University of Minho
School of Engineering

Alexandre José Costa Figueiredo

Optical Inspection of Electrical Connectors in Products for the Automotive Market

December 2021

Optical Inspection of Electrical Connectors in Products for the Automotive Market

Alexandre José Costa Figueiredo

UMinho | 2021

University of Minho
School of Engineering

Alexandre José Costa Figueiredo

Optical Inspection of Electrical Connectors in Products for the Automotive Market

Masters Dissertation
Integrated Masters in Physics Engineering
Devices, Microsystems and Nanotechnologies
Work carried out under the guidance of

Professor Doctor Eduardo Jorge Nunes Pereira

December 2021

DIREITOS DE AUTOR E CONDIÇÕES DE UTILIZAÇÃO DO TRABALHO POR TERCEIROS

Este é um trabalho académico que pode ser utilizado por terceiros desde que respeitadas as regras e boas práticas internacionalmente aceites, no que concerne aos direitos de autor e direitos conexos.

Assim, o presente trabalho pode ser utilizado nos termos previstos na licença abaixo indicada.

Caso o utilizador necessite de permissão para poder fazer um uso do trabalho em condições não previstas no licenciamento indicado, deverá contactar o autor, através do RepositóriUM da Universidade do Minho.

Atribuição-NãoComercial-CompartilhaIgual
CC BY-NC-SA

https://creativecommons.org/licenses/by-nc-sa/4.0/

Agradecimentos

A presente dissertação, embora esteja apenas em meu nome, não seria possível sem o auxílio, carinho e dedicação de várias pessoas, às quais deixo aqui o meu mais sincero agradecimento.

Em primeiro, sou eternamente grato aos meus pais, pois sem os seus esforços não teria a oportunidade deste percurso académico. Estiveram sempre presentes e acompanharam-me, não só nesta jornada, mas em todas da minha vida, e ensinaram-me a dar e ser sempre o melhor de mim. Ao meu irmão Afonso, que mesmo ainda em tenra idade, já muito "sabe e opina", deixo aqui o meu apreço, por nos relembrar da felicidade das pequenas coisas e trazer alegria em tantos momentos à nossa casa. A eles, o meu muito obrigado!

Diz se que é em momentos mais difíceis que as pessoas que mais se importam connosco aparecem, porém há algumas pessoas que são já constantes da vida, e "teimam" por ficar. À minha Ticha, por todo o carinho, conforto, dedicação e acima de tudo pela presença contínua, o meu muito obrigado!

Sou muito grato ao Professor Doutor Eduardo Pereira por ter partilhado comigo esta etapa académica e o seu conhecimento, por toda a ajuda no desenvolvimento desta dissertação, por todo o feedback e pelo estímulo do meu interesse na área de ótica. O meu muito obrigado!

Muito do trabalho aqui apresentado não seria possível sem o estágio curricular na Bosch, que me permitiu crescer, não só como profissional mas bem como pessoa. A toda a atual equipa do CoC Testing de Braga, deixo aqui o meu enorme apreço por tão bem me acolherem! Agradeço, de forma muito especial, ao Filipe Silva, meu mentor na empresa, por toda a orientação, feedback muito construtivo e estimulo persistente para a evolução, e ao João Paulo Silva, pela partilha constante de conhecimento e auxílio sempre pronto para a resolução de dificuldades. O meu muito obrigado!

Por fim, mas de igual valor, deixo um enorme obrigado a todas as pessoas, que mesmo não estando aqui referenciadas de forma singular, contribuíram, de uma ou outra forma, para esta etapa tão importante da minha vida. O meu muito obrigado!

STATEMENT OF INTEGRITY

I hereby declare having conducted this academic work with integrity. I confirm that I have not used plagiarism or any form of undue use of information or falsification of results along the process leading to its elaboration.

I further declare that I have fully acknowledged the Code of Ethical Conduct of the University of Minho.

Inspeção Ótica de Conetores Elétricos em Produtos para o Mercado Automóvel

Resumo

O mercado automóvel requer o controle de qualidade a 100% de todos os produtos. A inspeção ótica é o método preferencial para o controle de qualidade em fim de linha de produção porque é não destrutiva e tem tempos de ciclo baixos. Os produtos têm conetores elétricos com pinos metálicos que têm de ser verificados: posicionamento, integridade e coplanaridade. Muitos dos conectores estão integrados no interior de peças de plástico que também necessitam de ter a sua integridade analisada. Nesta dissertação são estudados diferentes métodos de perfilometria ótica, que permitam determinar a posição e/ou altura dos pinos, com uma tolerância de ±150 micrómetros. Entre as técnicas estudadas estão o uso de uma sonda confocal cromática, visão artificial com objetivas telecêntricas, fotografia computacional com formação de imagem plenótica, e o uso em simultâneo de estereoscopia e projeção de luz estruturada. Estas quatro técnicas foram testadas, tanto em *Electrical Connector Units* (ECU) como em *Standard Connectors* (SC), atendendo aos requisitos de cada tipo de conetor e às características de cada técnica. Para avaliar a aplicabilidade e sucesso de cada tecnologia, foram utilizadas medidas de capabilidade, o C_g e o C_{gk}. A sonda confocal cromática é apenas útil para medir a altura dos pinos dos ECU, e apresentou resultados razoáveis; a visão artificial com objetivas telecêntricas revelou-se excelente para determinar a posição dos pinos; a imagiologia plenótica demostrou ser o mais completo dos sistemas, visto ser o único capaz de fazer todas as análises necessárias, e com resultados interessantes; a estereoscopia com projeção de luz estruturada embora interessante para a análise da altura dos pinos, não apresenta valores aceitáveis para determinar as suas posições. Em suma, todas as técnicas analisadas têm os seus méritos, mas com uma tolerância tão apertada, não há apenas uma técnica que seja considerada superior em todos os aspetos às outras, sendo que a solução seria possivelmente a junção de duas das tecnologias disponíveis.

Palavras Chave: Inspeção Ótica Automática; Sonda Confocal Cromática; Objetivas Telecêntricas; Imagiologia Plenótica; Estereoscopia

Optical Inspection of Electrical Connectors in Products for the Automotive Market

Abstract

The automobile market requires 100% quality control of all products. Optical inspection is the preferred method for end-of-line quality control because it is non-destructive and has low cycle times. The products have electrical connectors with metal pins that must be checked: positioning, integrity and coplanarity. Many of the connectors are integrated into plastic parts that also need to have their integrity analyzed. In this dissertation, different optical profilometry methods are studied to determine the position and/or height of the pins, with a tolerance of 150 micrometers. Among the studied techniques are the use of a chromatic confocal probe, artificial vision with telecentric objectives, computational photography with plenoptic image formation, and the simultaneous use of stereoscopy and structured light projection. These four techniques were tested, both in *Electrical Connector Units* (ECU) and in *Standard Connectors* (SC), meeting the requirements of each type of connector and the characteristics of each technique. To assess the applicability and success of each technology, capability measures, C_g and C_{gk} were used. The chromatic confocal probe is only useful for measuring the height of the ECU pins, and has shown reasonable results; the artificial vision with telecentric objectives proved to be excellent for determining the position of the pins; plenoptic imaging has proved to be the most complete of the systems, since it is the only one capable of perform all the necessary analyses, and with interesting results; stereoscopy with structured light projection, although interesting for the analysis of the height of the pins, does not present acceptable values to determine their positions. In short, all the techniques analyzed have their merits, but with such a tight tolerance, there is not a single technique that is considered superior, in every aspect, to others, and the solution would possibly be to merge two of the available technologies.

Keywords: Automatic Optical Inspection; Chromatic Confocal probe; Telecentric Objectives; Plenoptic Imaging; Stereoscopy

Contents

List of Figures

List of Tables

List of Abbreviatures

AFM – Atomic Force Microscopy

AIAG – Automotive Industry Action Group

AOI – Automatic Optical Inspection

BDE – Best Depth Estimation

BrgP – Bosch Braga Plant

CCD – Charged-Couple Device

C_g – Potential Capability Index

C_{gk} – Critical Capability Index

CMM – Coordinate Measure Machine

CNC – Computer Numerical Control

CoC – Centre of Competence

DUT – Device Under Test

ECU – Electrical Connector Unit

FOV – Field of View

LED – Light Emitting Diode

MLA – Micro Lens Array

OCAI – Optical Calibration, Alignment and Inspection

OCT – Optical Coherence Tomography

OPD – Optical Path Difference

PDF – Probability Density Function

PoE – Power over Ethernet

ROI – Region Of Interest

SC – Standard Connector

SLD – Super Luminescent Diode

SLM – Structure Light Modulator

STM - Scanning Tunneling Microscope

VD – Virtual Depth

WLI – White Light Interferometry

Chapter 1

Introduction

The growth of a knowledge-based economy has reinforced the need for strategic partnerships that go past the traditional funding of research projects. With that in mind, there was a surge of partnerships between Industry and Universities. Such collaboration has numerous benefits. For the Academic side, it is a way to apply the knowledge and validate theories. For the students, it is an opportunity for training and skill development. For the Industry, it is a chance to apply state of the art technology developed by the academic side, in order to reduce cycle times and costs overall. For society in general, the creation of such workforce and technological advance resulting from those partnerships, will lead to an economical growth.

This thesis is a product of one of those partnerships. It is the result of the association of the optics group from the Physics Department of University of Minho and the Center of Competence (CoC) for Testing from Bosch Car Multimedia, S.A. in Braga (BrgP). The OCAI (Optical Calibration, Alignment and Inspection) project, where the dissertation is inserted, is part of Factory of Future, the third partnership between the two aforementioned entities. The main objective of the R&D Factory of Future program consists in generating advanced knowledge and technology in Portugal in the area of new technologies for manufacturing, which will be the basis of innovative solutions worldwide for the future of industrial manufacturing for the automotive industry. One of the objectives of the OCAI project is to develop cost effective innovative Automatic Optical Inspection (AOI) procedures for end-of-line quality control of electric connectors, integrated in a multitude of Bosch Car Multimedia products manufactured in the Bosch Braga plant. These connectors are usually integrated in the interior of plastic parts, leading to occlusion for laser scanning and stereoscopic cameras, and need to be verified for geometric integrity and co-planarity, with a tolerance of about ±150 micrometers.

Even though these collaborations can sometimes be complex and difficult to coordinate, the benefits outweigh the disadvantages and the success of the project between Bosch and University of Minho is a testament to this.

1.1 Connector Inspection

According to a recent study by Global Market Insights, Inc., the global connector market size is projected to cross the USD 75 Billion by 2026 (Ankit Gupta, 2020). This rise of market value is driven by the ever-growing requirement for fiber optic connectors. The automotive market is also a major customer for electrical connectors as with the increase of sensors, cameras and other electronic systems on newly developed vehicles the demand for connectors in each car has also increased. Besides the automotive connectors produced by Bosch, a big part of the products in the catalog of BrgP also have connectors, that can be damaged during the assembling or test process. Therefore, like most of industrialized products, an end-of-line inspection is needed to guarantee the quality of the product. This master thesis has the goal to test, compare and validate different technologies to fulfill the task of connector inspection.

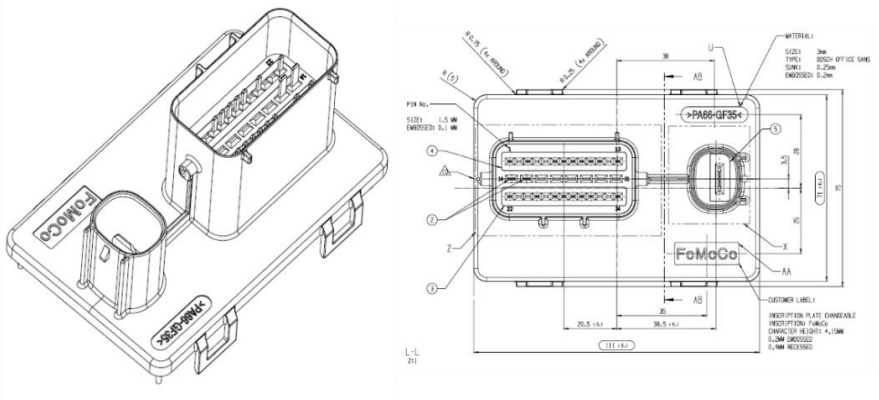

Figure 1 - Example of Electrical Connector Unit. In the technical drawing it is shown that the size is 11.1 cm x 7.1 cm.

Not all the connectors are the same. During the development of this thesis, two different types of connectors were analyzed. The first kind, the Electrical Connectors Units (ECU), produced by Bosch, and the second kind, Standard Connectors (SC), are the most common. ECU connectors, represented in Figure 1 are usually bigger than SC, Figure 2. This size difference can be observed in Figure 3, where both type of connectors are presented side by side. This difference will influence the technologies applied to each kind of connector. The ±150 micrometers tolerance is originated in the ECU analysis. In fact, for SC there is no defined value for tolerance, but in some cases those values are specified by the supplier.

Figure 2 - Example of two different SC: Fakra (top) and HSD (bottom) and commonly associated defects.

There are a few aspects related to the optical connector inspection. One important task is pin inspection, which involves various evaluations: presence of the pin, height of the pin (most suited to ECU analysis) and position of the pins according to a certain reference. The primary objective is to measure the latter two features with a ±150 micrometers tolerance. This is not an easy task, not only because of the tight tolerance, but due to the chosen reference. Ideally, the reference to measure the XY position of a pin would be the center of the connector, determined using the walls. But, since the walls are majorly formed by malleable polymers, they are easily deformed when subjected to forces, or thermal variations. These variations in the reference point can be enough to surpass the value of the previously mentioned tolerance.

Figure 3 - Size comparation between an ECU (left) and a SC (right).

Another relevant point to the analysis of the connector is to verify not only the integrity of the exterior plastic case, but also if the connector being inspected matches the one intended. Occasionally, a swap of the connectors can occur, and that error must be identified at the end-of-line inspection, using the color and shape of the plastic case, with the help of machine vision.

1.2 Dissertation Overview

Since this dissertation has the goal to test and compare different technologies, one must start by understanding how those technologies work. *Chapter 2* presents the state of the art of a range of different technologies with applicability to connector inspection, followed in *Chapter* 3 by the tests and results achieved for a number of those technologies.

Chapter 2

Literature Review

At the naked eye, a surface that looks flat may not always be as smooth as it seems. The family of profilometers is a set of meteorological measurement devices that are used in the determination of the roughness of a surface, waviness and height histogram, scratch and crack analysis, and paint and coating characterization. Using dedicated software tools, one can make a 3D reconstruction of the subject. For that to be possible, all the dimensions of the Device Under Test (DUT) must be known. Inside the family of profilometers, there are technologies that are limited to measurements in a single plane (XY plane), and therefore are used to determinate those coordinates. On the contrary, some technologies are incapable, or just unpractical to that same type of measurements, and therefore are used to find the depth of the DUT. To have a full 3D model, it is possible to combine one of each type of technologies, or then use instead a third type that can by its own give all the information on the three dimensions (Toru Yoshizawa, 2015).

A surface profilometer uses a high-precision data acquisition equipment to measure the different features on a given scale. A surface profilometer may either be contact or contactless. Contact based profilometers, as the name implies, need to make physical contact with the surface, normally using a sensitive stylus, which runs across the area under test. This method can register the deformation and the fluctuations of the surface through the variance of the stylus position. The non-contact methods for surface profilometry are, generally, a range of optical acquisition methodologies that obtain the surface information by emitting a light and then analyzing the emitted, reflected or scattered light. In a general way, the non-contact methods for profilometry are preferred over the ones that require contact because of the low invasiveness and improved measurements speeds.

Having in mind that the objective of this dissertation is to test and compare different technologies and evaluate those same technologies in the application of connector inspection, one must first understand how those techniques work. This theoretical study of the state of the art is presented in this *Chapter 2*. Figure

4 presents the technologies under study, which are sorted by different methods: contact or contactless, visual perception and type of scan.

To provide a better reading and comprehensive experience to the reader, a guideline must be provided. Having that in mind, in Sub-chapter 2.1 some useful concepts will be reviewed. Sub-chapter 2.2 is where the review of technologies is done, sorted by type of scan: it starts with Point Scan methods, followed by the ones under Line Scan, and ends with the methods based on Area Scan. To finish this Chapter 2 the measures of capability are presented, which evaluates the applicability of the technology to the problem, according to Bosch standards (Robert Bosch GmbH, 2019).

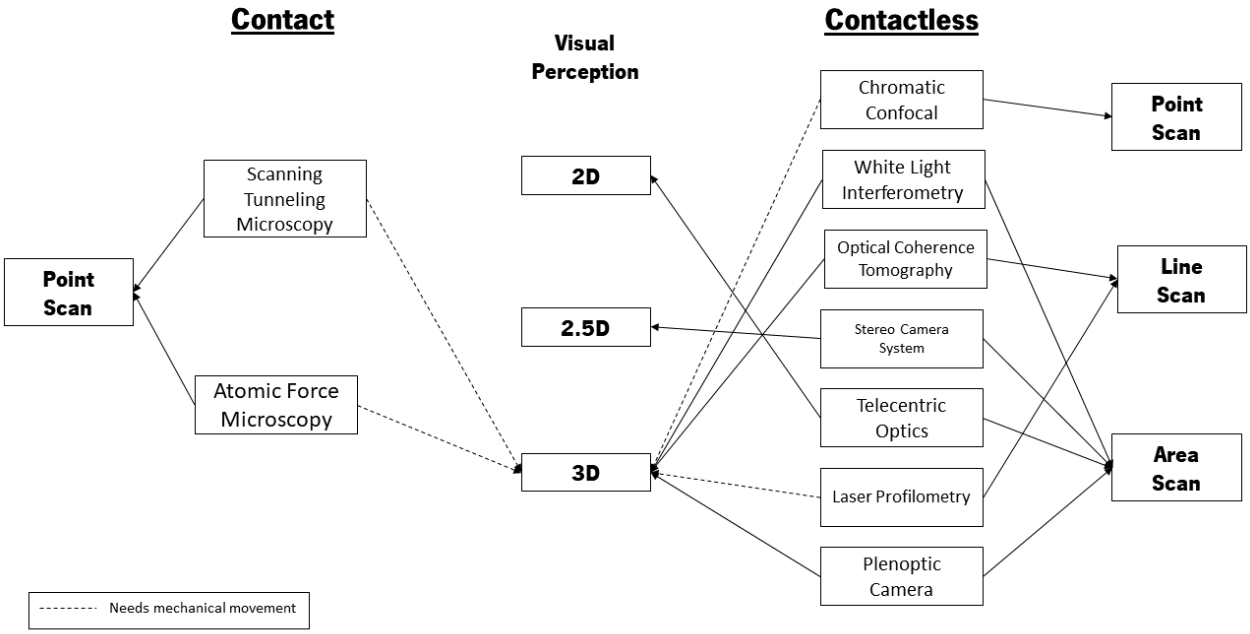

Figure 4 - Representational scheme of different technologies (Toru Yoshizawa, 2015) (Vision Doctor, s.d.) (Paschotta, s.d.) (Kerwien, 2014).

2.1 Concepts Review

2.1.1 Geometrical Optics

Inside *Geometrical optics* is the study of light as a ray. The reason why we use rays is that, like other successful models in physics, rays are crucial to our thinking, notwithstanding their shortcomings. The ray is a model that works well in some cases but fails to describe other situations, and it is valid only when the characteristic dimensions of the object being analyzed is much larger than the wavelength of the light source. In those occasions where this model fails, light can be thought about as scalar waves or electromagnetic waves, depending of the phenomena under consideration.

One instance where the ray is widely used is to explain and describe the object-image relation. Given an object and an optical system, one can describe the properties of the formed image, like its position, size and orientation, using the ray model. A schematic of this method, known as thin-lens model, is represented in Figure 5.

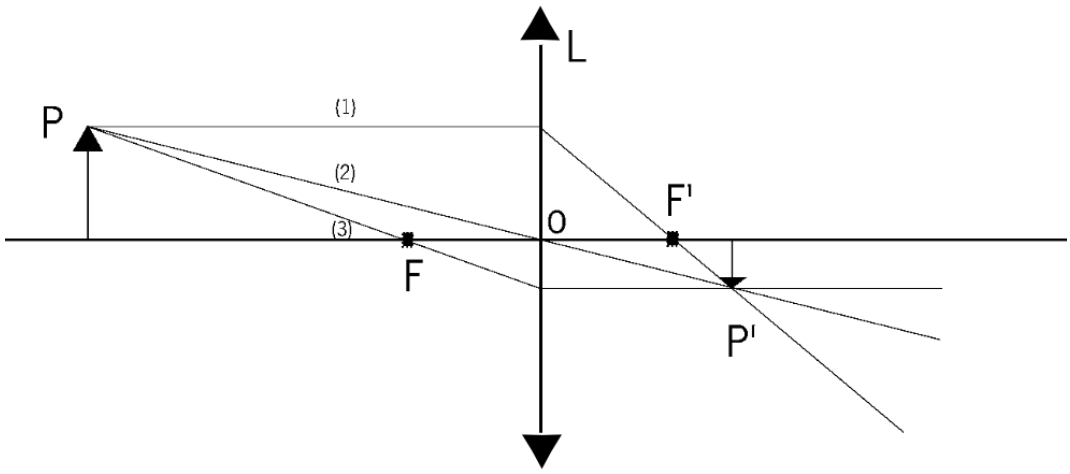

Figure 5 - Image formation principles under ray optics, paraxial model and thin lens model (three successive approximations).

Considering an object P, the respective image, as imaged through a lens L of focal length F, is P'. Knowing the position, size and orientation of the object, there are three rules to follow to know the same properties of the image formed. First: Rays parallel to the optical axis, when passing through the lens L, will

follow to the focal point F' of the system. Second: Rays that intersect the lens at the optical axis O, continue with the same angle. Third: Rays that cross the focal point F, when intersecting the lens L, will follow parallel to the optical axis. The object points P-P' are commonly referred to as conjugated points, as every light ray coming from P, irrespective of the angle, ends up on P' (Hall, 2008).

The understanding of light as a ray will be useful to better comprehend some technologies described over this dissertation, namely the Telecentric Lenses and the Plenoptic Camera.

2.1.2 Interferometry

Interferometry is one of the most versatile and powerful set of tools in the vast world of optics. Its applications range from the search for dark matter through gravitational lensing on a cosmological scale to control of CNC (Computer Numerical Control) machines of nanometer accuracy. Between these extreme cases, interferometry can be used for more simple situations like measuring distances.

2.1.2.1 Interfering waves

"Almost everyone has come across interference phenomena such as vivid colors in a soap bubble, or in an oil slick on a wet road" (Hariharan, 2003) An interferometry phenomenon occurs when two (or more) electromagnetic waves interfere with one another, provided that certain criteria (namely coherence) are achieved. The devices used for that evaluation, the interferometer, can measure the distortion of a wavefront caused by aberrations, badly manufactured optical components, or inhomogeneities in the material under inspection (case of connector analysis). This is done by measuring the interferogram, obtained by the interference of the complex amplitude distribution of at least two optical paths (Page, 2008).

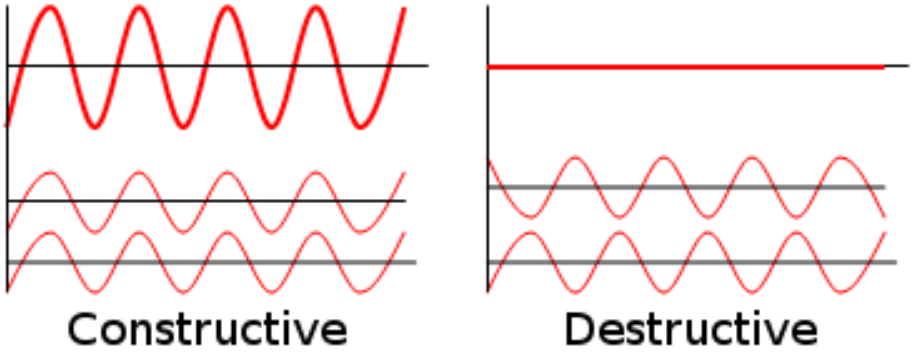

Figure 6 - Interference of two waves with equal wavelength, causing constructive interference, when both waves have no phase difference, and destructive interference, when the waves have opposite phases.

Mathematically, the interference of two light waves is the vectorial summation of their electrical field vectors. This summation can result in constructive interferometry, if their local fields point in the same direction, or destructive interferometry, in the case of opposite direction, as presented in Figure 6. Considering two waves, w_1 and w_2, traveling in the x-direction, with amplitude A, wavenumber $k = 2\pi/\lambda$, angular frequency of $\omega = 2\pi f$, and a phase difference between the two waves of φ , such that:

$$w_1 = A\cos(kx - \omega t) \tag{1}$$

$$w_2 = A\cos(kx - \omega t + \varphi). \tag{2}$$

Then, the resulting interference between these two waves will be constructive if φ is an odd multiple of π, and it will be destructive if it is an even multiple of π.

$$w_1 + w_2 = 2A\cos(kx - \omega t) : \varphi = n\pi, \quad n \in \ldots -4, -2, 0, 2, 4, \ldots \tag{3}$$

$$w_1 + w_2 = 0 : \varphi = n\pi,$$
$$n \in \ldots -3, -1, 1, 3, \ldots \quad (4)$$

2.1.2.2 Coherence

Like it was said before, for interference to occur, some conditions need to be fulfilled, namely a property of light called coherence. If this condition was not needed for interference to arise, then we would see it everywhere. A light source with a well-defined phase relation that is constant over time and space is said to be coherent. Incoherent light sources change their phase relation too quickly in time and space, causing interference to occur too fast, being impossible to see it and measure it. One of the most popular coherent light sources is the laser, that can present a visible interference pattern even if both waves have a very large path difference (Schmit J., 2019).

To quantify the coherence, l_c is used as a spatial measure, and t_c as the temporal measure. The coherence length, l_c, is the maximum path length difference between both beams that still shows an interference pattern. The coherence time, t_c, is expressed by the time the light needs to travel l_c with the speed of light c:

$$t_c = \frac{l_c}{c} \quad (5)$$

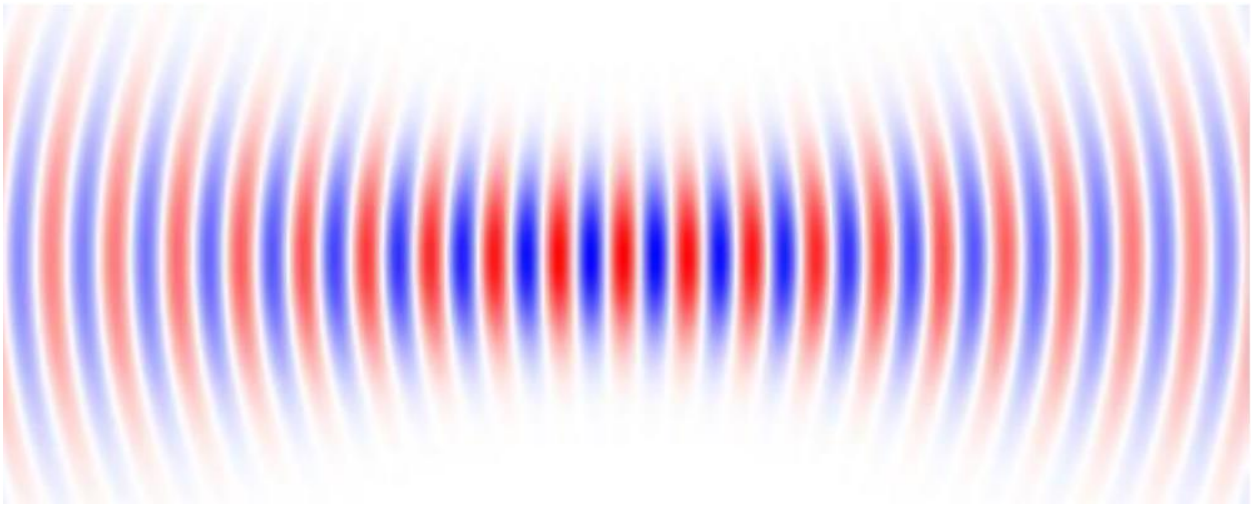

Figure 7 - Light source with high spatial and temporal coherence (RP-Photonics, n.d.).

The coherence time can be defined has the average time interval during which the light wave oscillates in a predictable way. The longer the coherence time, the greater the coherence time of the light source. If a light source was ideally monochromatic, the wave would have an infinite coherence length.

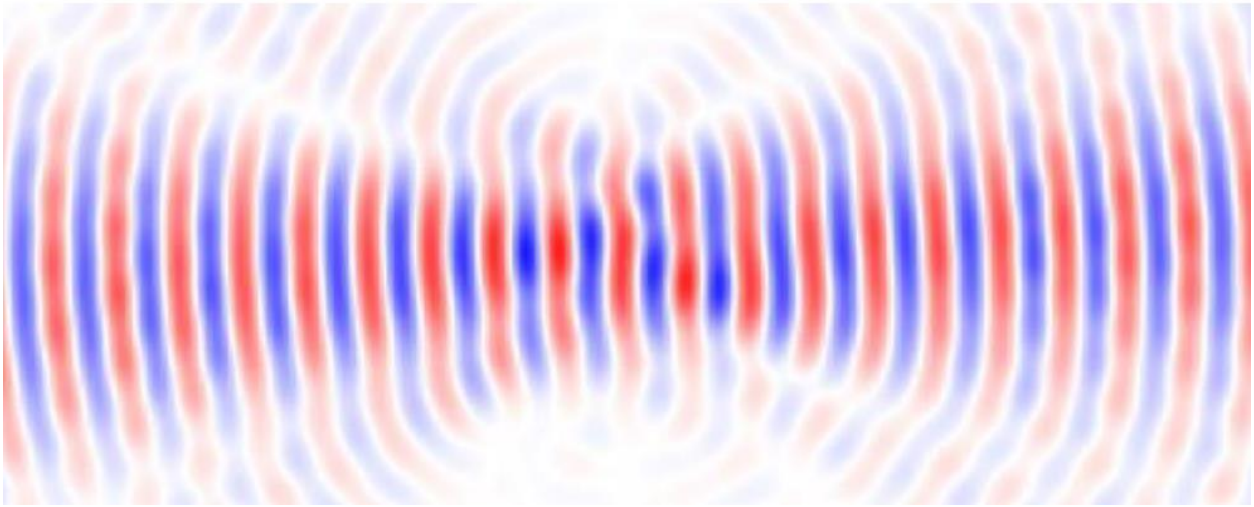

Figure 8 – Light source with good temporal coherence, but low spatial coherence (RP-Photonics, n.d.)

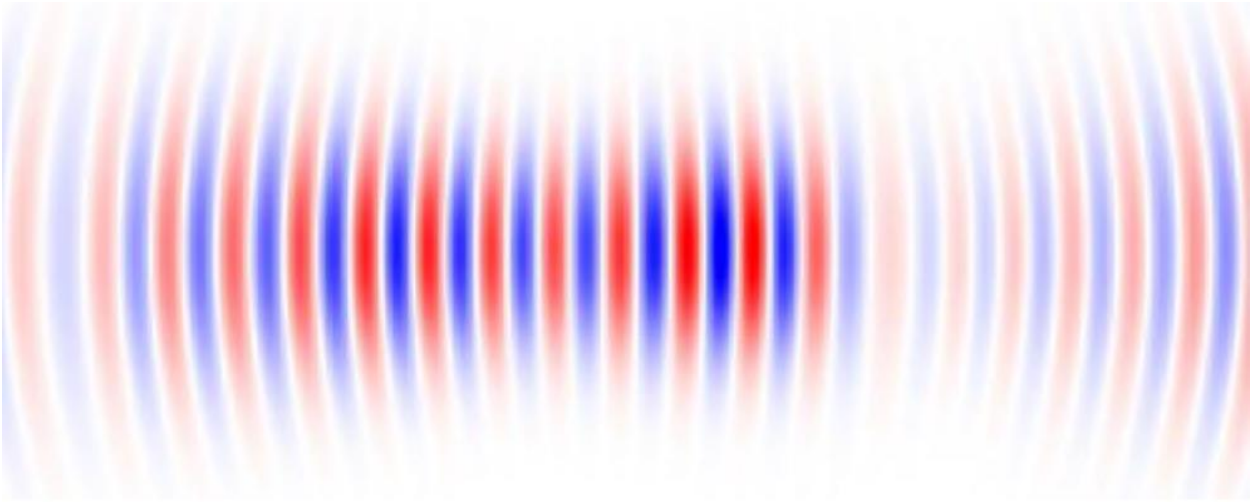

Figure 9 - Source with good spatial coherence, but low temporal coherence (RP-Photonics, n.d.)

Another condition necessary for interference to occur is polarization. In order for two beams to interfere, the electrical fields cannot be completely orthogonal, meaning that both beams should have the same polarization state.

2.1.2.3 Optical Setup

In practice, to create interference, we need two beams of light. Most of interferometers split the same light source in two parts, that travel slightly different paths to the detector. One of them goes practically direct to the detector, being called the *reference beam*. The other, the *object beam* interacts with the object under analysis before arriving to the connector. When both parts are reunited in the detector, interference is produced.

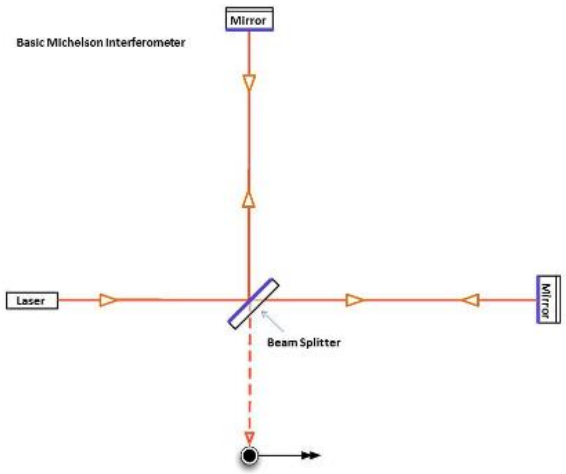

Figure 10 - Michelson's Interferometer: In measurement applications, one of the mirrors is replaced with the DUT.

One of the most known and used interferometer is the Michelson Interferometer, as presented in Figure 10. It is simple and explains the principle of interference perfectly. The coherent light source (laser) emits the light that is split in two beams by the *beam splitter*. Both beams travel approximately the same length before returning to the detector. On the detector both beams are superimposed and create the interference signal (Wiora G., 2013).

2.1.2 Optical Specification

In order to compare different equipment and to evaluate, at first sight, if it is suited for a task or not, there are commonly used some definitions that specify the devices in important aspects. Figure 11 presents a scheme of some of these technical specification concepts (Vision Doctor, s.d.).

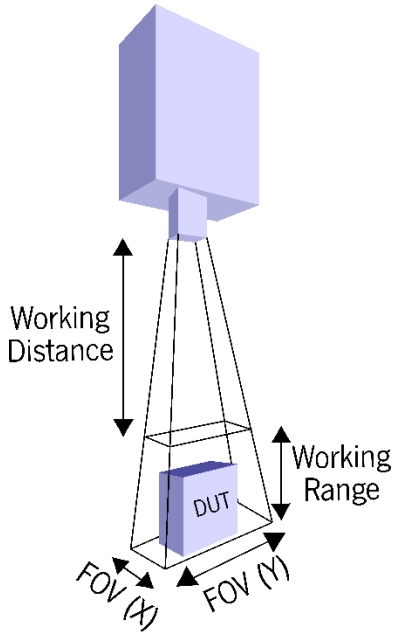

Figure 11 - Different concepts for specify an equipment.

The Working Distance (or Clearance Distance) is the minimum distance that an object must be away from the sensor in order to be correctly scanned and measured. If the DUT is closer than this minimum distance, the resulting data will be incomplete, and in the worst case, incorrect. The Working Range (or Measurement Range) is the difference, in vertical distance, between the minimum distance that can be measured *i.e.* the clearance distance, and the farthest point that the sensor can measure. Points outside the measurement range will most likely, not be measured, depending on the technology used. The Field of View (FOV) is the measure of the area in the XY plane, inside the measurement range, that the device can measure. The field of view can have different aspects: it can be a cone, a trapezium or even a cylinder. Understanding these concepts will be useful to better comprehend some technologies described in *Sub-Chapter 2.2*.

2.2 Technologies State of the Art

2.2.1 Point Scan

2.2.1.1 Contact Methods

The first tunnel effect microscope (STM – Scanning Tunneling Microscope) was developed by Roher and Binning in 1982 (G. Binnig, 1982). This enabled the non-destructive study of surfaces with an atom resolution, never seen before. The technique relies on the sweeping of a surface in parallel lines with the probe, that then would come together to form the topographic image of the sample. The sensor, or stylus, was revolutionary due to its dimension and construction. This system was the precursor of the more recent Atomic Force Microscopes (AFM), that are now used in most of surface investigation laboratories.

Electrical tunneling is a quantum effect that allows a current of electrons to occur between two surfaces really close to each other. The space between the two surfaces is considered a potential barrier, and the smaller the thickness (in the Angstroms scale), the bigger is the probability of the electron to cross it. This invention would lead to winning the Nobel Prize in the field of Physics by Roher and Binning in 1986.

Much like the STM working method, in the AFM a sharp tip, like the ones in Figure 12, is raster-scanned over a surface using a feedback loop to adjust parameters needed to image a surface, but instead of using the quantum effect of tunneling, it uses atomic forces to map the tip-sample interaction, that can be almost any type of force interaction – van der Waals, electrical, magnetic, thermal.

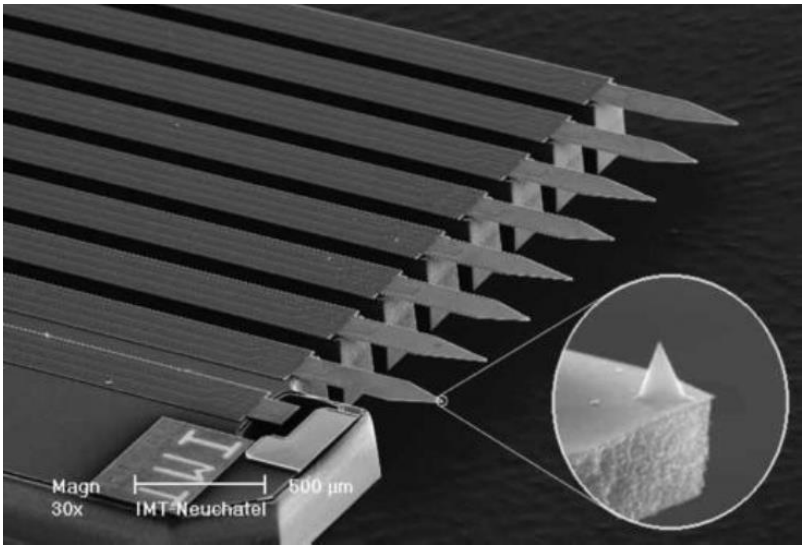

Figure 12 - Figure 6 - This image shows eight sharp tips of NASA's Phoenix Mars Lander's Atomic Force Microscope, or AFM. The AFM is part of Phoenix's Microscopy, Electrochemistry, and Conductivity Analyzer, or MECA (NASA, s.d.).

AFM has two operating modes: a contact mode, and a vibrating mode. The contact mode is more suited for measuring interatomic forces (Å), and the stylus is kept at with a regular force, changing its position when in contact with the surface. In the tapping or vibrating mode, the stylus oscillates at around 10^5 Hz close to the surface. This is more appropriate to soft surfaces, since the contact is not constant, and for long range forces, such as van der Waals and electrostatic forces (NanoScience Instruments, s.d.).

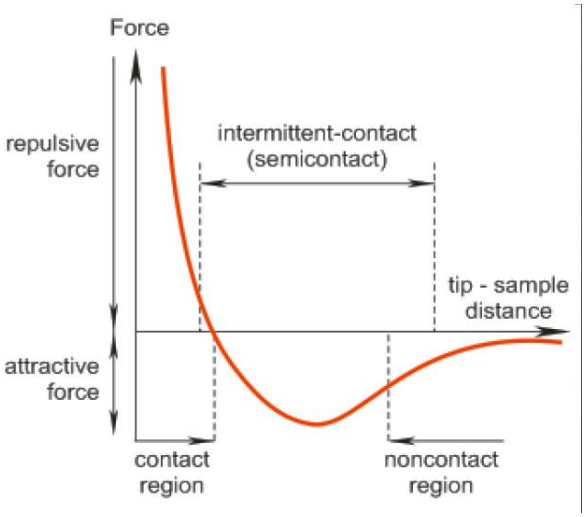

Figure 13 - Force-distance curve for Atomic Force Microscopes, where by Hooke's Law F=-kZ, F is the force, k the stiffness of the lever and Z the distance the lever is bent.

Atomic Force Microscopy is a well know and developed approach to the problem of profilometry, being used and continuously developed over the last 50 years. Although it has an incredible resolution and repeatability, it is not suitable for including in the production lines of BrgP, either by the impracticality of being a contact method or by the relatively long measuring times.

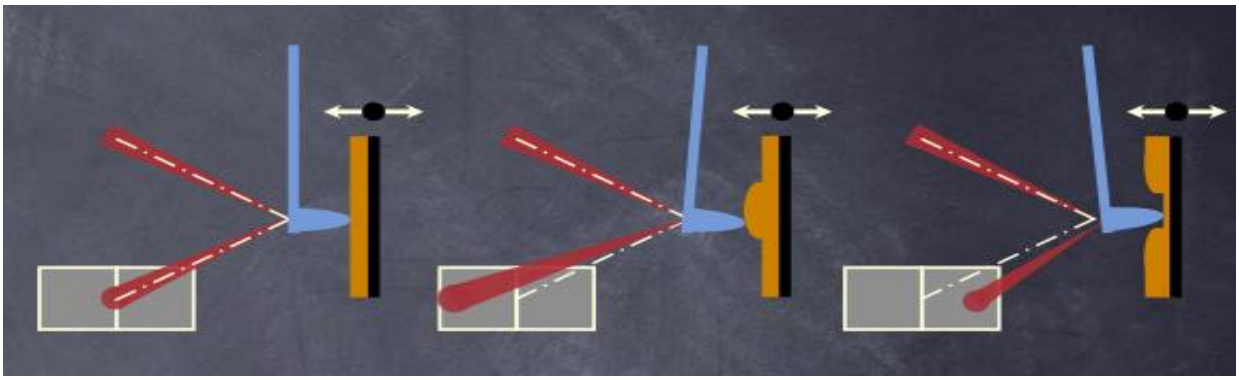

Figure 14 - Working method of an AFM. A laser, pointed to the tip, is used to track movements.

The alternative to mechanical profilometers, are the non-contact techniques, which rely mostly on optical methods, also known as optical surface profilometers.

2.2.1.2 Chromatic Confocal

Both Bosch and University of Minho already possess some experience with optical inspection technologies on connector inspection applications, one of them being the chromatic confocal technology.

Chromatic confocal probes are single point optical sensor built around a confocal coaxial setting that use chromatic dispersion and decoding to obtain the distance to the surface. Chromatic confocal probes can measure on, and through, transparent material, detect interfaces between materials and calculate thickness.

Figure 15 presents the most usual arrangement of a chromatic conformal imaging setup. The working principle is as it follows: when the point of focus is above (8) or below the surface being measured (7), the reflected light does not pass through the detector (3) pin-hole, leading to a detected intensity close to zero. In the other case, if the probe is on focus, meaning that the focal point is lying exactly on top of the surface (9), the reflected light will pass through the pinhole, causing a peak on the detector (Stil, SAS).

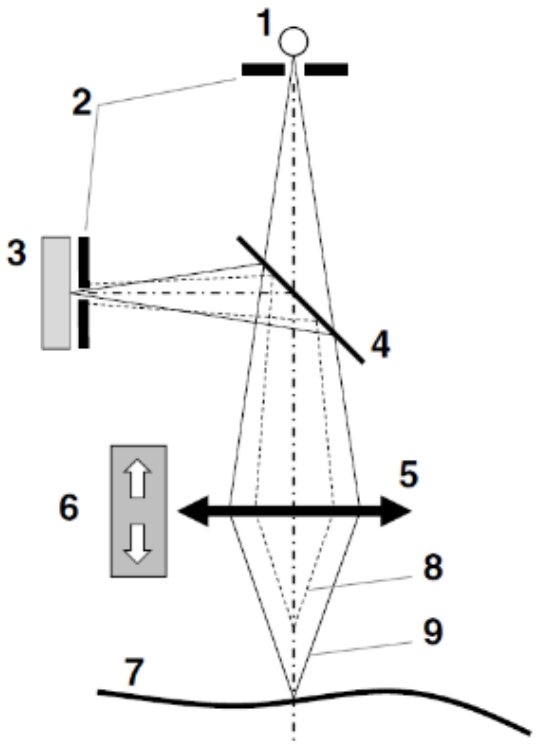

Figure 15 - Most usual implementation for Chromatic Confocal systems (Toru Yoshizawa, 2015).

The chromatic confocal probe is different from a usual imaging confocal microscope because the objective is replaced by a chromatic objective (5), that causes chromatic dispersion, and the photodetector by a spectrometer (3), which will decode the reflected light.

In most practical cases, the chromatic dispersion is something to avoid, since it generates different focal points for each different wavelength. However, in the case of chromatic confocal imaging probes, the chromatism present in the optical axis is used as a spaced-coding method, that associates a different wavelength to different depths.

STL SA, a manufacturer of these sensors, describes them as having an excellent spatial resolution regardless of ambient illumination and as being independent of the type of material in analysis, since it can work on transparent and opaque, specular or diffusing, polished or not materials. Also, the use of white light source and not of a coherent source (laser) completely eliminates all difficulties associated with speckle. Table 1 presents some specifications of chromatic confocal sensors available now in the market (Stil, SAS).

Examples of CHR Sensors for Profilometry

Specifications	Probe for Profilometry					
Measurement range (µm)	300	600	30,000	60,000	10,000	25,000
Resolution (nm)	10	20	100	200	300	800
Accuracy (µm)	0.1	0.2	1	2	3	8
Working distance (mm)	4.5	6.5	22.5	36	70	80
Spot size (µm)	5	4	12	16	24	25

Table 1 - Specifications of various Chromatic Confocal sensors.

Chapter 3.1 describes all experiments done and results achieved in the context of this dissertation.

2.2.2 Line Scan

2.2.2.1 OCT

The OCT, Optical Coherence Tomography, is part of the Low Coherence Interferometry family. It has a working principle similar to White Light Interferometry but uses near-infrared light instead of the white light source. These relatively long wavelengths will penetrate the scattering medium. However, it can be used in a more "standard" way, using only the reflections. It is a noninvasive, interferometric technique that provides real-time 3D images with micrometer resolution and depth penetration that can range from some millimeters to a few centimeters, depending on the technique employed and the material under study.

As with WLI, this technique also has long cycle time when inspecting large areas, that being one of the limiting factors. Both technologies are good alternatives to analyze small parts, in a non-invasive and non-destructive way, due to the great resolution they can achieve. However, they turn out to not be applicable to the connector inspection requirements, mostly due to the long cycle time (Nélida A. Russo, 2020).

A few measurements were done using an OCT, like the ones presented in Figure 16. These results were useful to compare with other technologies, and also to verify the correspondent results, as a ground-truth reference.

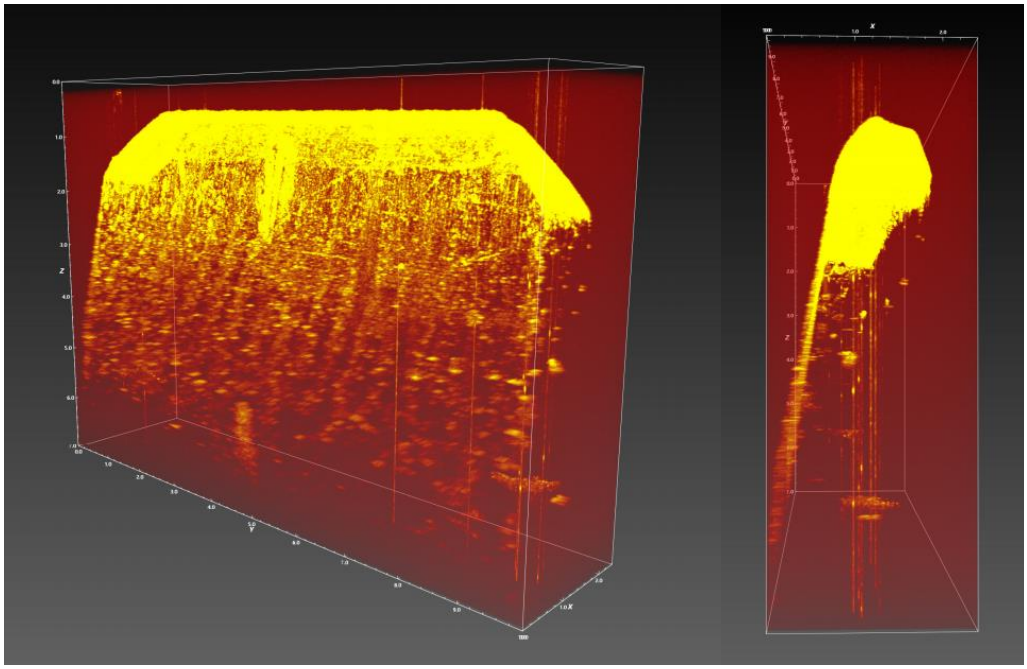

Figure 16 - Pin of an ECU scanned by an OCT: front view (left) and side view (right) (Thorlabs, 2017).

2.2.2.2 Laser Profilometry

The technique of triangulation is commonly used for determining spatial relations. This technique is widely used in diverse areas as cartography and the GPS (Global Positioning System). It can also be used to scan a surface, with the help of a Laser. Laser profilometry uses the principle of triangulation, where the laser point is projected on the DUT, and then observed (through a lens) by a sensor (Bradshaw, 1999).

This Laser Triangulation technique can operate in two different ways: as Point Scan, where, as mentioned above, only a point is projected and observed; and a Line Scan, where a line is projected instead. In both configurations, a mechanical scan is needed to obtain a 3D measurement. This second method can be achieved by replacing the laser point generator with a laser line generator. These two different methods are represented in Figure 17.

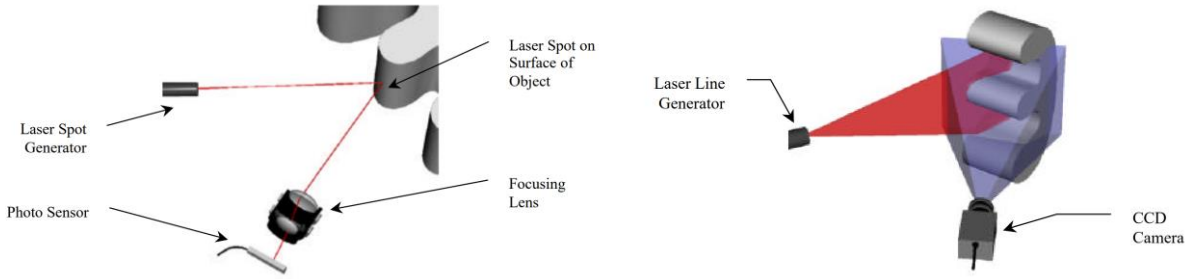

Figure 17 - Laser Triangulation, using Point Scan (left) and Line Scan (right) (Bradshaw, 1999).

In terms of sensors to scan a line, multiple sensors, stacked in top of each other, are required to measure the signal. But, it is often simpler, and cheaper, to replace the photo-sensors with a camera. The light quantity distribution of the reflected beam from the object is analyzed and the camera detects the pixel with the laser peak value (Tomasz GIESKO).

Usually, laser sensors are characterized by the resolution given in the micrometer scaler, but, for shorter ranges, these laser triangulation techniques are capable of sub-micron resolution. The Line Scan is more suited to our purposes, since the scan of the full DUT is required. The Point Scan technique would be possible, but the time and effort to scan the whole connector, point-by-point, would be just unpractical.

2.2.3 Area Scan

2.3.3.1 White Light Interferometry

Even though Interferometry can be used to scan a large area, White Light Interferometry (WLI), the technology studied in this dissertation, is more suited to perform scans in a smaller scale. Profilers based on white light interference (WLI) use broadband illumination, instead of coherent light, commonly used in classical interferometers, and work just like an array of optical focused sensors where each point of focused interference signal determines the profile. This method is well known by now and is widely used for measuring surfaces in a variety of subjects. It is known to have a good vertical resolution, being that in limit cases it can reach 300 picometers (Paschotta, s.d.).

A typical setup for this technique consists in a light source, a couple of lenses, a camera, and an interferometer, as shown in the Figure 18. The Michelson interferometer is the most used, but other solutions

are also possible. The light source is typically a light emitting diode (LED), incandescent lamp or a super luminescent diode (SLD). The camera works as the detector at the output of the interferometer. The distance between the mirror and the beam splitter must be equal to the distance between the beam splitter and the reference plane. To measure an object, it is necessary to move it along the optical axis in order to have its surface cross the reference. The light coming from the surface of the object will be superimposed with the light coming from the reference mirror, forming the white-light interference meaning that, if a surface point crosses the reference plane, the maximum interference will occur in the corresponding pixel of the camera. This means that to perform a measurement of a DUT in depth there is the need to move, either the DUT itself, the reference mirror, or the whole interferometer (Karthick Sathiamoorthy, 2010).

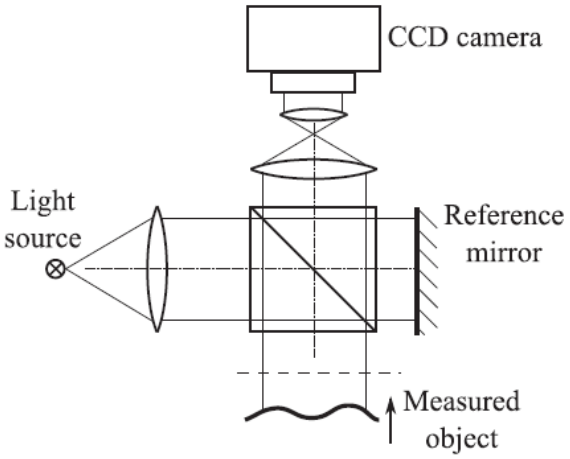

Figure 18 - Typical setup of a white light interferometer (Pavel Pavliček, 2019).

The usual light source used for this method falls within the visible spectrum (wavelengths between 380 and 750 nm), a low temporal coherence due to the wide wavelength bandwidth, and low spatial coherence due to it not being considered a single point light source.

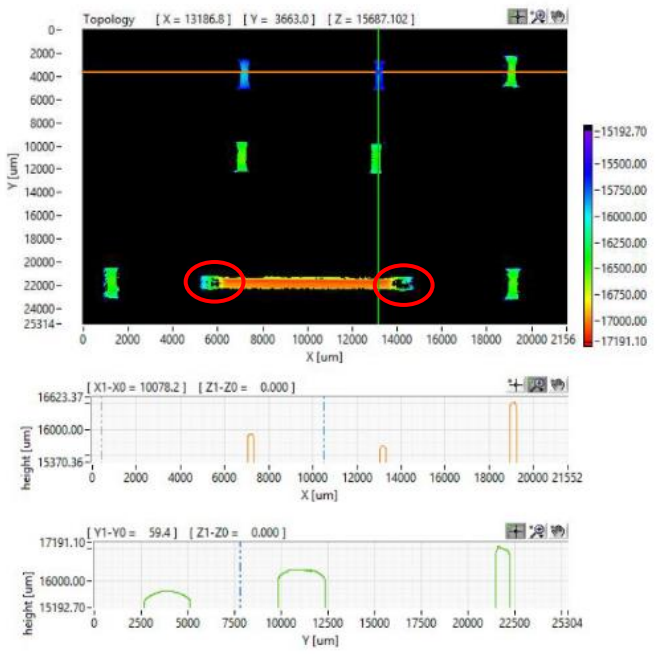

Figure 19 - Example of measurement with WLI technology. It is noticeable a loss of signal in the edges of the largest pin (marked with red circles).

The different wavelengths from the light source are mutually incoherent, and the superposition of fringes for different wavelengths will create white light fringes. If we have a monochromatic detector, it will observe the sum of all fringe intensities. The fringe where the maximum is located, which is where the greatest contrast is encountered, corresponds to the zero optical path difference (OPD). Away from that position, the observed intensities sum quickly falls as seen in the figure, and that is why the fringes are said to be localized (Schmit J., 2019).

The most important fact to know about WLI for topography is that the fringes are localized and can only be found near the zero OPD location, which occurs in the optimal focus position on the sample.

Bosch Car Multimedia S.A. (Portugal), namely the current CoC Testing department, had already the opportunity to test WLI technology in the past, in the context of connector inspection. From this experience, some system limitations were found. One of these drawbacks is the loss of signal at the edges of the pins, as seen in Figure 19. This limitation does not allow the use of the edge of the pins to find its XY position. Also, the cycle time and the total cost of the equipment were restrictions found by the team (Heliotis AG, 2017).

	Model A	Model B	Model C	Model D	Model E	Model F
Field of view	232 x 222 μm^2	580 x 560 μm^2	1.16 x 1.11 mm^2	1.47 x 1.41 mm^2	2.93 x 2.81 mm^2	5.86 x 5.62 mm^2
Working distance	2.52 mm	3.57 mm	3.57 mm	14.1 mm	55.8 mm	56.6 mm
Numerical aperture	0.5	0.4	0.3	0.17	0.11	0.07
Lateral resolution	0.8 µm	2 µm	4 µm	5 µm	10 µm	20 µm
Resolution RMS (phase mode)	50 nm (1 nm)	70 nm (1 nm)	100 nm (1 nm)	100 nm (2 nm)	100 nm (2 nm)	100 nm (2 nm)

Table 2 - Different models and its specifications available from (Heliotis AG, 2017).

The model tested (Model E) had a Field of View of 2.93 x 2.81 mm2, which is enough to scan a pin in a Standard Connector, but due to the larger size of Electrical Connector Units it will require additional linear actuators to cover the entirety of the surface of the DUT. If there was the need to have the whole connector analyzed, multiple line scans would be needed. As shown in Table 2 we can increase or decrease the FOV of the system, knowing that with a larger FOV part of the resolution will be lost.

2.2.3.2 Stereo Vision System

As it is known, a "normal" camera, with a "normal' lens, is only capable of capturing a bi-dimensional scene. Therefore, it is not possible, using a single camera + lens system to obtain depth information. One possible way to avoid this drawback is through stereoscopy. Humans, and many animals, use stereopsis as

a way to obtain the perception of a third dimension, using two bi-dimensional systems, the eyes. This same composed system can be simulated with cameras.

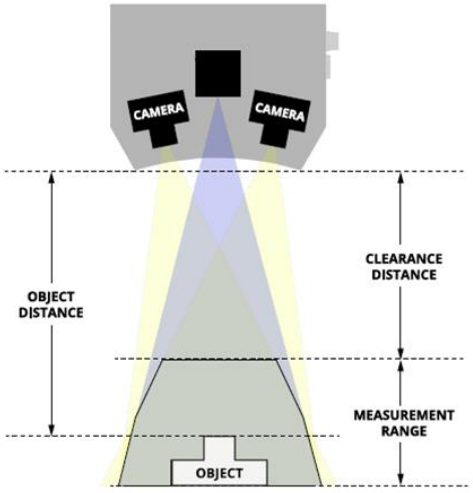

Figure 20 - Example of a Stereoscopic system.

In order to actually measure depths with such a system as the one presented in Figure 20, both sensors need to locate the same point on the DUT in the two images, with the two different viewing angles. Since the exact distance between the two cameras is known *a priori*, and the viewing angles are known, the distance to that point can be calculated.

This technique has some drawbacks; if a point under analysis is not visible to both sensors, then this triangulation will fail, meaning that occlusion is a problem. Besides that, this method requires computational power, alongside the two optical systems (Kerwien, 2014).

2.2.3.3 Optics

A photography can also be used to perform measurements on a scene, with the correct setup. Here are presented two ways to acquire the dimensions of a DUT, using photographic cameras and some sort of tool, namely a Telecentric Lens and a Micro Lens Array (MLA). But, for this to be possible, one other crucial point of optics must be approached: Illumination.

There are several ways to illuminate a scene, and, for different scenes and applications, different illuminations may be more suitable. In the context of this dissertation, three different illumination techniques were tested: Diffuse (or full Bright Field) Lighting, which splits into Flat Diffuse or Dome Diffuse; Dark Field Lightning; and Structured Lightning. Besides these three major techniques, another widely used approach in machine vision is Back Lighting, that does not have applicability in the Connector Inspection task due to the opacity of the DUT.

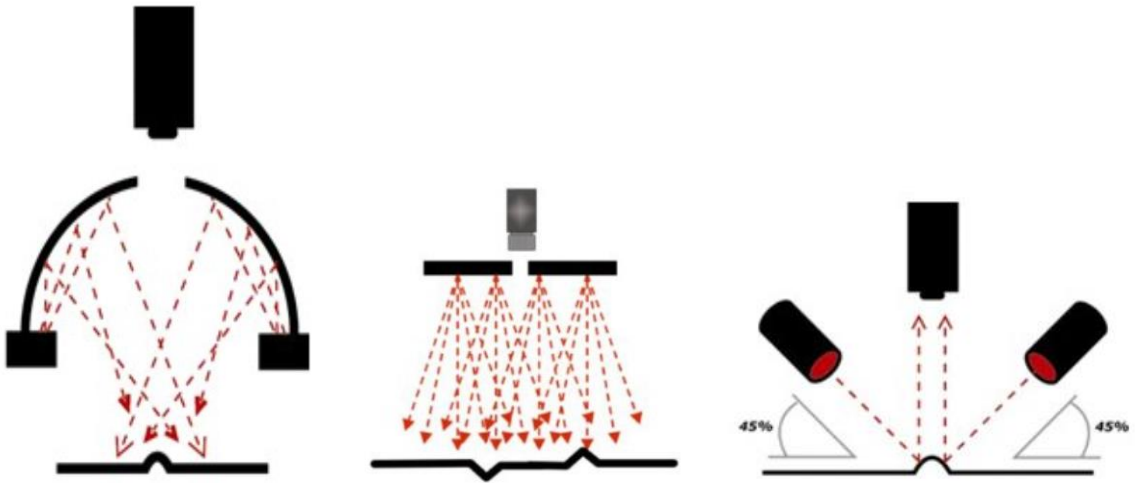

Figure 21 - Three different kind of illumination: Diffuse Dome, Flat Dome and Dark Field (from left to right).

It is possible to observe, in Figure 21, some of the more obvious differences, in terms of geometry, of the Diffuse Dome, Diffuse Flat (commonly referred as Flat Dome) and Dark Field (NI Engineer Ambitiously, 2019). The first two are the extensively used, since both can provide an even but multidirectional light in a large area. And, even though both provide diffuse uniform light, they have different influence in the final results. These results will be presented in 3.2.1.3.

Dark Field differs from other illumination systems in the angle that the light is emitted. These illuminators light is emitted at a shallow angle, which will provide a great contrast when a big change of depth occurs in the DUT, as can be seen in the pictures. This has proven to be useful for the vision software to check the integrity of the protective plastic case of the connectors, since most of that plastic is on a completely different level from all the other features.

Structured Light is the process of projecting a known pattern on to a scene. It can be used to measure depth differences by analyzing the way that the pattern deforms when striking a surface. In the topic of connector inspection, structured light is mainly used to find features, like the edges of connectors to provide stable references for referencing our measurements.

2.2.3.3.1 Telecentric Optics

High precision lenses are known to do a great job conveying contrast and color from object to image, but in terms of transferring accurate dimensions, they are not accurate especially if they have small focal lengths. Traditional lenses can be compared to a human eye: nearer objects appear larger than further objects. That is what we call depth perception. However, to a machine vision system, this can lower its accuracy, as a good vision system requires that the relationship between the dimension of an object and the corresponding dimension of the image to be well defined and unchanged. That is where telecentric lenses come in play.

Most of conventional lenses have angular fields of view such that as the distance between the lens and the object increases, the size of the image will decrease, meaning that a reduction of magnification occurred. This angular field of view will cause parallax, also known as perspective error, which will lead to a decrease in accuracy. The parallax error can be eliminated with the help of telecentric lenses. The main characteristic of these lenses is a constant, non-angular field of view, which means that these lenses will have the same field of view at any distance (Watanabe M., 1996).

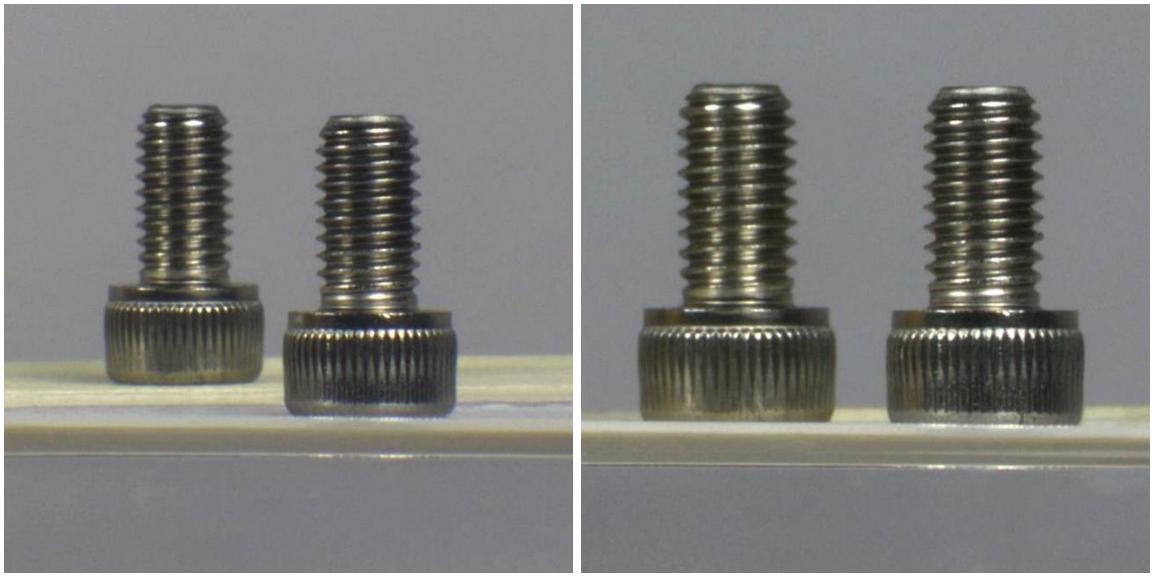

Figure 22 - Two screws, slightly separated from each other, captured by a regular zoom lens (left), and the same setup, captured by a telecentric lens (right) (Thorlabs, n.d.).

Telecentric lenses provide a way to present a uniform intensity image onto the camera, if the subject is uniformly lit. These lenses offer uniform collection by using a telecentric stop to provide an even angled cone of collection of light. This may not sound like much, but in fact most common lenses vignette the light that is not in the middle of the image field, causing the light at the edges to be reduced, as presented in Figure 23. Just looking at an image, most people might not even see this effect, as people are very tolerant to light level changes. However, given a vision system that is thresholding the light at some level in order to do the inspection, this light level variation is at least a nuisance. Even with adaptive thresholding, the limited dynamic range of cameras and the processing time taken for such filtering are both things that would be nice to not use up on something like light uniformity, given that the light sources themselves have become much better at presenting a uniformly lit field.

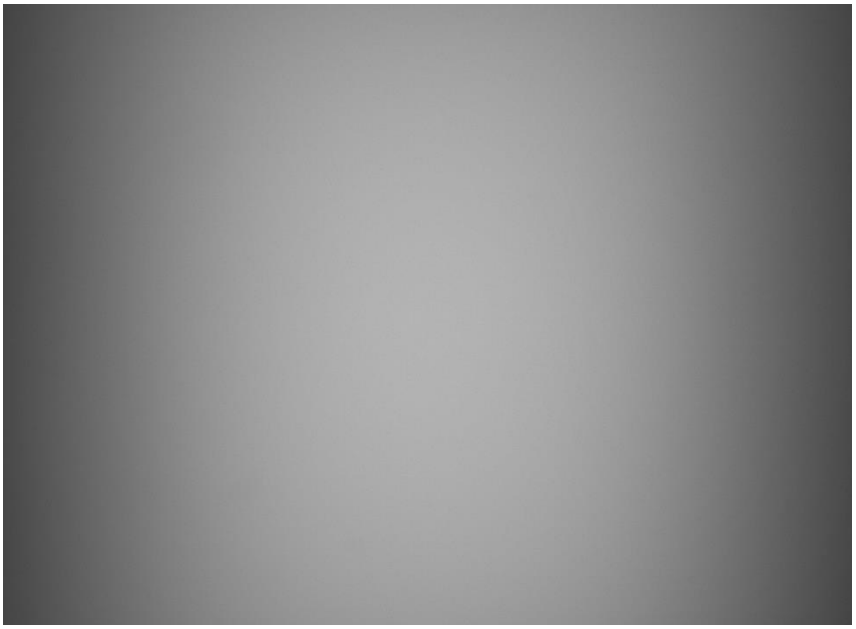

Figure 23 - Vignetting effect: The periphery of the image is less bright, when comparing with the center.

The second benefit telecentric optics provides is to produce an image that does not change in magnification for small shifts in the object distance. This means the system can be much more tolerant to shifts in the position of the part under inspection, both within the field and in distance, without the character of the image changing, either in terms of perspective view or magnification. This means a measurement made by a machine vision system can be tolerant to changes in distance to the part, without losing measurement accuracy.

In practice, no lens is perfectly telecentric. Th specification that quantifies the telecentricity is called telecentric angle, which tells the deviation from a perfect telecentric lens.

Object-space telecentric lenses

For the object-space telecentric imaging system, the entrance pupil is set at infinity. The easiest way to make a system object-space telecentric is placing a stop, *i.e.*, an aperture, between the lens and the detector and maintain the entrance pupil at infinity.

If we now consider an object that was displaced from the nominal focus position, then the transmitted rays will no longer meet the original image plane, meaning that, if the image sensor stayed in the same plane, the image formed will be somewhat blurred, but its height will not change. The magnification of the recorded image is fixed, and the correct object size can be determined (Thorlabs, n.d.).

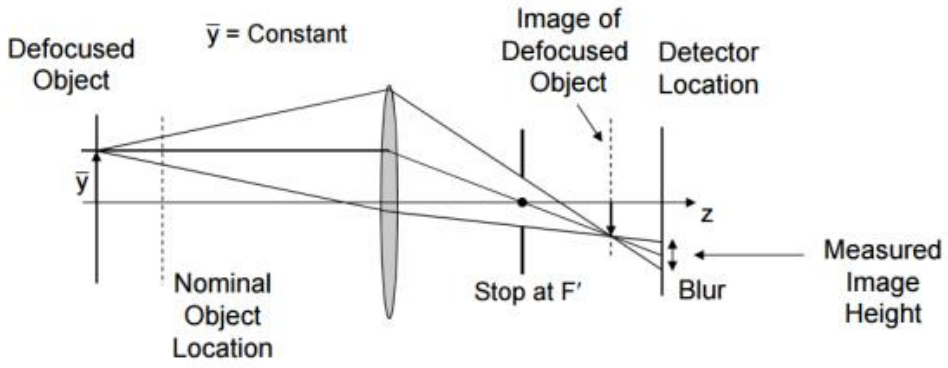

Figure 24 – Object-space telecentric lens. Stop is placed at the image side of the lens.

Object-space telecentric systems are usually used at close finite conjugates. The maximum object size is limited to approximately the radius of the objective lens due to vignetting considerations.

Image-space telecentric lenses

Contrary to the object-space, the image-space telecentric imaging system has the exit pupil set at infinity. Again, the easiest way to make this system is to place a stop aperture, but this time before the lens, in the front focal plane. The result is that the position of the image is independent of the chosen position of an image sensor; the drawback is that the resulting image will be blurred if the sensor is outside the focus.

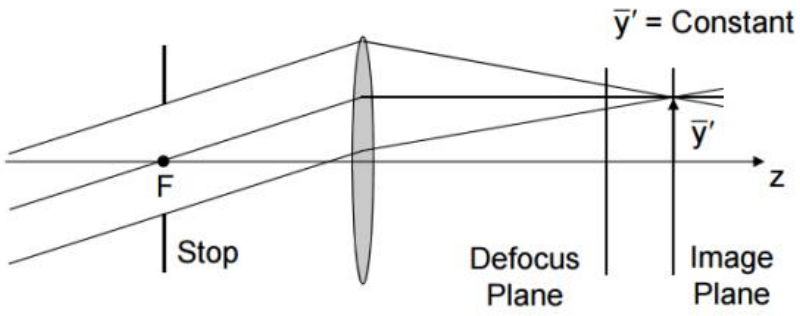

Figure 25 - Image Space telecentric lens. Stop is placed at the object side of the lens.

Double-sided telecentric system

When both previously mentioned methods are combined, lenses with bi-telecentry can be designed. That, however, is only possible with afocal optical systems. In this case, the stop is located at the common focal point, so that the chief ray is parallel to the optical axis both in the object space as well as in the image space. Since the ray bundle is centered on the chief ray, this condition guarantees that height of the spot forming the image is independent of axial object shift or image plane shift.

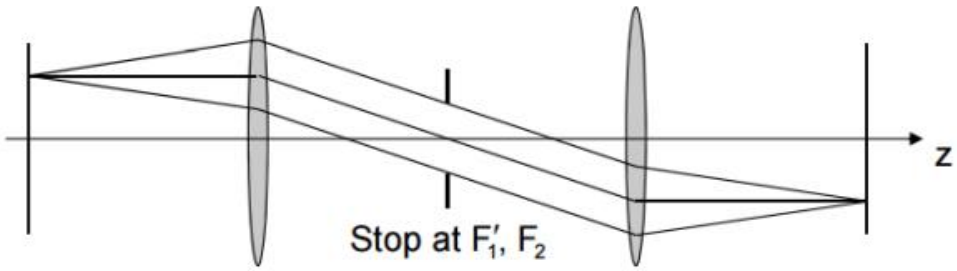

Figure 26 - Double-sided telecentric lens.

Telecentric optics does have its limitations. To be completely effective, there is some loss of light due to larger f-numbers, and the lens system does need to be larger than the part under inspection. However, with the great majority of precision metrology applications being the inspection of small part areas or features, telecentric optics has become a commonly used tool today.

To summarize the advantages and disadvantages of telecentric optics, one can say that, as positive points, this technology presents constant magnification, reduction of the fall-off of relative illumination from the optical axis to the borders of the image, no image distortion, no perspective errors, and no geometrical position uncertainty due to lighting. But, as main drawbacks, this kind of optics present a large f-number, which will lead to less light in the formed image, and the fact that the optic (usually) needs to be larger than the DUT (Opto Engineering, n.d.).

2.2.3.3.2 Plenoptic Imaging

The world around us is rich in information, and our eyes are capable of capturing a great amount of that information. For a long time, humans tried, through different ways, to capture and represent what our eyes see, being with paintings or sculptures. The first appearance of the photographic camera, commonly attributed to Joseph Nicéphore Niépce around 1825 (Masoner, 2019), was a big step towards the complete representation of a real scene. With such a device, with a single press of a button (not so simple in the first generations), one can perfectly capture the moment. The photographic camera turned out to be such a useful and popular device that nowadays we all carry a descendent of that device in our pockets.

The act of taking a picture is, nowadays, very simple: a number of settings are locked in by the photographer (or automatically chosen by the equipment), like the aperture, the exposure time and focus plane, and with the press of a button, the image is taken. If the result is not the desired one, then a new photo can be taken. That is where the plenoptic camera comes in.

The first person to propose the concept of a light field camera, commonly known as plenoptic camera, was the Franco-Luxembourgish physicist Gabriel Lippmann, around 1908 under the title "*La photographie integrale*" (Lippmann, 1908). While the normal 2-D camera only record the intensity of light on the image sensor, plenoptic cameras have the ability to capture the complete 4D light field.

Plenoptic Function and Lightfield

The plenoptic function, first described by Bergen and Anderson in 1991 (Edward H. Adelson, 1991), is set to describe the intensity of each light ray in the world as a function of wavelength, time, visual angle and viewing position. The word plenoptic its roots in the terms plen- (plenus) and opti- (optos), which means full and view/eye, respectively. Every single light ray in the space can be parameterized by a position with three dimensions, and a visual angle in two dimensions. If we add the time and wavelength, we get a total of seven dimensions (7D). The images and videos we see daily are just two-dimensional (2D) or three-dimensional (3D) special cases of the 7D plenoptic function. If we could capture this 7D function with a sufficiently high sample rate, we would be able, theoretically, to reconstruct views in any position and any time.

One possible representation of the plenoptic function is $l(x, y, z, \theta, \phi, \lambda, \tau)$. In this notation, the position of the light ray is described in Cartesian coordinates (x, y, z), the direction is parameterized by the spherical coordinates (θ, ϕ), and λ and τ denote the wavelength and time, respectively (S.C., 2014).

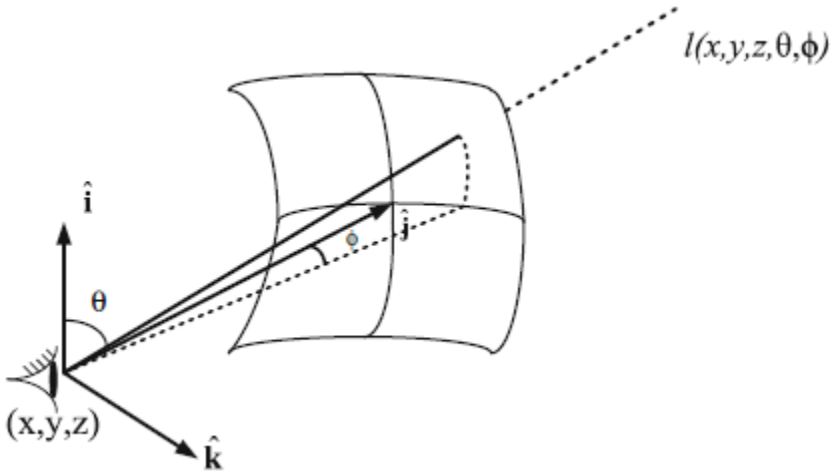

Figure 27 - Representation of a plenoptic function, as seen by a human eye.

If we assume a static scene, and that the wavelength is sampled using RGB channels, we can remove both λ and τ dependencies. Furthermore, in the free space, light rays have constant radiance along their path. In this case, we can reduce the 7D plenoptic function to 4D function, called light field.

There are several ways to capture a light field. It can be done with a "normal" 2D camera, if it is moved around the static object we are trying to capture, like it was done by M. Levoy and J. Shade in 1999 (Marc Levoy, 2000), when they scanned Michelangelo's statue. Other way to do it is using an array of cameras, all capturing a scene simultaneously. The third way consists in using a micro array of lens between the camera sensor and the main lens. This is the concept behind hand-held light field cameras.

Raytrix Camera

The first hand-held light field camera was developed by Ren Ng, during his PhD research in 2005 (Ng, 2006). He combined the idea of software refocus with the concept of light field camera. With his idea, he founded, in the following years, *Refocus Imaging*, which would later turn into *Lytro*, the first producer of consumer light field cameras, in 2012. The first commercially available plenoptic camera was manufactured by *Raytrix*, in 2010. The *Raytrix R11* used a 35 mm CCD sensor, with 40 000 microlenses and an effective resolution of 3 Megapixels. The product was targeted at industry and research sectors, and pricing was reportedly in the range of 20,000 to 30,000 Euros (LightField Forum, n.d.).

Micro Lens Array

Hand-held plenoptic cameras work using a Micro Lens Array, that allows it to capture the 4D light field with a 2D image. The ray of light leaves the source, goes through the main lens, and then into the MLA, arriving at the sensor the multiple result images. Another possible configuration is to use the MLA in front of the mains lens.

The MLA, derived from the Hartman-Shackman wavefront sensor (RP Photonics, n.d.), can have different arrangements. Two of the most common are the orthogonal configuration, and the hexagonal configuration. The hexagonal is usually preferred over other formations, because it provides a better coverage over the image plane, leaving smaller gaps between lenses.

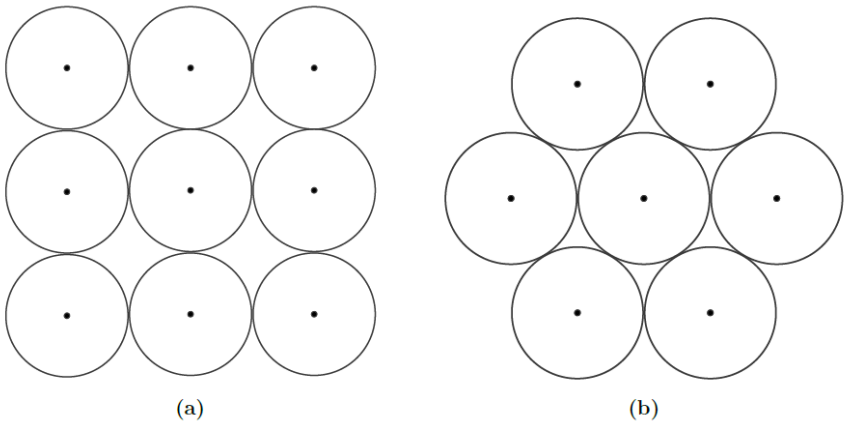

Figure 28 - Two conventional arrangements for MLA: orthogonal (a) and hexagonal (b).

In the first generation of plenoptic cameras, the focal length for MLA is equal to the distance from the MLA to the image sensor. Each of these micro-lenses will contribute with one-pixel value in the final image, meaning that the final image resolution is dictated by the number of micro-lenses, causing a rendered image with low resolution. This implementation has the advantage of requiring low computational power. This way is conceivable to manufacture compact cameras with built in rendering capabilities (Cunha, 2015).

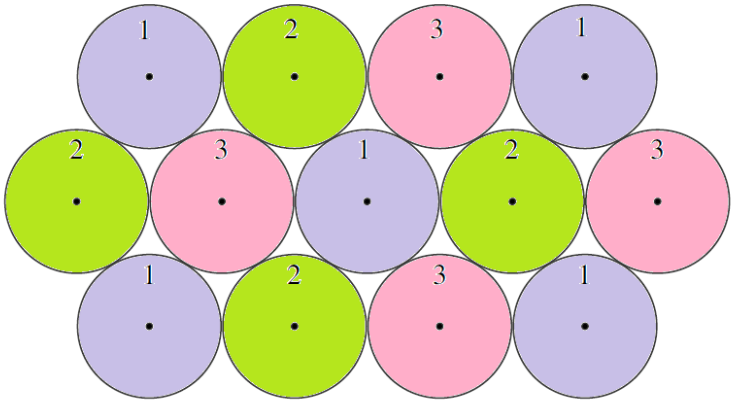

Figure 29 - Arrangement of an MLA with three different kind of lenses.

To solve the low-resolution issue, and to better use the available resources, the Plenoptic 2.0 concept was presented by Georgiev (Todor Georgiev, 2009).The main difference from the standard plenoptic camera is that the MLA is placed after the point where the image is formed. Another improvement proposed by Georgiev was to introduce, in the MLA, three types of lenses, each with a different focal length. This

implementation allows for a better resolution, and a larger depth of field. The fact that each micro-lens type has a different focal length, means that different ranges will be in focus *i.e.* far away planes will be in focus in one type of lenses, while closer planes will be in focus in another type of lenses. In Figure 30 shows that, while some micro-lenses are in focus, others are not.

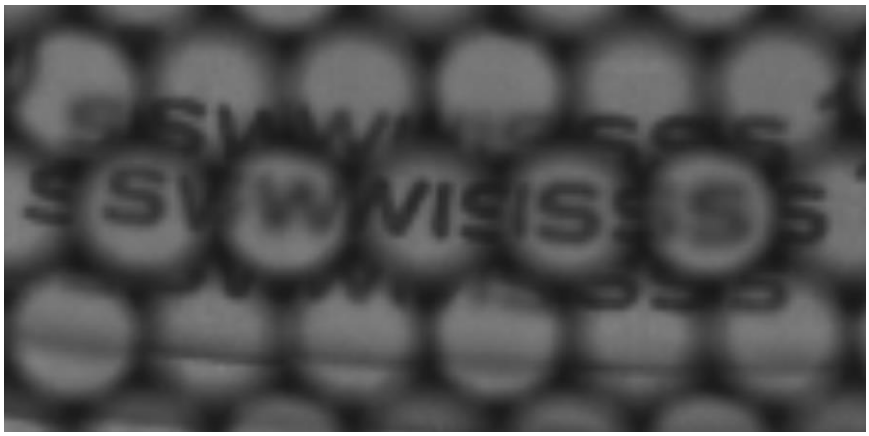

Figure 30 - Example of an image with a MLA with different focal lengths: in some lenses, the text is in focus, while in others it is out of focus.

One advantage that plenoptic cameras have, when comparing to a stereo camera system is the reduction of occlusion. When a stereo camera system is pointed at an object with big differences in height, some parts of the objects will only be visible to one of the cameras, and occlusion will occur. But, if a plenoptic camera is used instead, the same object will, most likely, not be a problem, since we no longer have only a pair of objectives, but we have a large number of lenses, closely spaced to each other. This way, if some feature of the DUT is occluded to some lenses, it will be visible to others.

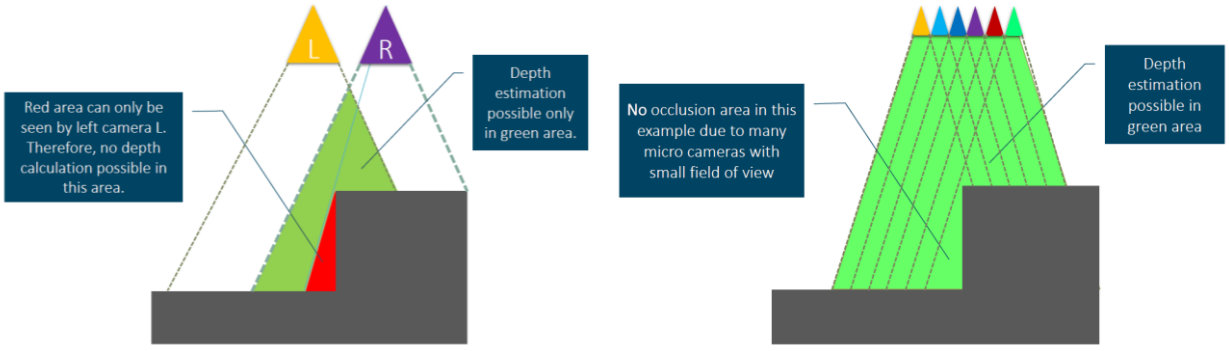

Figure 31 - Situation where occlusion can occur: case of a Stereo Camera System (left) and a Plenoptic Camera (right) (Perwass, 2014).

Image Formation in a Plenoptic Camera

Plenoptic imaging uses, as a starting point, the thin lens imaging model. The transition between a thin lens and an optical system it is very straight forward. It can be used the exact same model as the thin lens in an optical system, and the transition required no approximation, physical or mathematical, besides the already present paraxial aproximation.

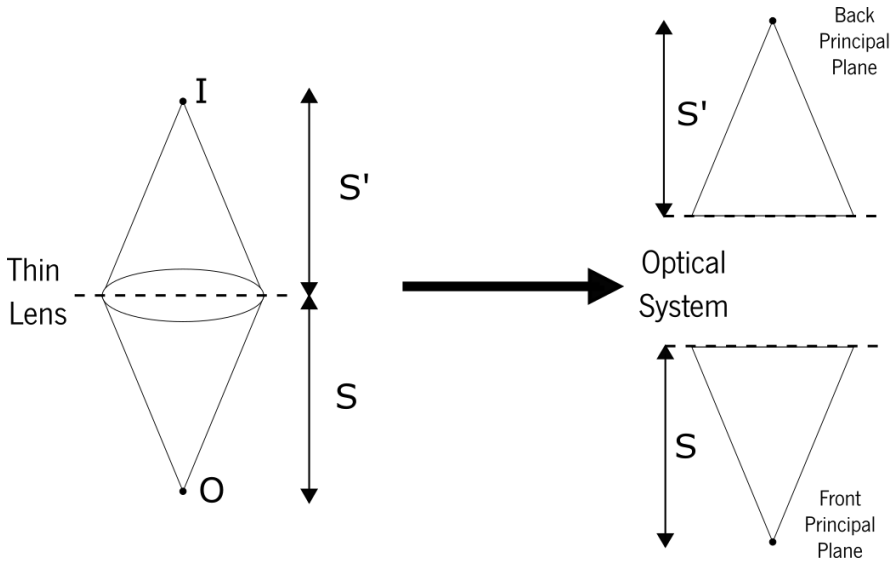

Figure 32 - Image formation: from the Thin Lens model to an Optical System.

$$\frac{1}{s} + \frac{1}{s'} = \frac{1}{f} \tag{6}$$

The equation and scheme above describe the image formation in a "normal 2D" camera. Like it was said before, the Plenoptic 2.0 introduced the MLA between the main lens and the camera sensor. So, instead of recording the only image originated from the main lens, each of the micro-lenses will intercept the rays, and will provide different images in the sensor plane.

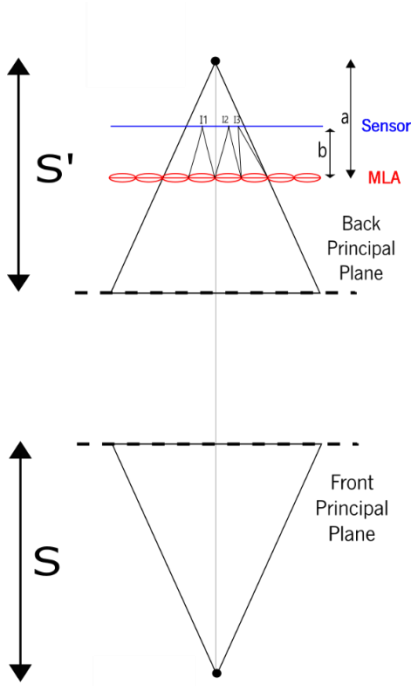

Figure 33 - Multiple image formation, due to the presence of the MLA in front of the imaging sensor.

The plenoptic camera, alongside doing what a "normal 2D camera" does, it is also capable of providing depth information. There are two steps required for this technology to provide a depth estimation of the object: Estimation of Virtual Depth (VD) followed by a mapping of VD's into real world distances.

Virtual Depth is the ratio of the distance between the MLA plane and the back principal plane (*a*), and the distance between the MLA and the sensor (*b).* Due to the presence of the MLA, each point of the object is represented by (at least) three images in the sensor. Then, from the difference of the same point in the three images, by standard triangulation one can estimate where the object would be. This process of VD estimation is, therefore, dependent of the system being able to identify the same point in the three images, which means that the Plenoptic technique requires good contrast. For technical reasons, VD as a minimum value of 2.

The second step is then to map the VD calculated in the previous step into distance in the object space. This means that, for each optical system used in a Plenoptic camera, there needs to be a calibration file.

2.3 Capability Measurements

To ensure the capability of measurement of a given measuring system there are specific tools and procedures that can be used. Those procedures are documented in the Booklet 10 from BCM (Robert Bosch GmbH, 2019) and comply with the requirements according to AIAG (Automotive Industry Action Group) Measurement System Analysis, as explained in the literature "Process Capability Analysis" (Polhemus, 2018).

The *Capability Index*, C_g, and the *Critical Capability Index,* C_{gk}, will be the indicators that will classify a measurement system as capable or not capable, according to Procedure 1 of Booklet 10. This Procedure requires that a characteristic has a lower and upper limiting value (LSL and USL), so that the tolerance (T=USL-LSL) is defined. The standard requires that each characteristic is measured 50 times on a reference sample but in special and documented cases 25 measurements could also be accepted. Then, the C_g value can be calculated using *Eq. (7)*, and C_{gk} using *Eq. (8)*, where s is the standard deviation of the measured values, $\bar{x}$ is the mean value of those same measurements, and x_m denotates the known value of the reference sample. This reference value is measured using an alternative and precise instrument, like a Coordinate Measuring Machine (CMM). Following Bosch standards, for a measurement system to be considered capable of performing a measure, both C_g and C_{gk} must be equal or greater than 1.33 (Robert Bosch GmbH, 2019).

$$C_g = \frac{0.2 \times T}{6 \times s}, C_g \geq 1.33 \quad (7)$$

$$C_{gk} = \frac{0.1 \times T - |\bar{x} - x_m|}{3 \times s}, C_{gk} \geq 1.33 \quad (8)$$

Chapter 3

Results and Discussions

During the development of this master dissertation and having in mind the technologies described in *Chapter 2*, I had the opportunity to try and explore the main benefits and drawbacks of some of those techniques. Many of the equipment necessary for testing was already available at Bosch and at the University. These technologies were:

- Chromatic Confocal
- Telecentric Lenses
- Plenoptic Imaging
- Stereoscopic Imaging

Over the next subchapters, it will be described the work developed in each technology.

3.1 Chromatic Confocal

The optical head used in these practical experiments was the CL5-MG35, by Stil. It has a measuring range of 12000 µm, a working distance of 26,6 mm and a spot size of 24,3 µm. The controller was the CCS Prima 2 (Figure 34). The connection between the controller and the optical pen is done by optical fiber, and the data transfer from the controller to the computer is done using a RS232 – RS422 connection (Stil, SAS).

Figure 34 - Controller CCS Prima 2.

For this setup, different light sources could be used, besides the one built into the pen. In all tests below, the internal white light source was used. This technology is also capable of measuring the thickness of a layer, but, since the main objective is to acquire a profile of the connector, the measuring mode was set to Chromatic Confocal Distance.

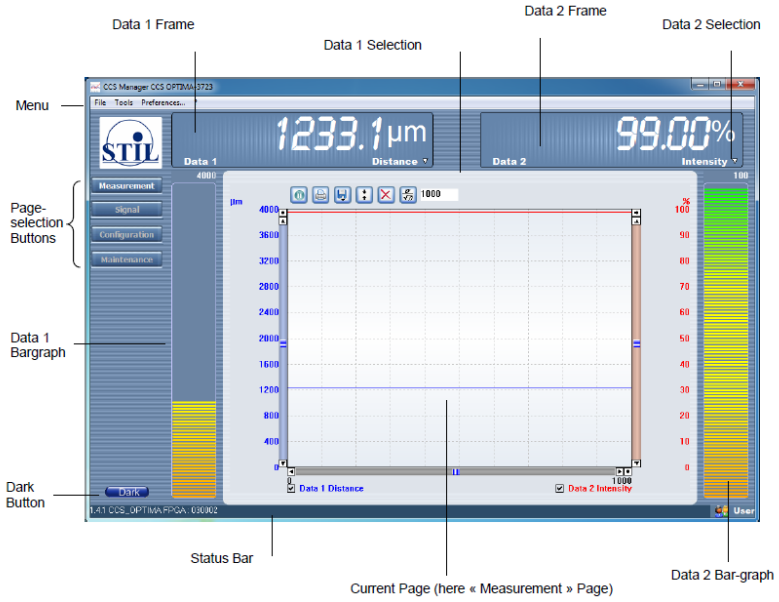

Figure 35 - Stil software interface. The data points are shown in the measurement area. If more than one optical pen is connected to the controller, there is the possibility to observe information from both stylus at the same time.

Figure 35 shows the basic interface of the software. It is simple and intuitive to use, having options to export data as .csv files, or the graphic as an image, evaluate the values in real time, change the number of samples acquired, and some additional functionalities.

3.1.1 First Practical Experiment

The first work done with the Chromatic Confocal Pen was to understand how the technology works, and, with that purpose, I tried to get a representation of the connector under study in the software.

When the probe is blind, meaning that no light is entering through the lens, there is still a detected signal, called the dark level, which may be generated by electronic noise of the components, or photonic noise of the detector. In order to remove this effect, an initial calibration should be performed before measuring any data. This can be done on the CSS unit, pressing the "dark" button, or in the software. These steps are well documented in "CCS Optima User Manual". After this is done, one is ready to start the testing.

The first steps were done to understand how the acquisition frequency of the probe, f_{probe} affects the measurements. The most affected factor was the scanning speed. With a high f_{probe} value, more values will be acquired per amount of time consequently reducing cycle time. So, with a higher f_{probe} value, we can move the subject faster, being able to sweep a larger area.

Another factor that was dependent of the f_{probe} was the working range, that is the difference between the "highest and lowest" points that the system can measure. The experiment told us that, the higher the f_{probe}, the lower the working range.

That means that a compromise should be made regarding the f_{probe}: if we choose a high frequency, we can measure more points in the same amount of time, "covering more ground", but we lose range in the optical axis; on the other hand, if a lower frequency is chosen, the working range will be greater but it will take longer to measure the same amount of points. During the remainder of this experiment, the lowest f_{probe}

was chosen, 100 Hz, since time was not a major factor and the main point was to get familiarized with the technology.

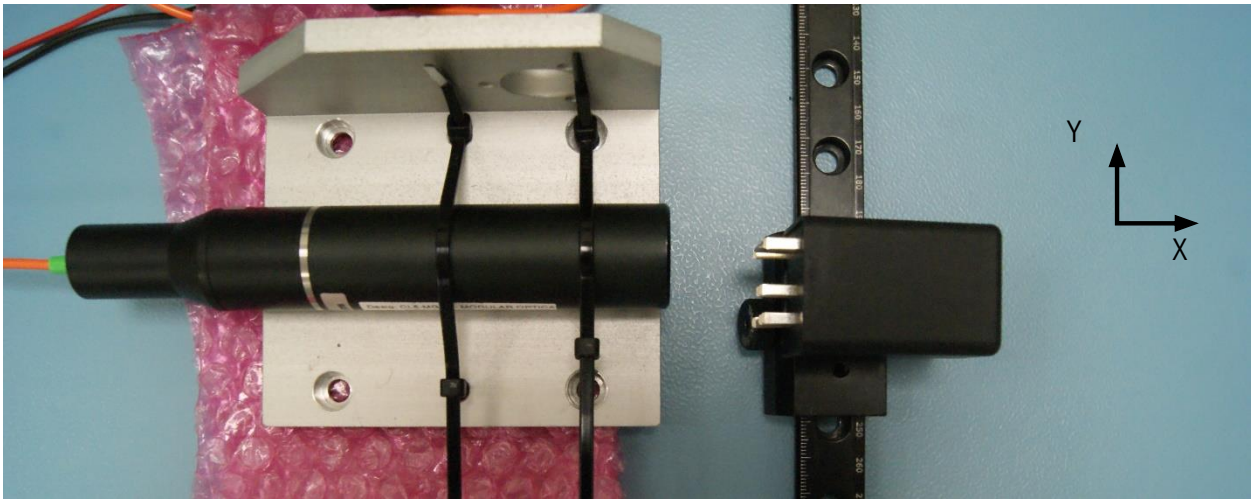

Figure 36- First setup used for testing. The Chromatic Confocal system

The setup was at it shows in Figure 36. From now on, it will be assumed the optical axis as the *X*, and the axis where the connector is moved as *Y*. A rail was mounted in order to move the connector more smoothly along the *Y*-axis, avoiding the vibrations caused by human handling.

Figure 37 represents one of the most successful measurements, where the profile of the connector was most accurately transcribed into the software. The width of the pins is not the same because the movement along the Y-axis was manual, and therefore uncertain.

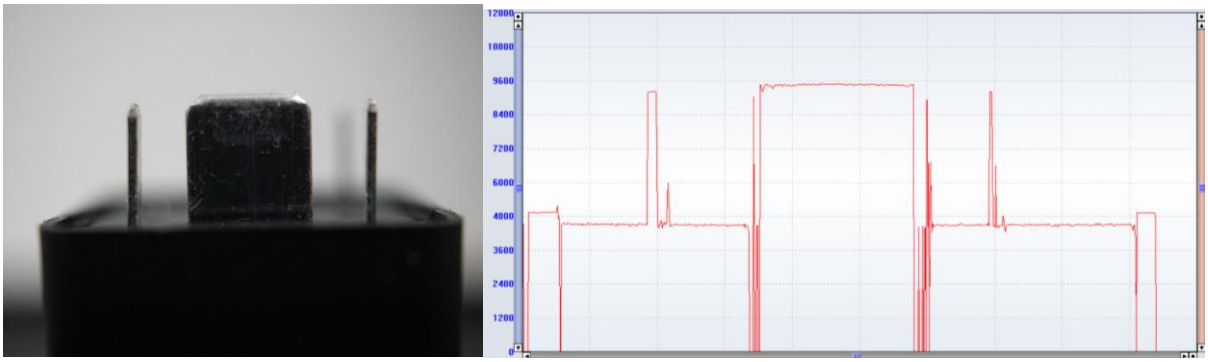

Figure 37 – Side profile of the connector and corresponding data acquired from the chromatic confocal imaging system.

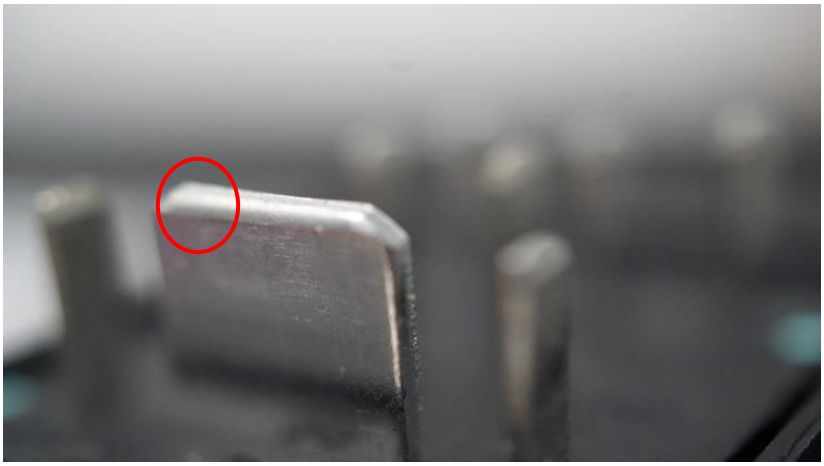

Figure 38 – Corner of the pin. This slope causes most of the reflected light to not enter the pin-hole of the optical pen.

The most difficult points to measure occurred in the transitions between the lowest point, the "base" of the connector, and the highest point, the pin itself. At each of those steps, it is visible in the data that some of the values are zero. That represents one of the limitations, not only of this technique, but also of most of the techniques based on reflection. When the ray hits the slope, most of the light will not be reflected through the objective. In that case, not enough light will be received by the detector, causing the detection algorithm to generate a non-measured point. In practice, most surfaces have a certain level of roughness, that will lead to a diffuse reflection, causing some light to be reflected into the detector, which may or may not be enough to cause a peak in the data chart.

In connectors as the ones presented in Figure 39, it was not possible to measure both the outer protective case of the connector and its lowest point. That indicates that the working range is too small for this purpose, even though the f_{probe} was the lowest possible.

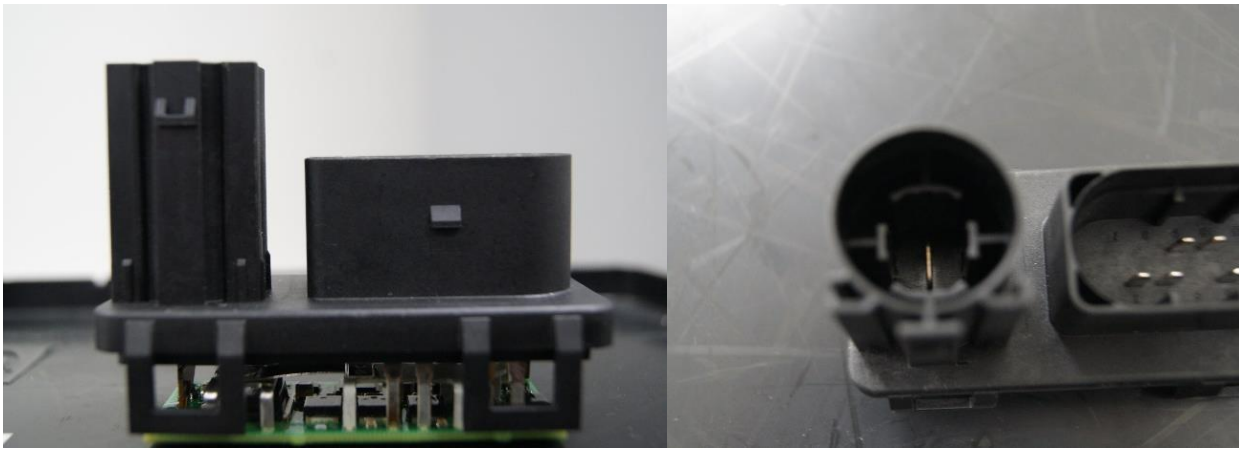

Figure 39 - Examples of connectors in which it is not possible to obtain data from both the protective case and the bottom of the connector at the same time due to the limited working range.

3.1.2 Second Practical Experiment

Having in mind the knowledge and information acquired in the previous experiment, a more controlled setup was mounted, in order to test the full capabilities of this technology, in the context of connector analysis, more specifically of the ECU connectors. This setup has two motorized linear axes, to achieve a more precise and exact movement of the CCS pen.

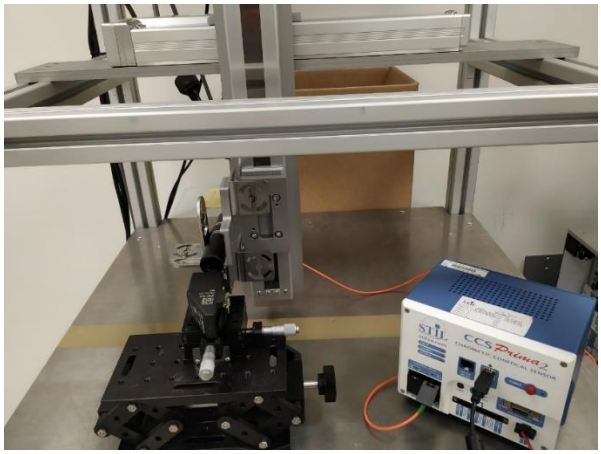

Figure 40 - Chromatic Confocal Setup. CCS Prima 2 controller, the optical pen, and a system of 2 motorized linear axis.

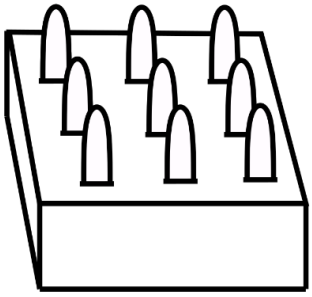

Figure 41 - Representation of an Electrical Connector Unit.

In this experiment, the same exact points of the pin and the base were measured 50 times, to do the capability measurements, performing a scan transversal to the pin, as shown in the representative Figure 42 (a).The pin profile shown in Figure 43 corresponds to a 2.5mm section of the connector. For these measurements, the optical pen was set with a frequency of 100 Hz, to utilize the full range of the pen, and the axis moved at 0.5 mm/s.

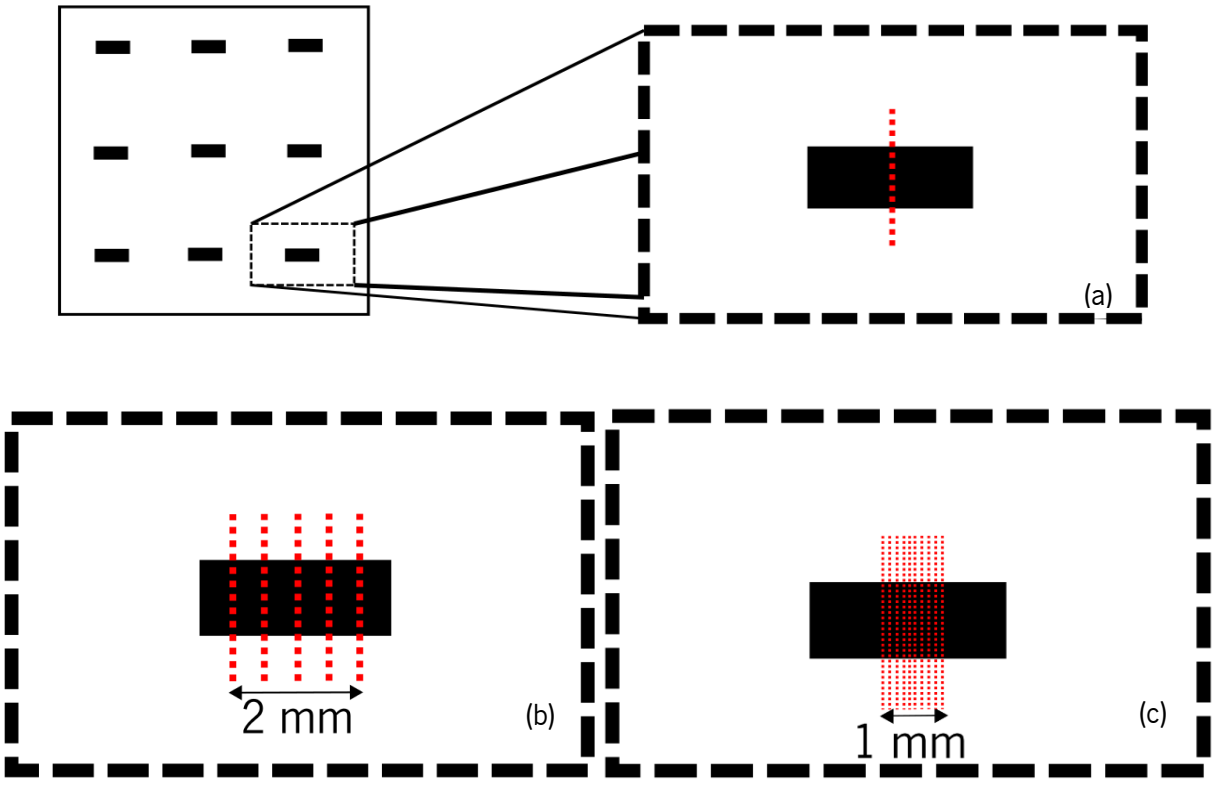

Figure 42 - Representation of the scans performed on the ECU.

In order to evaluate the height of the pin, some data processing was needed to split the values of the pin itself, and the base of the connector. The pin is characterized by values above 10200 µm and the base is drafted with all the values below 1500 µm, as explained in Figure 43 (these values represent the distance to the optical pen itself). Unwanted reflections occurred constantly, in the transitions from the base of the connector to the top of the pin, and are represented by values that either are zero, or some random peak, like the ones presented in Figure 43. These values were excluded and were not used to calculate either the base of the connector or the top of the pin.

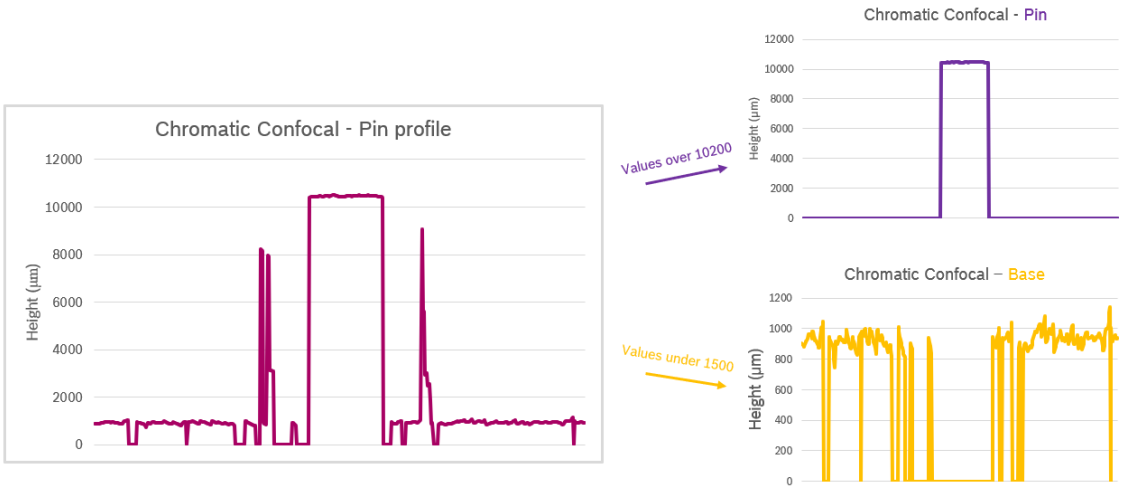

Figure 43 - Explanation on how the data is treated to identify the data points from the pin and from the base.

Having measured 50 time the same points, both from the pin and base, an average was calculated to estimate the value of the height of the pin, knowing that this value is the subtraction of the mean value of the tip of the pin and the mean value of the base. The results are presented in Table 3. Good value of C_g (>1.33) was achieved, with a tolerance of ±150 µm, even though the base of the connector presented more deviation, due to its roughness.

Mean Value Pin	10461.03 µm	Standard Deviation Pin	0.94 µm		
Mean Value Base	927.59 µm	Standard Deviation Base	2.56 µm		
Mean value Height	9533.43 µm	Standard Deviation Height	2.67 µm	Tolerance	300 µm
				Cg	3.74

Table 3 - Values of the measurements of the pin in the same point.

Knowing that the system has capability when analyzing the same point, the next step was to perform the same measurements in different points of the pin, slightly separated from each other. First, 5 different points were measured 50 times, covering a 2 millimeters range in the pin top, as shown in the representative Figure 44.

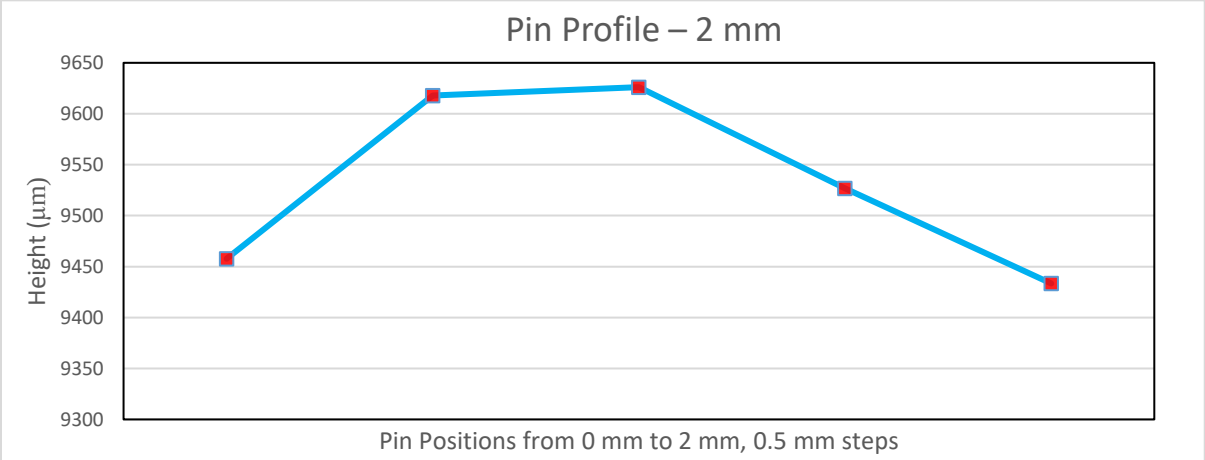

Figure 44 - Profile of the pin achieved by measuring the same points (red points) 50 times across a 2 mm range.

Again, for each of the individual section measured, the measurements of height achieved good values of C_g. All these points, representative of the pin height, measured inside a 2 millimeters range on the top of the pin, had a maximum variation between themselves of around 150 micrometers. This is a large value, since it is half of our tolerance of 300 micrometers. So, to confirm these variations, the top of the pin was measured again. This time only a 1 millimeter range was measured, with 0.1 millimeters steps, so we would have more points, close to each other, to compare.

The same good values of capability were achieved on these singular points. But now we can observe that, for two adjacent points a variation of 90 micrometers is present.

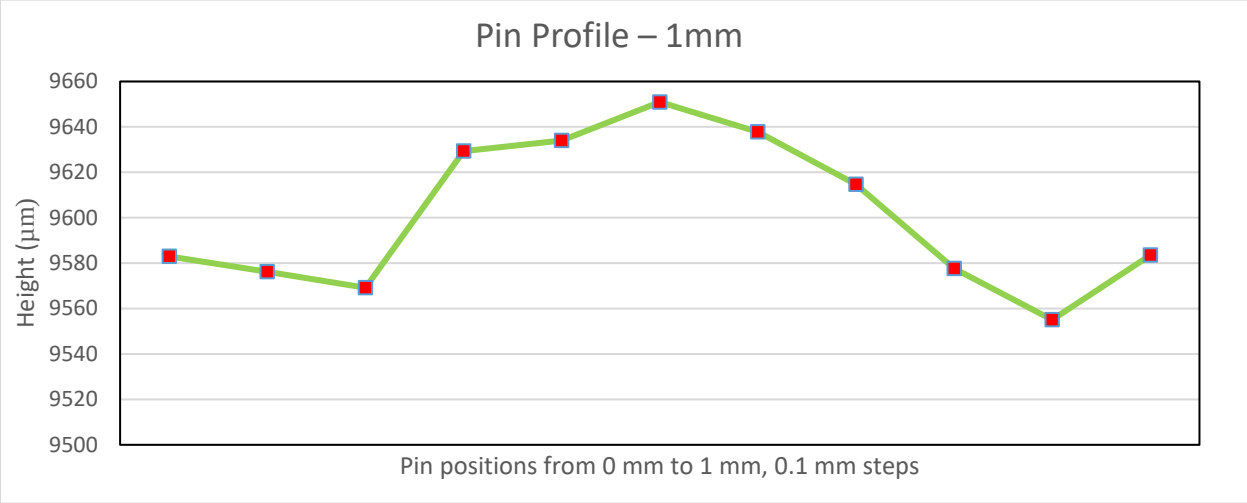

Figure 45 - Profile of the pin achieved by measuring the same points (red points) 50 times across a 1 mm range.

From these experiments with the Chromatic Confocal technology, we can infer some conclusions about its application to the connector analysis problematic: even though that for measuring the exact same point, good values of capability are achieved, if a slightly separated point (0.1 millimeters spacing used in the experiment) is measured instead, that can mean a 90 micrometers variation. This kind of variations presented by the Chromatic Confocal technology were not in line with the measures performed by the OCT equipment.

So, if we cannot guarantee that the exact same point is being measured, Chromatic Confocal technology will present low capability.

3.2 Telecentric Optics

Telecentric lenses were an important point of study during the internship at Bosch, due to its applicability for connector inspection. Since this kind of lenses do not cause perspective error or image distortions there will be no geometrical position uncertainty, which is ideal for maximum accuracy when measuring the positions of pins. In fact, the first prototype of the connector inspection machine consisted in a camera with a telecentric lens and different illuminations.

Figure 46 - Example of the small working range presented by Telecentric Optics. Though the pins are in focus, the back of the connector is not.

A drawback of telecentric lenses is the small working range, as one can observe in Figure 46.

3.2.1 Connector Inspection Machine Prototype

This first machine prototype has the main goal of optical connector inspection, including all the major factors on evaluating the DUT, being the pins position, its height, the integrity of the whole connector, or if its color and housing shape matches the one intended. This machine has, as main focus, the analysis of SC since those were the connectors present in the target DUT, but all the process was done having ECU in mind. Thus, the height of the pins is not a major task in this development, since that characteristic is not usually evaluated in SC.

Our initial prototype machine has, on the hardware level, 3 essential components: the camera, the lens and an illuminator. Each of these components is chosen to guarantee the best results, according to the characteristics of the DUT.

Figure 47 – First Connector Inspection Machine Prototype for SCU Analysis: Camera, Telecentric Lens and Flat Dome.

3.2.1.1 Camera

The camera that was chosen for this project is a Manta G-1236 1.1" from Allied Vision. It is a 12 Megapixel color camera, with a pixel size of 3.45 x 3.45 (µm) and a sensing area of 14.2 x 10.4 (mm). This is a PoE (Power over Ethernet) camera which means it can be connected to a computer via Ethernet port, requiring no external power source.

Besides all the technical factors, the choice of this camera is also the result of the experience of Bosch with Allied Vision cameras, that are widely used in BrgP facilities.

3.2.1.2 Lens

For the first prototype, two telecentric lenses were tested, a DTCM111-64H-AL and a DTCM111-48-AL, both from Vico Imaging (Vico Imaging, n.d.). The main difference between the two is the Field of View one has a 49 x 36 (mm) FOV, while the other has a 35 x 27 (mm) FOV. One of the contributing factors to the choice of lens is that the FOV must be bigger than the area under inspection. If we go for the bigger lens, we gain on the FOV but we lose on resolution, so there is always a commitment to be made.

3.2.1.3 Illumination

Like every other optical testing setup, illumination is a big part of the arrangement and can make or break every system. For this prototype we tested a few different illuminators: a dome, a flat dome, a dark field, an adjustable dark field and a structured light illuminator.

Both the Dome and the Flat Dome can easily provide a uniform illumination on the DUT, but they will have different use scenarios. Compared to the Flat Dome, the Dome can provide a higher contrast on the DUT, as presented in Figure 48, which will improve the image quality and make it easier for the software. On the other hand, the Flat Dome is more practical, and can be easier to integrate into a machine due to its compact size and rectangular shape. Some products will not fit into the Dome due to its dimensions. This can almost always be fixed, by custom-making a Dome, which can lead to an increase of the total cost of the machine. Another advantage of the Flat Dome is the possibility to use polarized light, which, with the correct setup, can help to reduce the specular reflections.

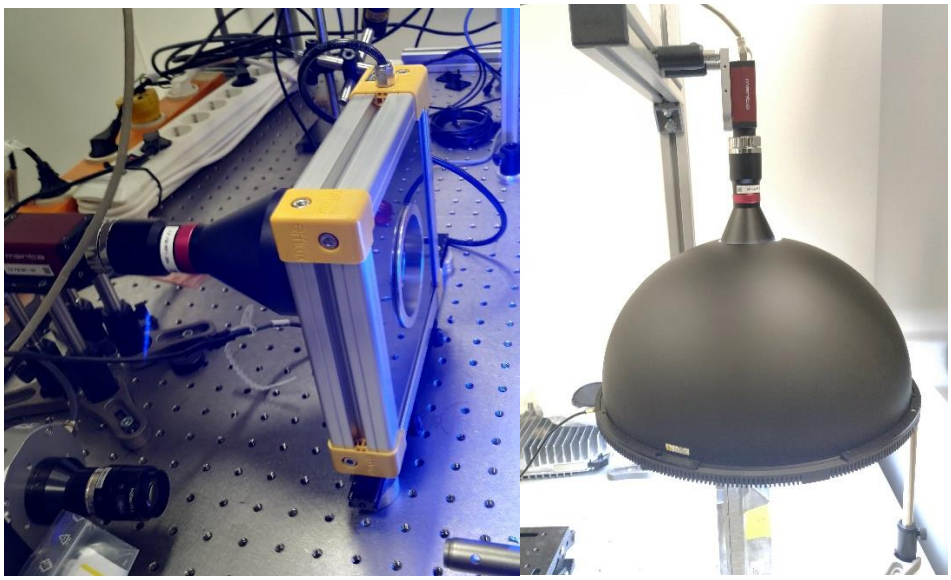

Figure 48 – Flat Dome (left), Dome (right)

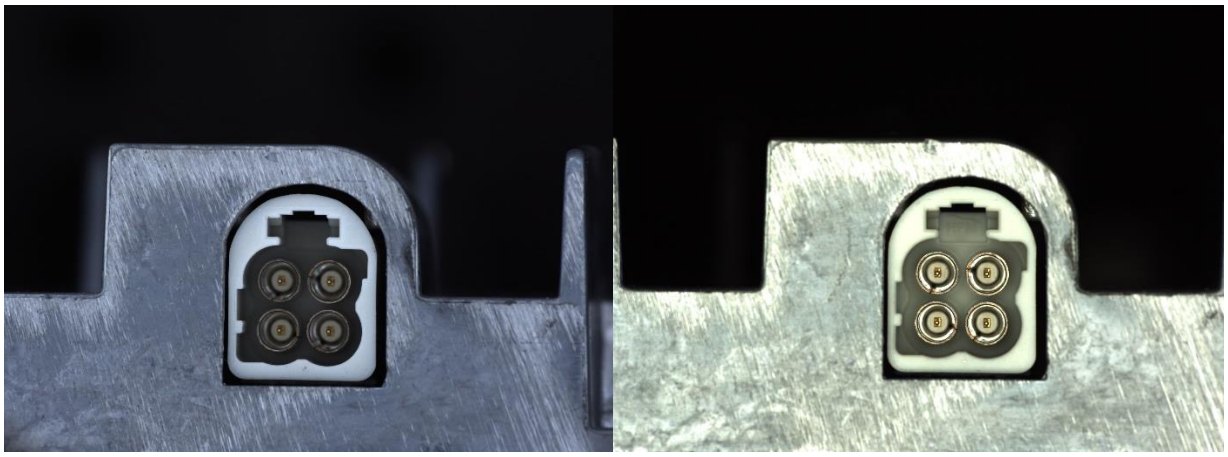

Figure 49 - Two HSD Connectors: on the left, image with Dome; on the right, image with Flat Dome

For the Dark Field to be useful, it must be placed extremely close to the DUT, in the order of a few millimeters, which in some cases can be a problem. For those situations, an adjustable Dark Field illuminator can be used. The main difference is that the emitted light angle can be adjustable, which allows us to place the illuminator farther away from the DUT. Of course that if the emitting angle is increased too much, the illuminator will stop producing the high contrast.

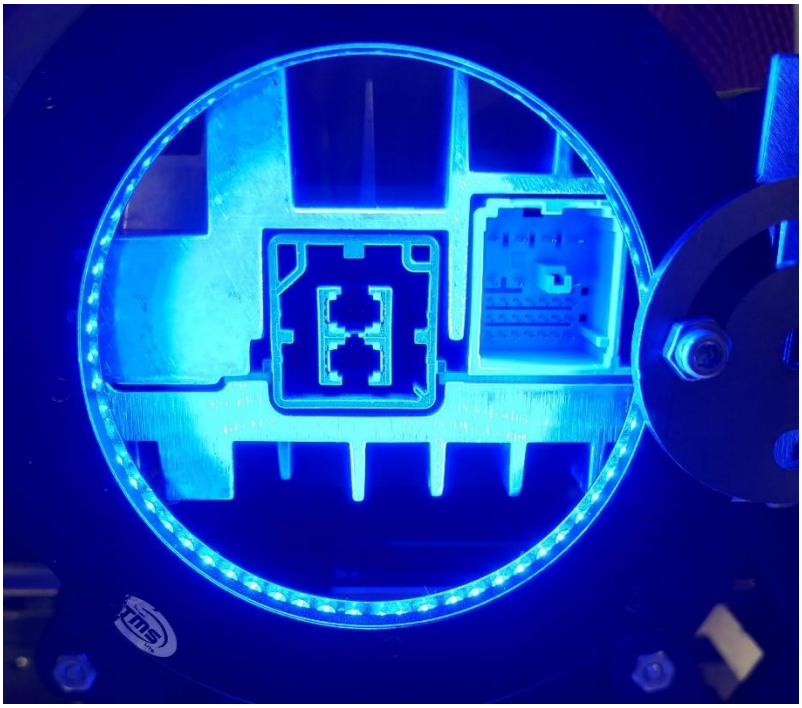

Figure 50 - Example of the Dark Field illuminator: a ring of blue LEDs, with a low emitting angle.

Most of the times, these illuminators cannot provide enough illumination for the analysis of the whole connector, so a second shot with another illuminator must be taken, which will increase the running time.

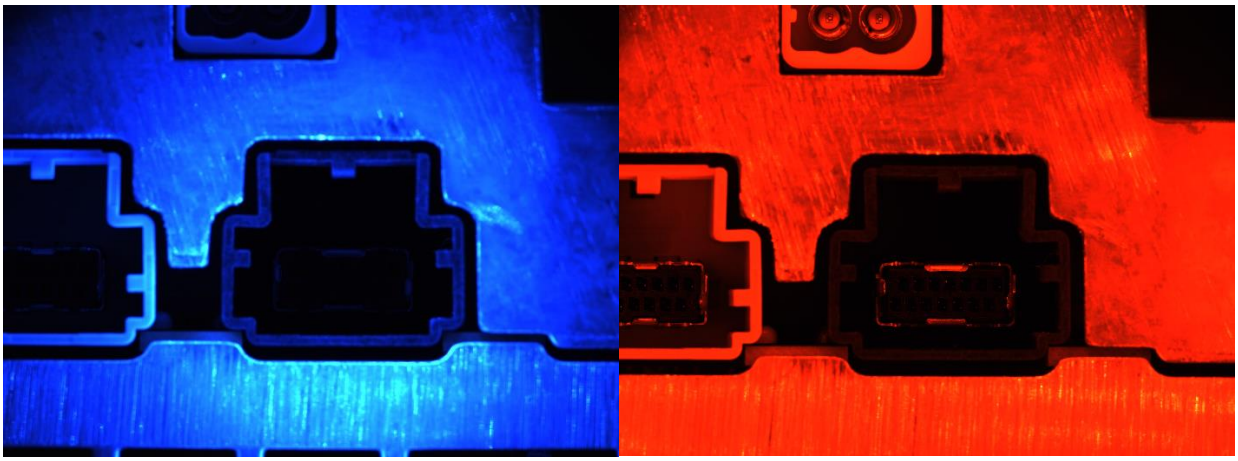

Figure 51 - Connector under Dark Field illumination (blue, on the left); Dark Field adjusted with around 20 degree angle (red, on the right).

A Structured Light was also tested. The one used for the prototype is an EFFI-Lase-PSV V2, with a Cross mask that can project a grid. It is mainly used for Electrical Connector Units, and not so much for Standard Connector Units, due to the size of the pins, and is especially useful on ECUs to define and find a

reference point other than a pin. Running this light for too long uninterruptedly causes fluctuations in brightness which have a negative impact in the consistency of the measurements. Therefore, the light was turned on and off for each measurement.

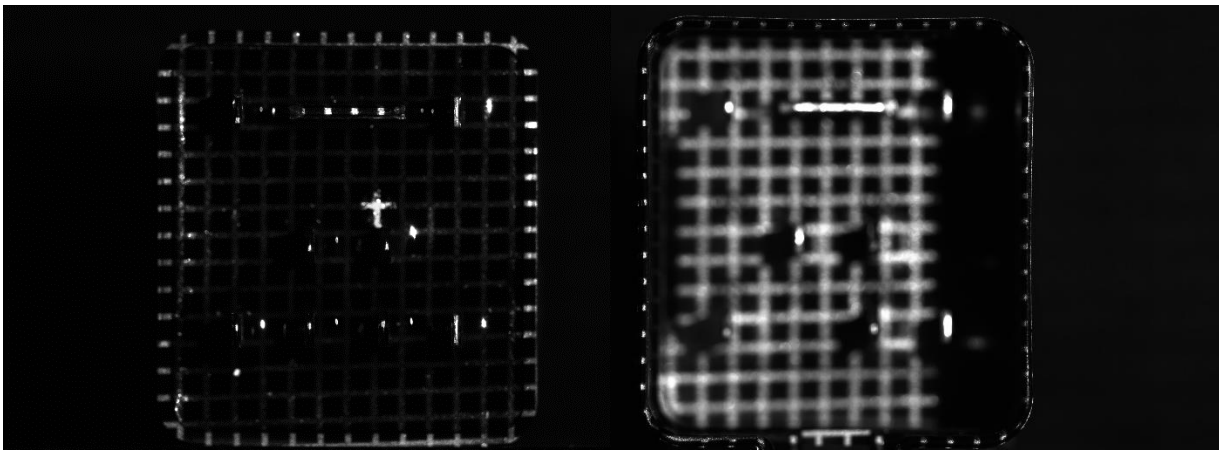

Figure 52 - Two different connectors under Structured Light Illumination, with a grid pattern projected.

3.2.1.4 Machine Vision Software

To analyze the images resulting from telecentric optics, and to perform measurements, it is needed a machine vision software. For this prototype, there were two options for the software, but the one tested the most by me was Sherlock by Teledyne DALSA. The interface of the software is presented in Figure 53. In this software, one can acquire images directly from the camera and create a *recipe* (called an *Investigation*, in the context of this software) to process them, in order to obtain the required values: number of pins, position of the pins in relation to a reference, color and shape of the connector, and to evaluate the integrity of it.

There are several different ways to implement the process for these measurements, using the array of tools available in the software. These tools can be separated in two groups: Pre-processing, which will apply different filters in the image, or, in some way, alternate the image; and Algorithms, which do not alternate the image but will output the actual results needed. Using a subset of these two different tools, the images can be processed, and the analysis can be done.

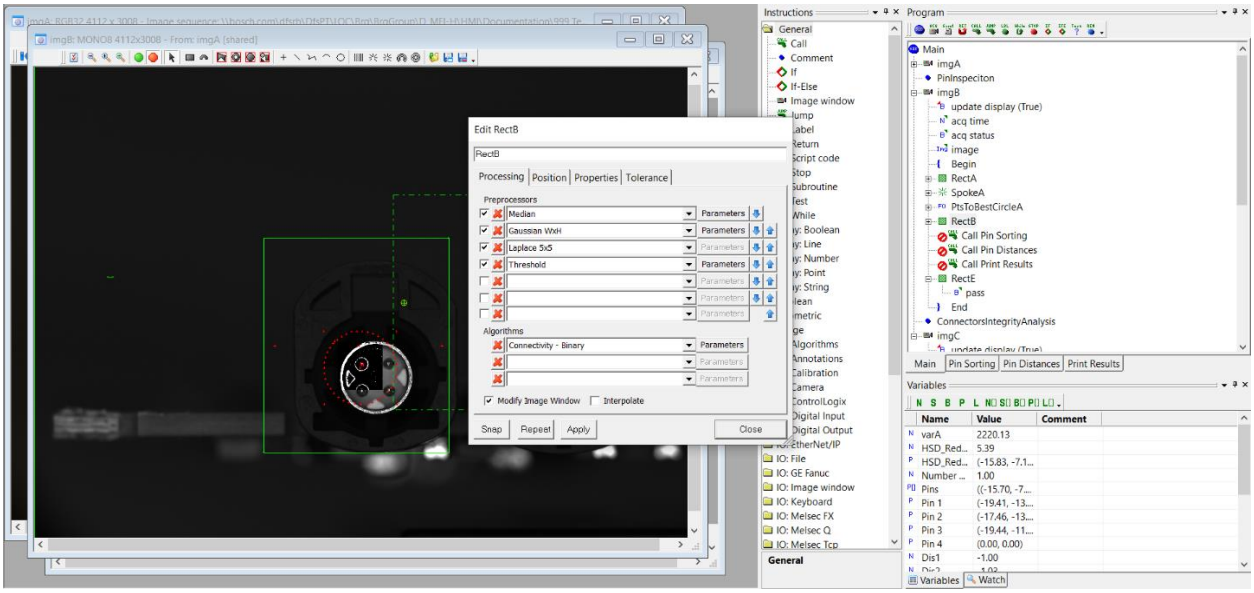

Figure 53 - Screenshot of the working interface of Sherlock.

When inspecting connectors, one important task is to acquire the position of the pins. But those positions need to be measured relative to a reference. For that to be possible, that reference point needs to be selected, and, for different connectors, different reference points will be chosen, according to the characteristics of the connector. There are three major ways to reference the position of the pins: use a stable feature, like a metal ring; use the walls to determine a reference; or use a pin as reference.

One kind of reference used is to check the concentricity of a pin, relative to a metal ring, or metal jack. Connectors that have that metal jack are presented in Figure 54.

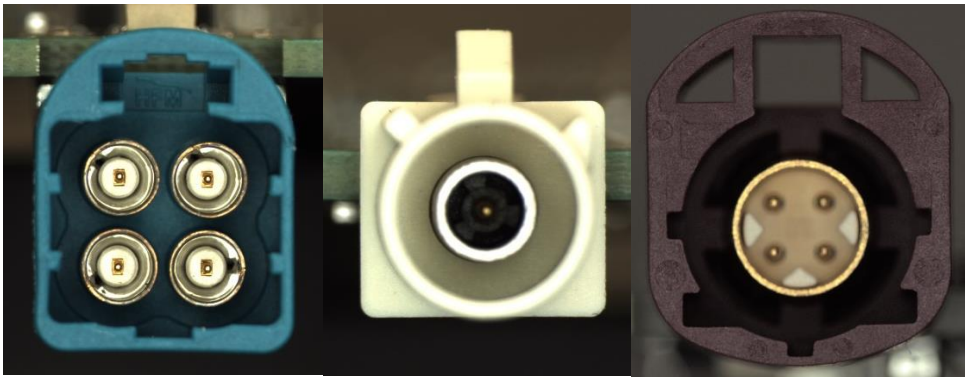

Figure 54 - Examples of connectors that use the center of the metal ring as reference: HFM (left), Fakra (center), HSD (right).

In this kind of connectors, we first determinate the center of the pin, then the center of the metal ring, and subtract those values. This is one of the most used methods to reference the positions of the pins in the XY plane, in SC, since it is reliable because of the sturdiness of the metal part, and due the large number of parts that have that ring.

The most conventional way to determine a reference for a connector, mostly for ECUs, is to use the walls to calculate that position, drawing two perpendicular lines and computing the intersection between both.

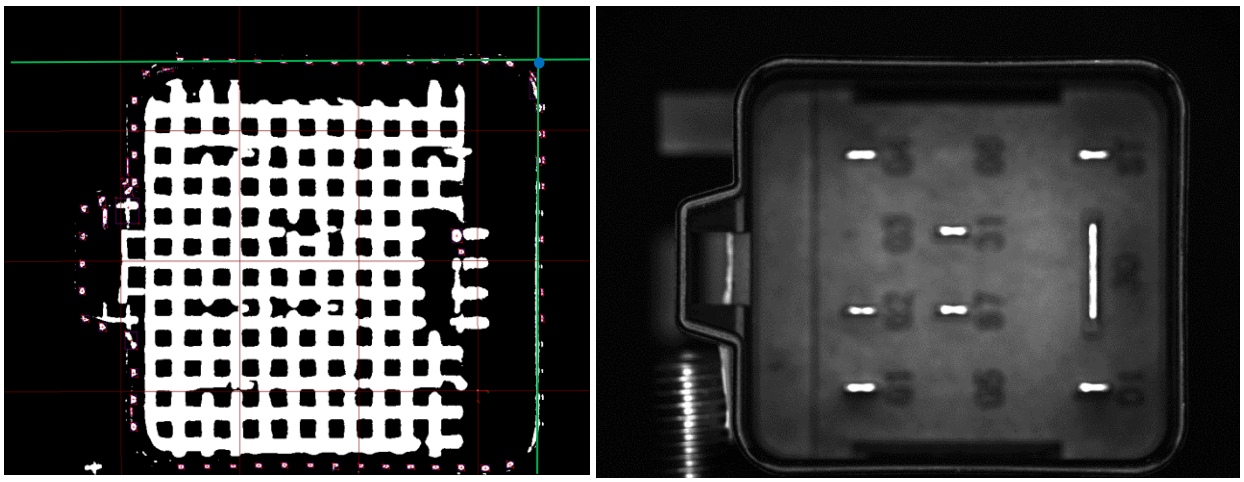

Figure 55 - Example of connector where the walls are used to determine the reference point.

But, when using the walls, not always the center of the connector is the reference point. Figure 55 shows an ECU where a structured light is used to better analyze and identify the walls of the connector. And, in this example, the reference point is not the center of the connector but a corner instead.

Figure 56 shows another kind of connector that, due to the good contrast achieved in the connector walls, those can be used to calculate a reference point.

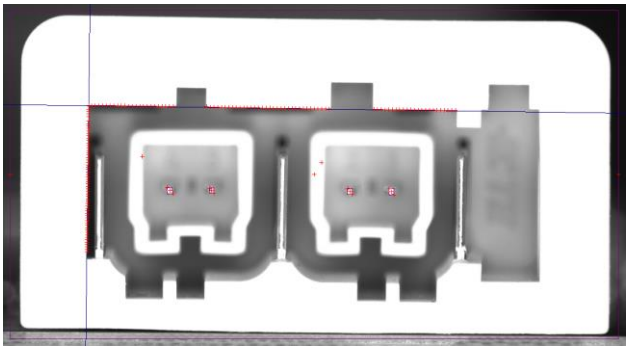

Figure 56 - MATEnet connector, where walls are used to calculate the reference point.

When there is no such sturdy feature as a metal ring, and the walls do not have good contrast, like the ones presented in Figure 57, one possible solution is to use a pin as reference (usually the first pin). This is not an ideal solution, because a feature that was supposed to be tested is being used as reference, but when nothing else is reliable, it is a safe approach.

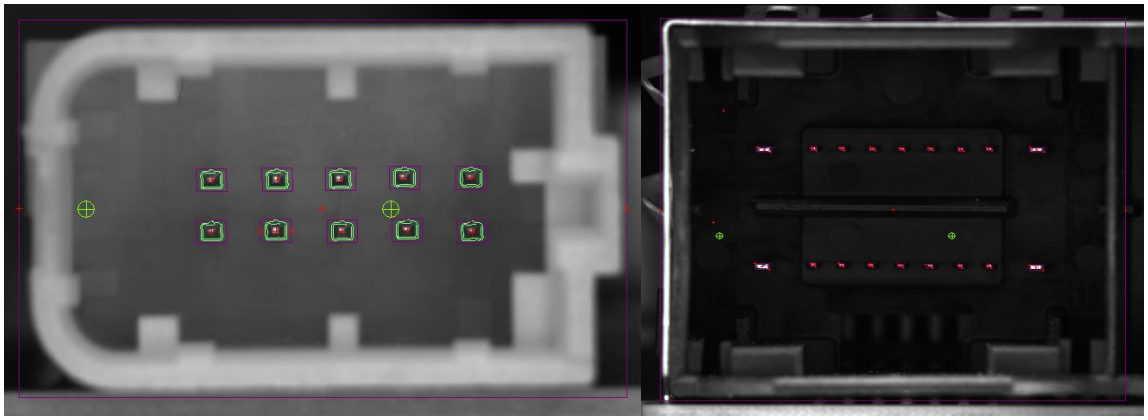

Figure 57 - Example of two connectors where a pin is used as reference. Images processed by Sherlock.

These three methodologies described above are the most used at the moment in BrgP to define a reference for measure the pins in the XY plane, according to the type of connector under study, and the characteristics of that same connector.

3.3 Plenoptic Imaging

The integral photography applied to connector inspection was an important point studied during this Master Dissertation, due to the lack of precedent studies in this application. Having the previous knowledge of University of Minho and Bosch Car Multimedia in a different context, plenoptic imaging was a possible viable solution to inspect the whole connector using only a single shot. For the following tests, a Raytrix R42 was used. It is a C-Mount camera with a maximum lateral resolution of 10 Megapixels.

The Raytrix camera, being a plenoptic camera, captures the Lightfield of a scene, and can output that information as a single file. But, in order to analyze the values captured, the Lightfield must be converted. The RXLive software, which comes with Raytrix cameras, can convert a .ray file (Lightfield information) into different images, that hold different information: RAW Image, an image containing the unprocessed micro lens images; Total focus, which is a “normal” picture of the scene, where every point (inside the available range) is on focus, and 3D Depth Image, a .tiff file where for each pixel can be found x (mm) in the red channel, y (mm) in green channel and z (mm) in blue channel, apart from other file types. The last one is the one used to perform the measurement of the DUT (it can output the distance from camera, or the elevation from a chosen reference). But, as mentioned before, in order to obtain the values in millimeters, a conversion from dimensionless Virtual Depth must be made, using a chosen algorithm.

3.3.1 Initial Testing

The first point of study was to choose a light source that could lead to the best results, having in mind that, for plenoptic imaging, good contrast is needed in order to perform good measurements. These first tests also had the objective to get familiarized with the data acquisition process using the Plenoptic Camera. These initial tests were performed using the standard pre-calibrated 50mm Ricoh objective, and different connectors were analyzed, both SC and ECU.

To evaluate the results, three different graphics were drawn for each connector, using a PDF (Probability Density Function): one for VD, one to express the Elevation from Reference and another for the Distance from Camera.

At first, we started by experimenting with an He-Ne laser, since it is well-known coherent light source. But it does not have the capability of causing contrast in the DUT. So, a beam expander was introduced in the system. This equipment not only did the obvious task of enlarging the spot size of the laser, but also caused some grain to appear. The grain formed did not provide enough light to the whole connector, due to the small size of the grain. So, the observed results were not good enough, and the technology was not able to acquire the necessary data. One possible solution was to change the size of the grain. This arrangement proved to be unpractical and somewhat expensive for the purposes.

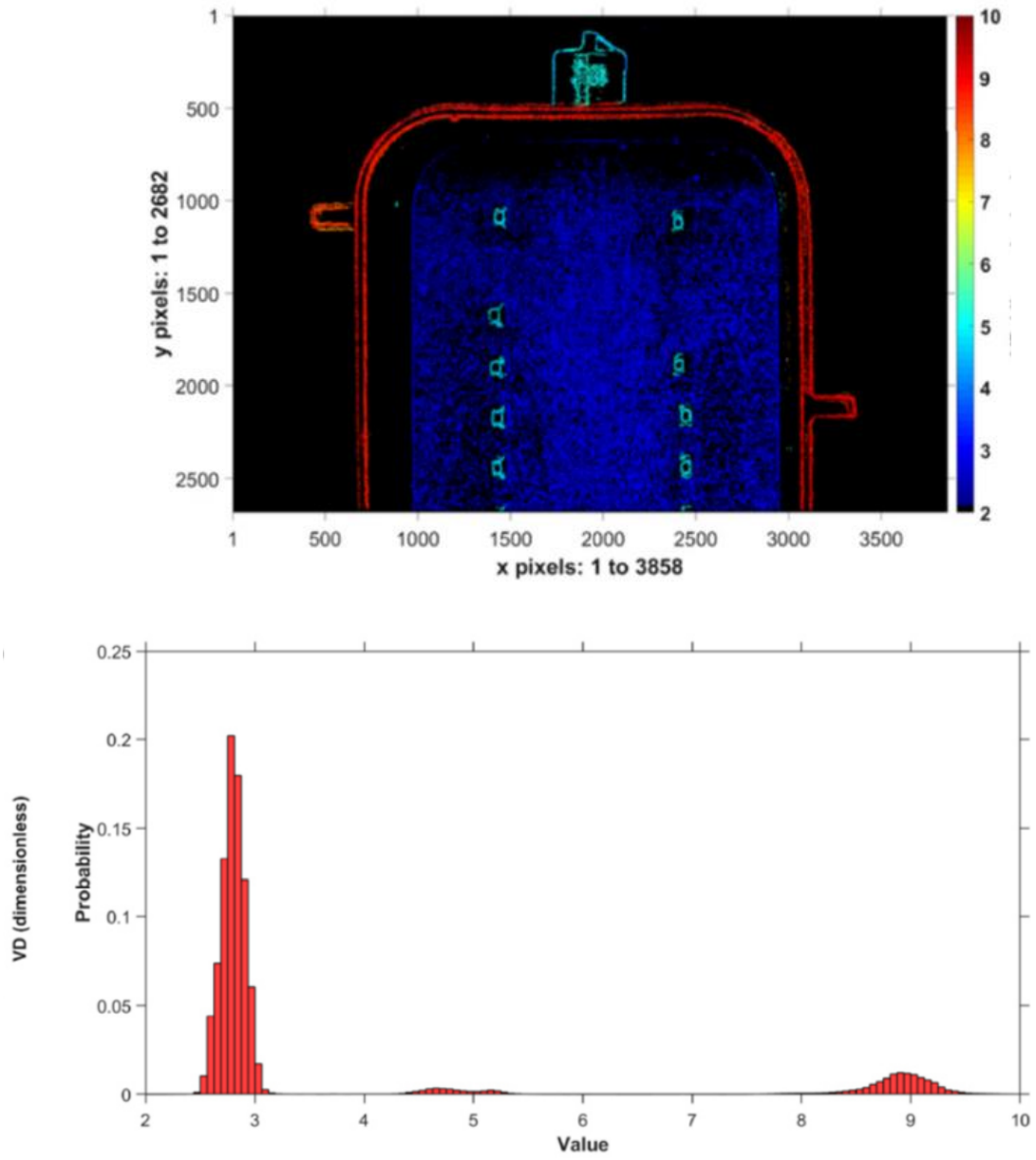

Figure 58 - Example of an ECU measured with Raytrix R42, and correspondent PDF graph of the virtual depths.

The other option available for lighting was to use 4 white LED bars mounted around the camera and lens, which resembles the Diffuse Flat Dome (Figure 48, from the previous *sub-chapter)*. Instantly the results were better, at first sight, still having to demonstrate the validity of the measurements using the Capability tests described in Section 2.3.

3.3.2 Testing Different Algorithms

As mentioned before, for the plenoptic technique to output "real world" measurement distances, a conversion from dimensionless Virtual Depth must occur. For that, there are different algorithms available, and some of them are provided by Raytrix. The RXLive software also gives the user the option to perform Pre and Post Processing in the image. So, in the following tests both of those factors were tested. To do that both an ECU and a SC were used. The results of these experiments are presented in *ANNEX A*.

To make this comparation, the first step was to compare the two algorithms available, Depth Path and Raycast, both without any Pre or Post Processing. The Depth Path algorithm is the more consistent, see in Figure 59, as it presents a more smooth and uniform curve. Also, the shape of the values in VD is transcribed to the Elevation from Reference graphic. This behavior is consistent across the multiple measures presented in *ANNEX* A. These results indicate that, between these two options, the Depth Path is more suited for the purpose.

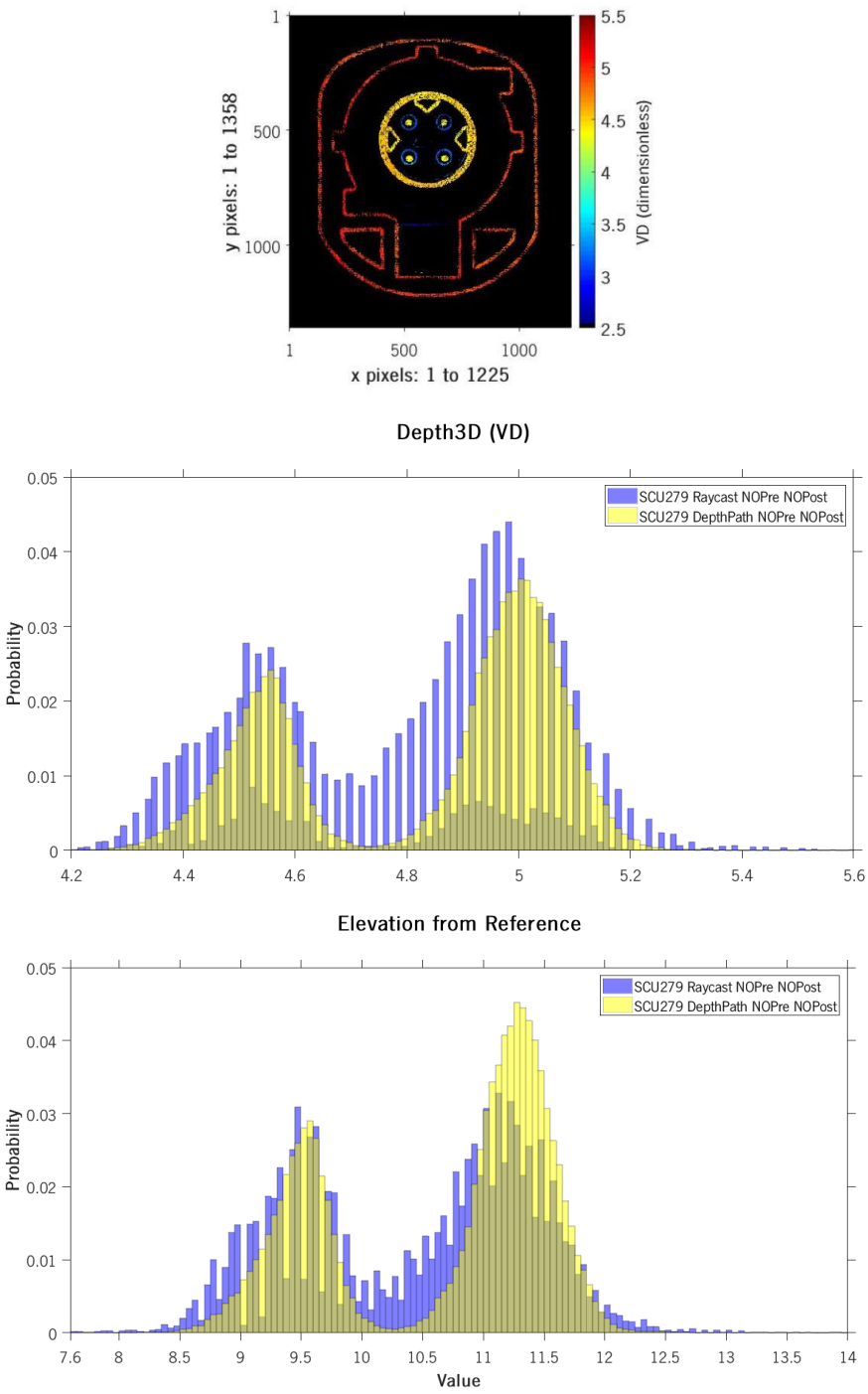

Figure 59 - Histograms of the two algorithms under test (probability estimated as PDF): Depth Path and Raycast, applied to a SC.

Having this result, the choice was to keep testing the Depth Path algorithm. The next step was to choose a set of Pre and Post Processing functions, apply them to the images, and compare the results with the ones without Pre and Post Processing. This comparison is presented in Figure 60. As one can see, the

shape of the curves is similar, but the one with Pre and Post Processing is smoother. Another point to notice is that there is a clear shift in the values. This indicates that, Pre and Post Processing must be used with caution, since it can lead to unwanted changes in values.

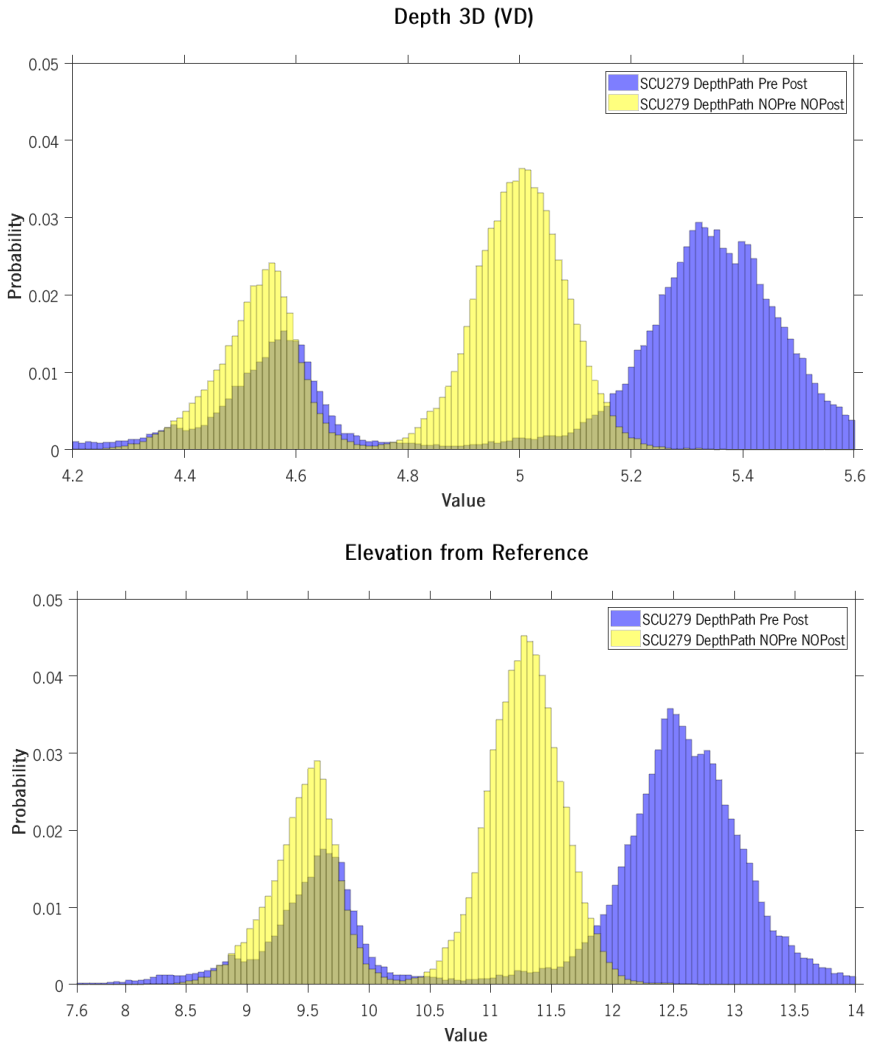

Figure 60 - Comparison between images with and without Pre and Post Processing, using Depth Path algorithm.

With these results, it seems that with no Pre and Post Processing, the Depth Path algorithm is more suited for the application, and the choice of Pre and Post Processing functions can influence the results in a negative or positive way. This will be confirmed in the next sub-chapter.

3.3.3 Siemens Star as Device Under Test

For these next tests, the ECU and SC were substituted by a Siemens Star. It consists in a pattern of dark "spokes" on a white background, that radiate from the center. In concept, these spokes become narrower as they come close to the center, and they only touch each other in that point. Since the main objective is to test the technology, this pattern is a good target since it provides enough contrast in the stripes and it can be settled at a known distance. With this setup, the histograms like the one presented in Figure 60 should approximate a single vertical bar. The narrower the bar, the better the results.

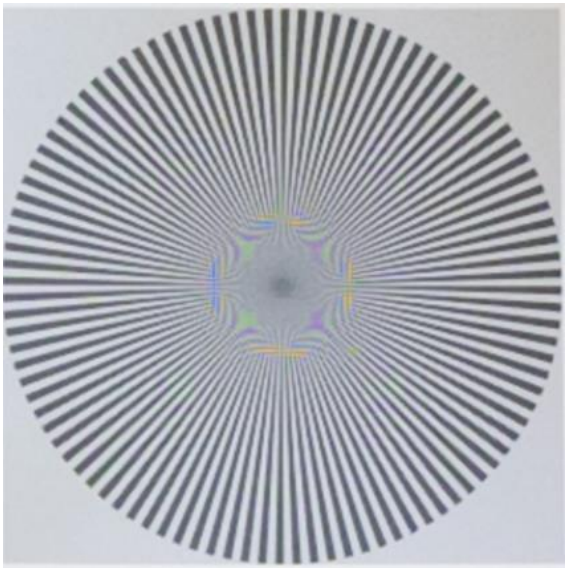

Figure 61 - Siemens Star

The software presented, as an option for Pre and Post Processing, a set of functions and value called Best Depth Estimation (BDE). Attracted by the suggestive name, this was the set tested. And so, for these trials using the Siemens Star as DUT, four different conditions were compared: BDE with Depth Path; BDE with Raycast; No Pre and No Post Processing with Depth Path; and No Pre and No Post Processing with Raycast. These measurements can be found in *ANNEX B*. In this setup, the Siemens Star was placed in a micrometric linear vertical stage, parallel to the lens.

From the results presented both in Figure 62 and *ANNEX B*, the more evident observation is that when there is No Pre and No Post Processing, the histogram is wider and not as tall, when comparing with

the results from BDE. In this aspect, the BDE results are better. The Mean Values and the Standard Deviations were also computed for each of the 4 conditions, and can be found in Table 4 and Table 5, respectively.

As stated in Table 4, the mean values in all 4 conditions are similar. But the values for the standard deviation is a different case. Both algorithms, when using BDE, perform much better than without it, presenting lower standard deviation. The highest standard deviation is shown by Raycast without Pre and Post Processing (confirming the results from 3.3.2), and the lowest is presented by Raycast again, but with BDE. So, from this experiment, we can infer that, to obtain the lowest standard deviation, we should use Raycast with BDE, and it will not lead to shifts in values, as the one presented in Figure 60.

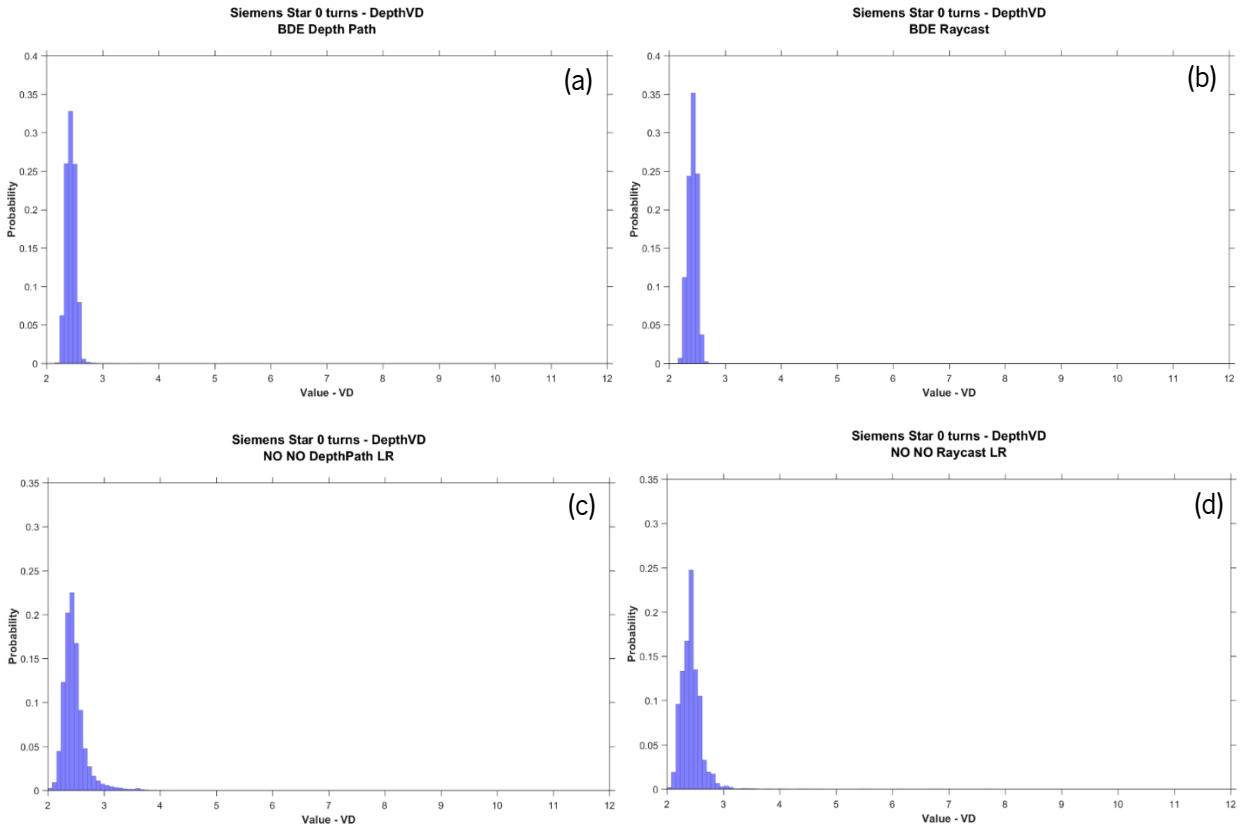

Figure 62 - Histograms of the Siemens Star, under 4 conditions: (a) BDE with Depth Path; (b) BDE with Raycast; (c) No Pre and No Post Processing with Depth Path; and (d) No Pre and No Post Processing with Raycast

Objective	Minimum Mean Value (mm)	Maximum Mean Value (mm)
BDE Depth Path	0.58	20.40
BDE Raycast	0.46	20.40
NONO Depth Path	0.82	19.85
NONO Raycast	0.74	20.80

Table 4 - Mean Values for the 4 conditions under study. Values in millimeters.

Objective	Mean Standard Deviation (mm)	Minimum Standard Deviation (mm)	Maximum Standard Deviation (mm)
BDE Depth Path	0.63	0.36	1.05
BDE Raycast	0.36	0.31	0.48
NONO Depth Path	1.77	0.72	3.14
NONO Raycast	2.73	2.10	3.19

Table 5 - Standard Deviation Values for the 4 conditions under study. Values in millimeters.

Even though the Raycast algorithm, with BDE Pre and Post Processing presents a low standard deviation, it is not low enough when the tolerance is ±150 μm. This value seems even worst knowing that these measurements were performed using a target with well-defined contours and good contrast.

3.3.4 Testing Different Objectives

Having the last paragraph in mind, and given that the values obtained were not good enough, the immediate modification to increase axial resolution (thus decreasing the tolerance for axial depth estimation) is to use a higher focal length. That alteration occurred through the objective. Besides the precalibrated 50mm Ricoh objective, two more were tested: an 75 mm Double Gauss and a Telecentric. To test these objectives, and having in mind the previous results, the Raycast with BDE was used. These results are available in *ANNEX C*.

The results of this comparison between objectives is, in short, represented by the graphic in Figure 63, and is a critical result for this technology. For the same distance, the Double Gauss lens presents the higher variation, which will lead to an increased resolution (making better use of the VD range). This does not come without a cost: increasing the resolution, through a higher focal length, will be traded by vertical working range.

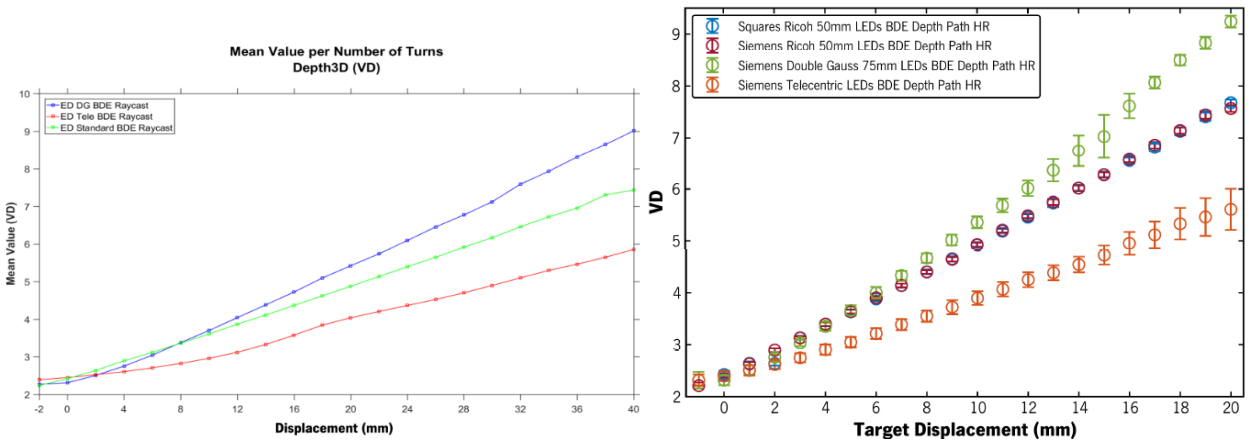

Figure 63 - Comparison between lenses: 75 mm Double Gauss, standard 50mm Ricoh and Telecentric.

The histograms from the Telecentric lens starts as tall and narrow as the other objectives, but when increasing the turns, meaning higher VD, it quickly falls, and the histogram becomes wide, as the one presented in Figure 64, which means high standard deviation. This means that the Telecentric objective, although still possible to use with a Plenoptic Camera, gives much poorer results. This may be an expected

result, since telecentric imaging is optically designed to minimize differences in perspectives, which is the feature used for plenoptic depth estimation.

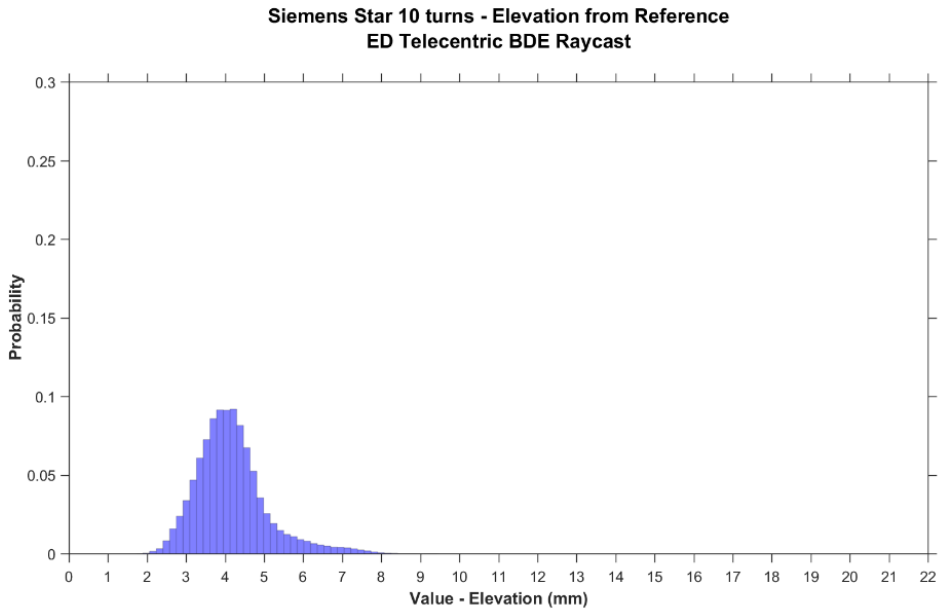

Figure 64 - Histogram of Telecentric Objective (using Raycast with BDE).

On the other hand, the Double Gauss 75 mm lens presents the sharpest and tallest histograms, as one my expect by the higher focal length. In fact, the histogram from Figure 65 is the closest from the ideal that was achieved. This indicates that this objective may have the potential to achieve the resolution necessary for the specifications.

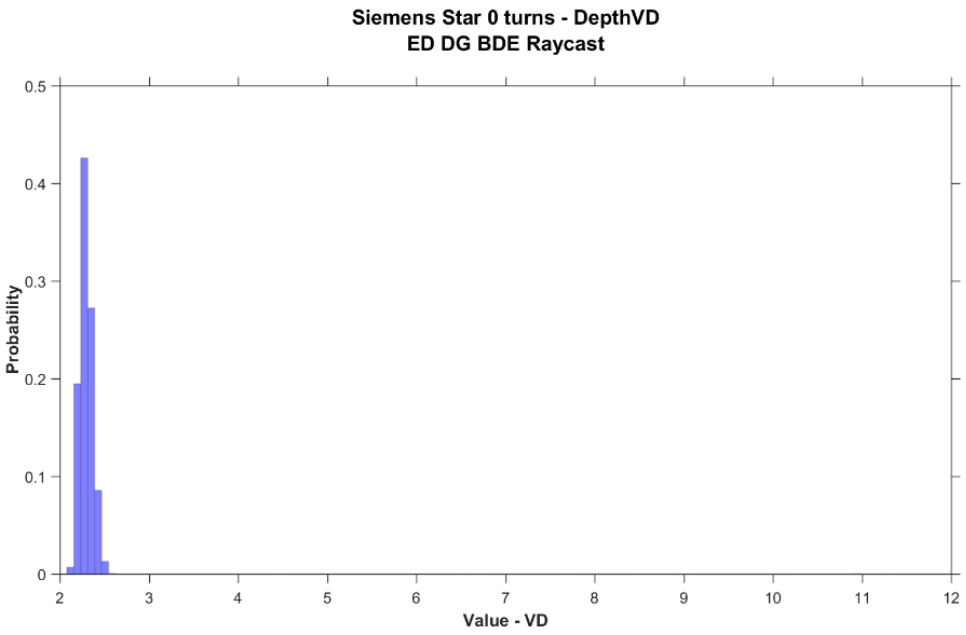

Figure 65 - Histogram of Double Gauss Objective (using Raycast with BDE).

One may ask why all the results presented in section 3.3.4 are expressed in VD. The reason is because there are no calibration files, both for the Double Gauss and Telecentric lens. The calibration is needed in order to convert VD values into "real world" values. This process of calibrating an objective for the Raytrix camera was performed during the last Innovation Project between University of Minho and Bosch, and it will be repeated for the current one.

3.3.5 Lens Calibration for Depth Estimation

As explained in *2.2.3.3.2* Plenoptic Imaging uses the VD in order to estimate depth values. But, to convert the VD into real world values, it is needed a calibration file. The 50 mm lens was calibrated by Raytrix, but for the 75 mm Double Gauss there was no such file. The process to obtain a calibration file is far from trivial, but fortunately, the team already had already validated this process (Silva., Nunes-Pereira, & Forte, 2019), and was now a matter of replicating the work with the different optical objective

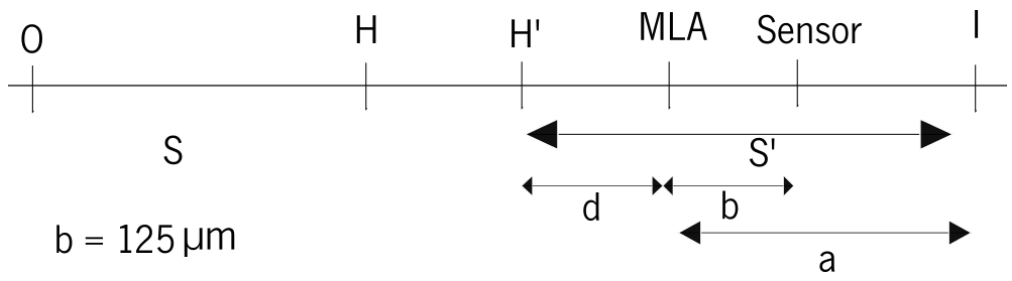

Figure 66 - Principal planes for the plenoptic model.

To obtain this calibration, a relation between VD and S' must be found. Having the relations of the **Erro! Fonte de referência não encontrada.**, and the equations $\frac{1}{S} + \frac{1}{S'} = \frac{1}{f'}$, and $VD = \frac{a}{b}$, one finds that

$$VD = \frac{S'}{b} - \frac{d}{b} \tag{9}$$

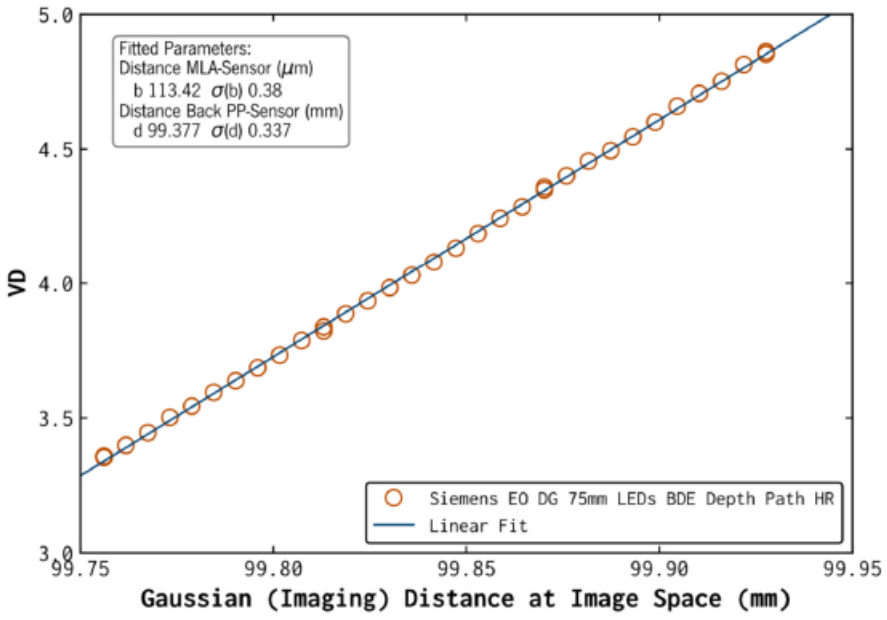

Figure 67 - Relation between VD and real distance for the 75 mm DG lens.

With this expression, knowing the values of VD and S, both given by the Raytrix software, one can make a linear adjustment to find *b* and *d*. The process to obtain the calibration file started by placing a target (Siemens Star) in front of the optical system, and acquire the values of VD and S, while measuring the real distance. This is presented in Figure 67. The result of *b* is different of what it was expected, since S. Moises, *et al* (Silva., Nunes-Pereira, & Forte, 2019) had found that b=125µm, and now the result was b=113µm. The value of *b*, the distance between the MLA and the sensor, is a fixed distance by hardware, and should be equal for both lenses. The difference is not major, since the error percentage is around 10%. Now, with these values of *b, d*, VD we can find the values of S', and given that $\frac{1}{S} + \frac{1}{S'} = \frac{1}{f}$, with f=75mm, we can determinate all values of S, the distance in the object space.

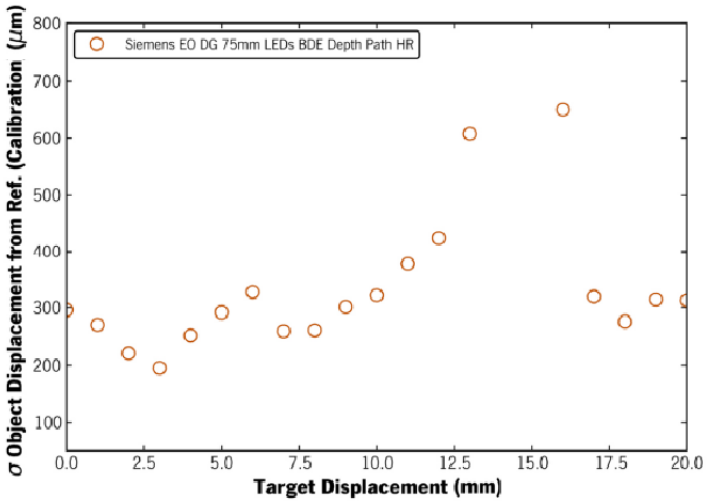

Figure 68 - Standard Deviation values between the calibration values and the measured values, for the 75mm DG lens.

Analyzing the values of VD and S, it is now possible to estimate the values of standard deviation, which are presented in Figure 68. The values of standard deviation for this 75mm DG lens seem to be larger than the standard 50mm lens, which is not what was expected. But, from Figure 63 it is already visible the higher dispersion in the values of VD for the 75mm lens. The reason this may occur is due to the apertures of the lenses: the MLA has an f/2.8, while the 75mm DG lens has f/4 to f/30, being always smaller than the MLA aperture. One possible solution is to this problem is to try this same process with a lens that has the same aperture as the one of the MLA.

3.4 Stereoscopic Imaging with Pattern Light Projection

The last technology documented in this Master Dissertation is the use of Stereoscopic Imaging, paired with Pattern Light Projection, more specifically the Gocator 3506. The aggregation of these two technologies is seen as a possibility to integrate in a single equipment for both axial and lateral analysis. The main function of this device would be to measure the height of pins, when required by a costumer, and to help in the connector integrity examination, namely, to evaluate the plastic housing.

3.4.1 How the device works

The device used in the tests described in *Chapter 3* is a Gocator 3506, by *LMI Technologies,* and it is marketed as "the highest-resolution 3D snapshot sensor on the market" (LMI Technologies, Inc, n.d.) by the company. As it was said above, the Snapshot sensor uses both stereoscopy and projection of structured light in order to obtain a 3D visualization of the DUT. The target must remain stationary during the camera exposure of the light patterns.

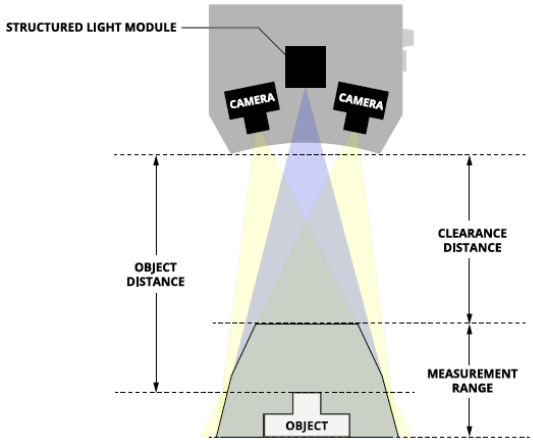

Figure 69 - Schematic of a Gocator device. It uses a pair of stereo cameras and a Structured Light Module.

Figure 69 shows some important concepts for understanding the setup of a Gocator device. The field of view has the aspect of a cone, meaning that is smaller at the near end and enlarges as it reaches the end of the measurement range. At the near end of the field of view, where it has the smallest value, it is also where it has the highest resolution. So, it is recommended that the DUT should be placed as much as possible close to the Gocator sensors while still within the measurement range from the clearance distance, when resolution is critical (LMI Technologies, Inc, 2020).

Gocator 3506 Specifications	
Scan Rate (Hz)	3
Imagers (megapixels)	5
Clearance Distance (CD) (mm)	87.0
Measurement Range (MR) (mm)	25.0
Field of View (mm)	27.0 x 45.0 - 30.0 x 45.0
Repeatability Z (um)	2.0
Resolution XY (mm)	0.020 (CE) - 0.025 (FE)
VDI/VDE Accuracy (mm)*	0.012

Figure 70 - Gocator 3506 Specifications (LMI Technologies, Inc, n.d.)

A Structured Light Modulator (SLM) produces a sequence of high resolution and contrast light patterns, with the help of a blue LED. The two cameras capture the reflected light from different viewing angles. Then the sensor can use either the *stereo correlation* or the *independent triangulation* to generate 3D points from the light pattern.

Stereo correlation means that the sensor locates the same point on the physical target in the two images captured at different viewing angles. Since the exact distance between the two cameras and the viewing angles are known, the distance to the point can be calculated. For stereo correlation to work and produce a 3D data point, the point on the target must be visible to both cameras. Stereo correlation may produce more stable measurements on targets with a simple shape but will be affected by occlusions on targets with complicated shapes and protruding features.

Independent triangulation means that each camera independently triangulates off the LED light pattern, based on the calibration process that takes place when the sensor is manufactured. Since a snapshot sensor has two cameras, a point on the physical target only needs to be visible to one of the cameras in order

to generate a 3D point. Independent triangulation may improve performance on targets with complicated shapes that can cause occlusion, but it relies on the sensor's internal components being fully stable.

The Gocator 3506 is powered by 24V and connects to a PC with an Ethernet port. To use it, there is no need to install any software, since it runs using a Web Interface (Figure 71).

Figure 71 - Gocator Web Interface.

3.4.2 Testing on a Calibration Plate

A calibration plate was used as the DUT for these first tests, as shown in Figure 72. The use of this calibration plate is to simulate a connector, with 4 different pins, with different heights and thickness, and 9 holes. The objective was to use the pins to perform the capability test along the Z axis (height), and the holes to assess the performance on the XY plane. Those measurements are known and can be found in *ANNEX D*. The result of a scan in the calibration plate is presented in Figure 73.

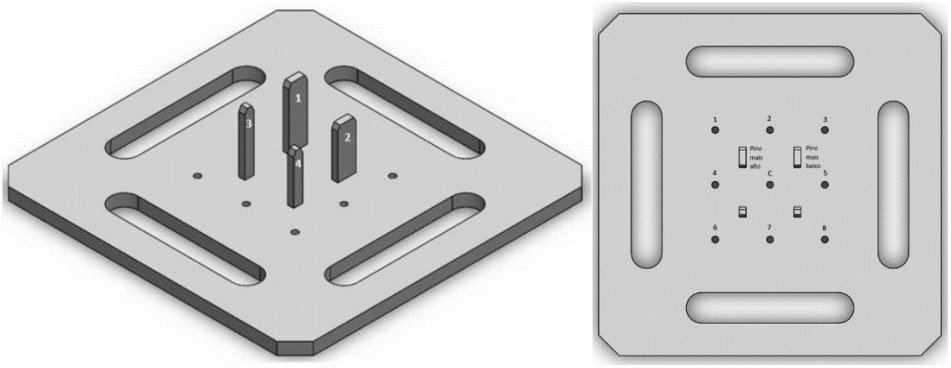

Figure 72 - Calibration plate used for testing the Gocator 3506.

The first thing that was immediately obvious when trying to perform a scan was that the performance time was long, around 8 to 10 seconds. A possible workaround for this problem was to reduce the FOV. to the necessary, meaning that it could be reduced to only the connector, or the part of the connector being analyzed. With this alteration, the scan time was reduced to around 1 to 2 seconds when analyzing only one pin, and to around 4 seconds when analyzing the 4 pins.

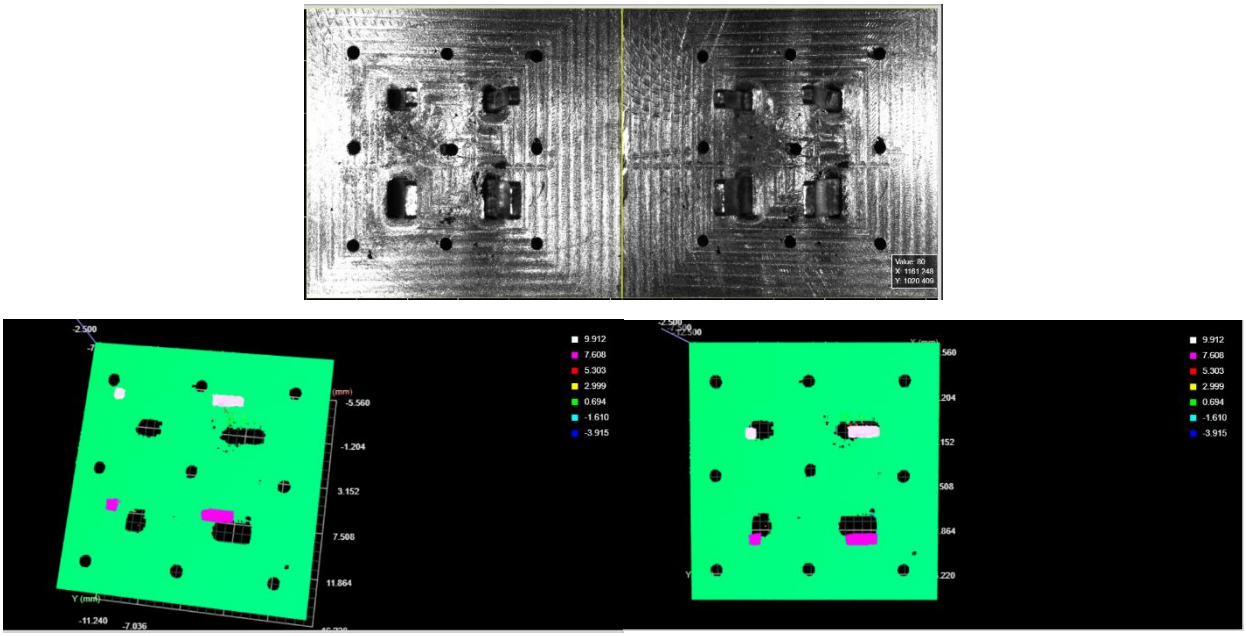

Figure 73 – Result of scanning the calibration plate with Gocator 3506: View of each of the two cameras (Top); 3D point cloud generated (bottom).

There are a few different ways to measure the height of the pins. The one chosen on these trials was to create a section, as shown in Figure 74, and then compare the values of the base with the top of the pins,

using an average of the points of interest. The results of this measurements can be found in *ANNEX E1*. In short, both C_g and C_{gk} presented good values, ranging from 5.19 to 20.07, meaning that, following Bosch norms for Measurement and Test Processes (Robert Bosch GmbH, 2019), this device has capability to perform the analysis along the Z axis, for a 300 micrometers tolerance (which is the value we are trying to achieve for Electrical Connector Units).

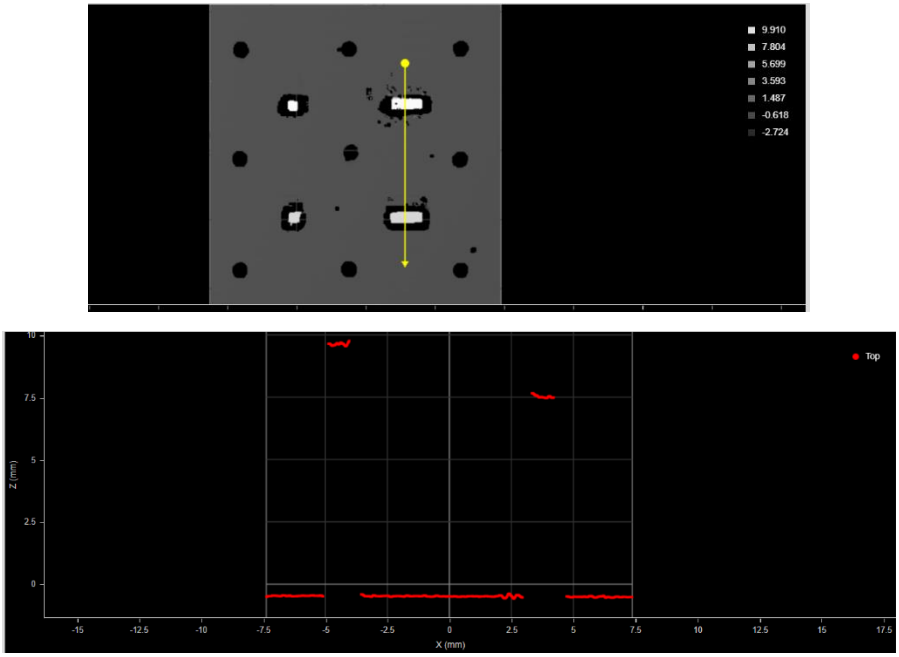

Figure 74 – Section of the Calibration Plate, containing 2 pins, and the respective graph of heights.

To assess the performance of the Gocator 3506 on the XY plane, was used the *Surface Hole* tool, that, as the name implies, will find holes or any shape that resembles a hole, and return various information about it, like the value of the radius or the X and Y positions.

First, to test if the system has repeatability, the holes were measured 25 times each, the values of X and Y were obtained, and the C_g was calculated. Again, those values, available in *ANNEX E2*, were all above 1.33, meaning that repeatability was achieved for the tolerance of 300 micrometers.

Next, the value of the distance from the center of each hole to the center of the central hole was calculated using the prior points. The goal was to compare with the known vales from the calibration plate. Again, all the distances were repeatable, but when comparing with the real physical distance, they did not

match. When applying the C_{gk} formula, most of the results presented a negative value (*ANNEX E3*), when it should be above 1.33 to be acceptable.

3.4.3 Testing on real connectors

The next steps were to try to apply the same techniques to real connectors, both Electrical Connector Units and Standard Connectors. The results were mixed, more on the negative side.

Scanning an ECU was not much different from scanning the calibration plate, since the pins resemble each other. So, the results from an ECU are, in every way, similar to the ones from the calibration plate. Figure 76 presents the result of such scan. In order to obtain the scan with good results, there was the need to apply some filters, like *Space Filling* and *Smoothing*, as presented in Figure 75. Even then, some pins (e.*g.* the DI), presented some noise, that does not correspond to the actual values. To calculate the height of the pins, a similar technique as the one used in the calibration plate can be used, as demonstrated in Figure 77.

Figure 75 - Filters available, applied to the direct measurands.

Figure 76 – Result of a scan of an ECU (left) and the real connector (right).

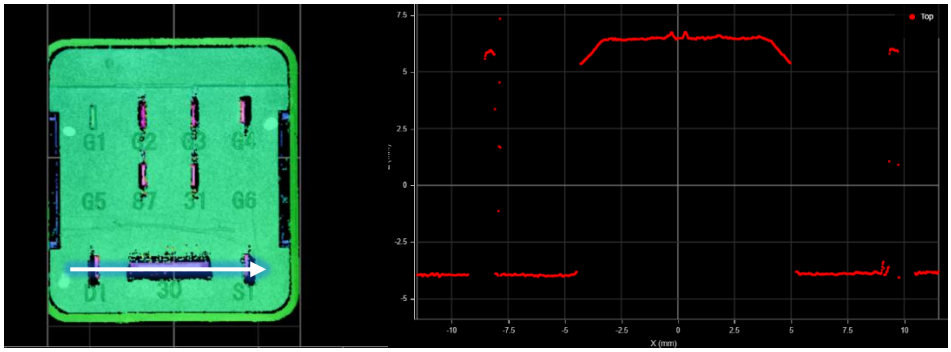

Figure 77 – Section across the 3 bottom pins of the connector (left) and the correspondent heights graph (right)

Scanning a SC proved to be a much harder task. Both the size and the shape of the pin, alongside with some unwanted reflections presented in some connectors caused trouble to correctly measure an SC. As one can observe in Figure 78 and Figure 79, it is hard to identify the pins because of all the noise. Different filters like the ones mentioned above were applied, alongside with others such as *Median*, but with close to no improvement on the results. These difficulties can be attributed to the shape and size of the pins, as the outer plastic case is perfectly represented into the 3D scan.

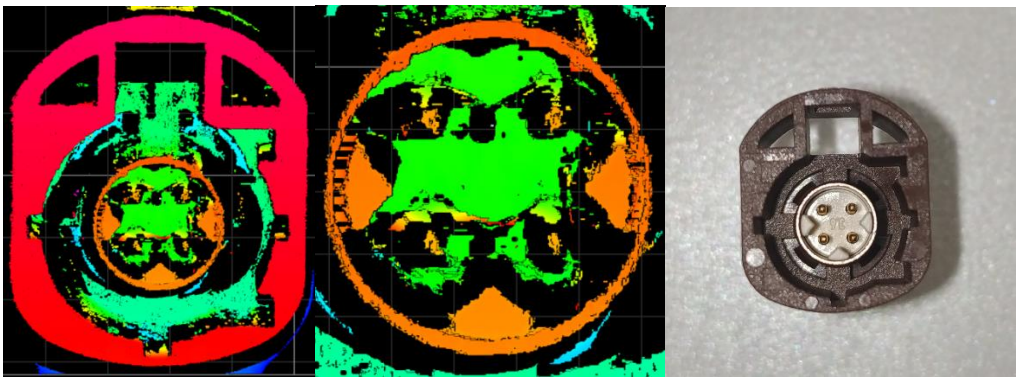

Figure 78 – HSD connector 3D scan (left), the center metal ring with pins (middle) and the real connector (right).

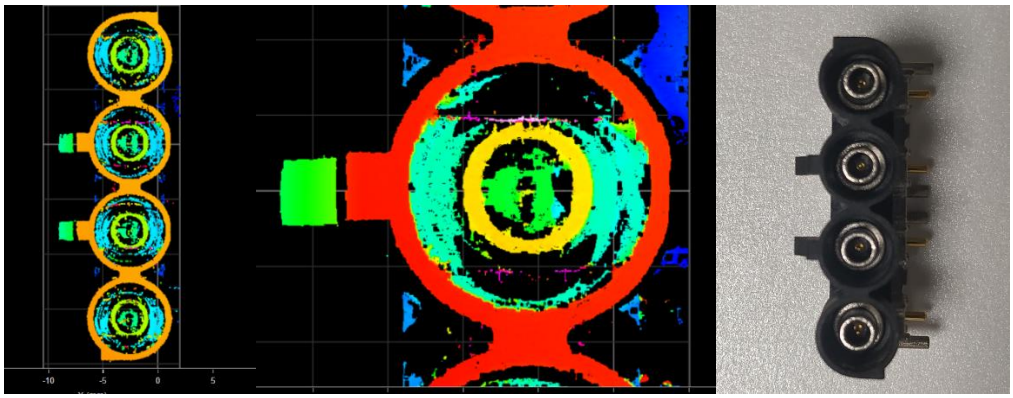

Figure 79 – 3D scan of a typical SC connector (left), the center metal ring with the pin (middle) and the real connector (right)

Aside from the problems when trying to find pins, other issues raised when analyzing both types of connectors. The implementation of a solid enough *job* (name of a recipe in the Gocator software) proved to be hard. Using the *Part Detection* or the *Model* features often caused the found model to be in different positions from the one trained, or even failed to find the same part that was used to train the model. This means that if we cannot guarantee that the part is placed in the same position, it can be hard to perform accurate measurements.

So, as a conclusion for the analysis of this equipment, when using a Calibration Plate, it was proven that the Gocator 3506 has the capability to perform the height measurements, but the same did not prove true for the measurements in the XY plane, where it failed when performing the C_{gk} capability test. For real connectors, the sizes and different shapes of the pins caused many complications, and alongside with the difficulties to create a robust *job*, it is possible that the Gocator 3506 is not ready yet to be integrated in the prototype of the connector inspection machine, for the Pin Inspection task. However, the device can be a

possible solution for the connector integrity evaluation, since it can provide a real 3D view of features of larger sizes.

Chapter 4

Conclusion

The summary of the technologies studied during this Dissertation is presented in Figure 80, as a comparison between techniques. In order to better evaluate each technology, the tasks were separated, because a technique may be the best to acquire the position of the pin, but completely fail to determine the color of the connector, per example. Also, there is the separation between ECU and SC, due to the different characteristics and requirements of each type of connector.

Chromatic Confocal technology proved to be capable of accurately measure heights, according to Bosch standards. But it also suffers greatly with light scattering and unwanted reflections, making it hard to analyze the resulting data. Also, it fails in every other task other than measure the height of the pins in an ECU. It is not applicable in SC since the pins are, most of times, too small. And there is a strict correlation between the number of pins analyzed and the cycle time, being this technique based on a Point Scan. However, it is a possible solution to complement the gaps of Telecentric Lenses.

The use of telecentric optics for connector inspection is a viable option, mostly for determining the position of the pins. Having a good resolution and no distortion errors caused by the lenses will lead to good results. The fact that one can chose the size of FOV and adapt it to the connector in mind is an advantage, comparing with other technologies. From experience, not all connectors are as easy to analyze, with telecentric lenses, due to the lack of contrast between the connector protective plastic and the background, for example. But these difficulties can be overcome using different sources of illumination, changing the focal point of the system or even using polarization. The more obvious down point for this technology is that, from the way that it was implemented, the height of the pins cannot be determined. So, to offer a complete analysis of the connector, telecentric lenses could be paired with a technique like laser profilometry or chromatic confocal.

The pairing of Stereoscopic Imaging with Pattern Light Projection, implemented in the Gocator 3506 device, has the potential to be a solution for the connector analysis problematic , since it provides XY coordinates to analyze the position of the pins, a 2D shot that allows to evaluate if the protective plastic case of the connector is damaged and the presence of unwanted features, and offers a cloud point of heights, failing only to analyze the color of the connector. But, in the way that the device is implemented, it is still not possible to do these analyses with the targeted resolution. The detection of pins can be unreliable due to the presence of noise, mostly in SC, making it hard to industrialize the process. But even in the analysis of the position of pins in an ECU, the capability measurements were not satisfactory for the connector inspection process. The height analysis, when the pins can be found, presented motivating results, making this an interesting device to keep studying and improve.

At last, the Plenoptic Imaging technique, which has proven to be an all-in-one solution. It is a technology not widely used in the industry, but with potential to be applied in more AOI processes. It allows us to join both 2D (working as a "normal" camera) and 3D (using the plenoptic depth estimation). Most like Telecentric Optics, with the Plenoptic Imaging technique, one can change the lens to fit the necessary. Yet, its much difficult with light field imaging, since the plenoptic depth estimation requires a calibrated lens. Based on the experience, the computational processing necessary to estimate depths is sensitive to several computational artifacts, so, even if the plenoptic total focus image is able to locate the features, the depth estimation algorithm may fail. The 50mm Ricoh precalibrated lens did not provide axial or depth resolution compatible with Bosch standards. However, the higher focal length 75 mm Double Gauss lens seemed to accomplish the task, result that still need to be proven with a different lens, that matches the aperture of the MLA. This gain on the resolution came at the cost of axial working range, which is a relation hard to balance.

To complement the work developed during this Dissertation, there are a few tests that I would like to perform. First, and more obvious, to complete the calibration of the 75 mm Double Gauss lens, in the context of Plenoptic Imaging, and perform capability measurements with that setup. It would be interesting to quantify the relation between axial resolution and working range. Second, I would like to apply a Laser Profilometer to connector analysis, giving that it is a Line Scan, meaning that would not be as time consuming as the Chromatic Confocal technology, and I am expecting similar results. Third and last, It would be interesting to

scan the Calibration Plate, referred in 3.4.2, with all the technologies available, making the results of the comparation much more objective.

Summary of Conclusions	Advantages	Disadvantages	ECU			SC						Cycle Time
			PIN			PIN			Housing	Coding	# PINs	Color	
			Position	Height	Axial Range	Position	Height	Axial Range					
Chromatic Confocal	1. Good axial resolution	1. Requires additional equipment for inspection of pin position 2. Highly susceptable to light scattering and vibrations 3. Cycle time greatly depends on number of pins	F[8]	B	?	⊗	⊗	?	⊗	⊗	⊗	⊗	D[9]
Imaging with Telecentric Lens	1. No parallax error 2. Selectable FOV 3. Low Cost 4. Flexibility of lighting setup	1. Requires additional equipment for height measurements	A[1][2]	⊗	⊗	A[1][2]	⊗	⊗	B	B	A	A[3]	B
Plenoptic Light Field Imaging	Minimizes impact of optical oclusion	The balance between axial resolution & FOV/ /lateral resolution is difficult to achieve	A/B (?) Lateral Resolution TBD [6]	A Axial Resolution 100-150um [6,7]	A/B (?) min. 30mm [7]	A/B (?) Lateral Resolution TBD [6]	A Axial Resolution 100-150um [6,7]	A/B (?) min. 30mm [7]	A	A	A	A	A
Stereoscopic Imaging with Structured Light	1. 2.5D solution 2. Good axial resolution	1. Difficulty analyzing smaller pins 2. Compromise between FOV and cycle time 3. Poor lateral resolution	C	A	?	D[1][4]	B	?	B[5]	B	D[1][4]	⊗	C

A	Very Good/Good
B	Satisfactory
C	Mediocre
D	Insufficient
F	Failure
-	Not Evaluated
⊗	Not Applicable
TBD	To Be Determined

[1] - Depends on size of pin (smaller pins are harder to inspect)
[2] - Lack of a stable reference negatively impacts inspection
[3] - Color cameras only
[4] - Ghost points can have a negative impact
[5] - Shows potential, needs further analysis
[6] - Varies with focal length/FOV
[7] - Based on 50mm focal lens
[8] - Possible but unreliable and slow
[9] - Depends on number of pins

Figure 80 - Summary of the technologies studied during this Dissertation.

References

Ankit Gupta, A. S. (2020). *Connector Market Size By Products.*

Bradshaw, G. (1999). *Non-Contact Surface Geometry.* Dublin: Trinity College.

Cunha, J. A. (2015, September). Improved Depth Estimation Algorithm using Plenoptic Cameras. *Master Dissertation*. Coimbra.

Edward H. Adelson, J. R. (1991). *The Plenoptic Function and the Elements of Early Vision.* Cambridge: MIT Press.

G. Binnig, H. R. (1982). *Surface Studies by Scanning Tunneling Microscopy.* American Physical Society.

Hall, P. R. (2008). Lenses, Prisms and Mirrors. In T. Yoshizawa, *Handbook of optical metrology : principles and applications.* Taylor & Francis Group, LLC.

Hariharan, P. (2003). *Optical interferometry.* Elsevier Science.

Heliotis AG. (2017). *Note to Feasibility Analysis for Connector Inspection.*

Karthick Sathiamoorthy, T. A. (2010). *Construction and Validation of a White Light Interferometer.* Halmstad.

Kerwien, N. (2014). *3D goes digital: from stereoscopy to modern 3D imaging techniques.* Beijing. doi:10.1117/12.2073658

LightField Forum. (n.d.). *HISTORY OF LIGHT FIELD PHOTOGRAPHY*. Retrieved July 15, 2020, from http://lightfield-forum.com/what-is-the-lightfield/history-of-light-field-photography-timeline/

Lippmann, G. (1908). Épreuves réversibles donnant la sensation du relief. doi:10.1051/jphystap:019080070082100

LMI Technologies, Inc. (2020). *Gocator 3210 & 3500 Series Sensors User Manual.*

LMI Technologies, Inc. (n.d.). *Gocator 3506 Datasheet*. Retrieved from https://downloads.lmi3d.com/gocator-3506-all-one-3d-smart-snapshot-sensor-datasheet

Marc Levoy, K. P. (2000). The digital Michelangelo project: 3D scanning of large statues. New York: ACM Press/Addison-Wesley Publishing Co.

Masoner, L. (2019, March 1). *A Brief History of Photography and the Camera*. Retrieved August 9, 2020, from https://www.thesprucecrafts.com/brief-history-of-photography-2688527

NanoScience Instruments. (n.d.). *NanoScience*. Retrieved from Stylus Probes: https://www.nanoscience.com/techniques/optical-profilometry/stylus/

NASA. (n.d.). *NASA*. Retrieved from Phoenix Mars Lander: https://www.nasa.gov/mission_pages/phoenix/images/press/AFM_Tips.html

Nélida A. Russo, E. N. (2020). OCT in Applications That Involve the Measurement of Large Dimensions.

Ng, R. (2006, July). Digital Light Field Photography. *Doctor Thesis*. Stanford University.

NI Engineer Ambitiously. (2019, March 5). *A Practical Guide to Machine Vision Lighting*. Retrieved December 2, 2020, from https://www.ni.com/de-de/innovations/white-papers/12/a-practical-guide-to-machine-vision-lighting.html#section-53685227

Opto Engineering. (n.d.). *Telecentric lenses tutorial: Basic information and working principles*. Retrieved July 5, 2020, from https://www.opto-e.com/resources/telecentric-lenses-tutorial

Page, D. A. (2008). Interferometry. In T. Yoshizawa, *Handbook of optical metrology : principles and applications.* Taylor & Francis.

Paschotta, R. (n.d.). *RP-Photonics*. Retrieved from Optical Profilometers: https://www.rp-photonics.com/optical_profilometers.html

Pavel Pavliček, E. M. (2019). *White-light interferometer without mechanical scanning.* Olomouc: Joint Laboratory of Optics of Palacky University and Institute of Physics ASCR.

Perwass, D. C. (2014). Light Field Cameras for metric 3D measurements. Kiel: Raytrix.

Polhemus, N. W. (2018). *Process Capability Analysis: Estimating Quality.* New York: CRC Press.

Robert Bosch GmbH. (2019). *Booklet 10 - Capability of Measurement and Test Processes.*

RP Photonics. (n.d.). *Shack–Hartmann Wavefront Sensors*. Retrieved January 26, 2021, from RP Photonics Encyclopedia: https://www.rp-photonics.com/shack_hartmann_wavefront_sensors.html

RP-Photonics. (n.d.). *Coherence*. Retrieved June 9, 2020, from RP-Photonics Encyclopedia: https://www.rp-photonics.com/coherence.html

S.C., C. (2014). Plenoptic Function. In *Computer Vision.* Boston: Springer. doi:https://doi.org/10.1007/978-0-387-31439-6_7

Schmit J., P. A. (2019). White Light Interferometry. In C. Springer, *Handbook of Advanced Nondestructive Evaluation.*

Silva., M. A., Nunes-Pereira, E., & Forte, P. M. (2019). Single shot plenoptic optical imaging inspection of a head-up display: projection distance, astigmatism, field curvature, and distoritions.

Stil, SAS. (n.d.). *CCS Prima: Operating and maintenece manual.* Saint Hilaire: STIL SAS.

Thorlabs. (2017). TELESTO-II-1325LR. *TELESTO SERIES SD-OCT SYSTEMS*.

Thorlabs. (n.d.). *Telecentric Lenses Tutorial*. Retrieved June 7, 2020, from https://www.thorlabs.com/newgrouppage9.cfm?objectgroup_id=10762

Todor Georgiev, A. L. (2009). Superresolution with Plenoptic 2.0 Cameras. Optical Society of America.

Tomasz GIESKO, A. Z. (n.d.). *LASER PROFILOMETERS FOR SURFACE INSPECTION AND PROFILE MEASUREMENT.* Radom: National Research Institute.

Toru Yoshizawa, T. W. (2015). Surface Profilometry. In T. Yoshizawa, *Handbook of Optical Metrology Principles.* Yokohama: CRC Press.

Vico Imaging. (n.d.). *DTCM Series High Precision Bi-Telecentric Lens*. Retrieved January 2021, from Vico Imaging.

Vision Doctor. (n.d.). *Optic basics*. Retrieved from Vision Doctor: https://www.vision-doctor.com/en/optical-basics.html

Watanabe M., N. S. (1996). Telecentric optics for computational vision. *Computer Vision — ECCV '96.* Berlin: Springer.

Wiora G., W. M. (2013). Optical Interferometry. In C. Y. Wang Q.J., *Encyclopedia of Tribology.* Springer, Boston, MA.

ANNEX A

1. **SC** algorithm comparison

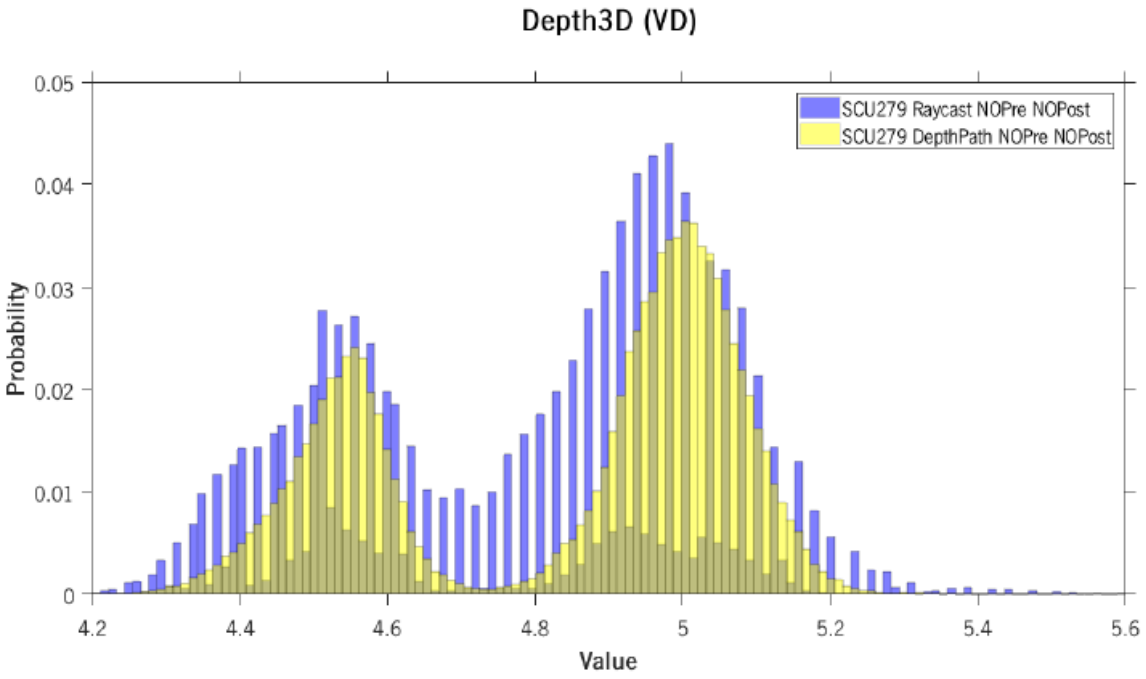

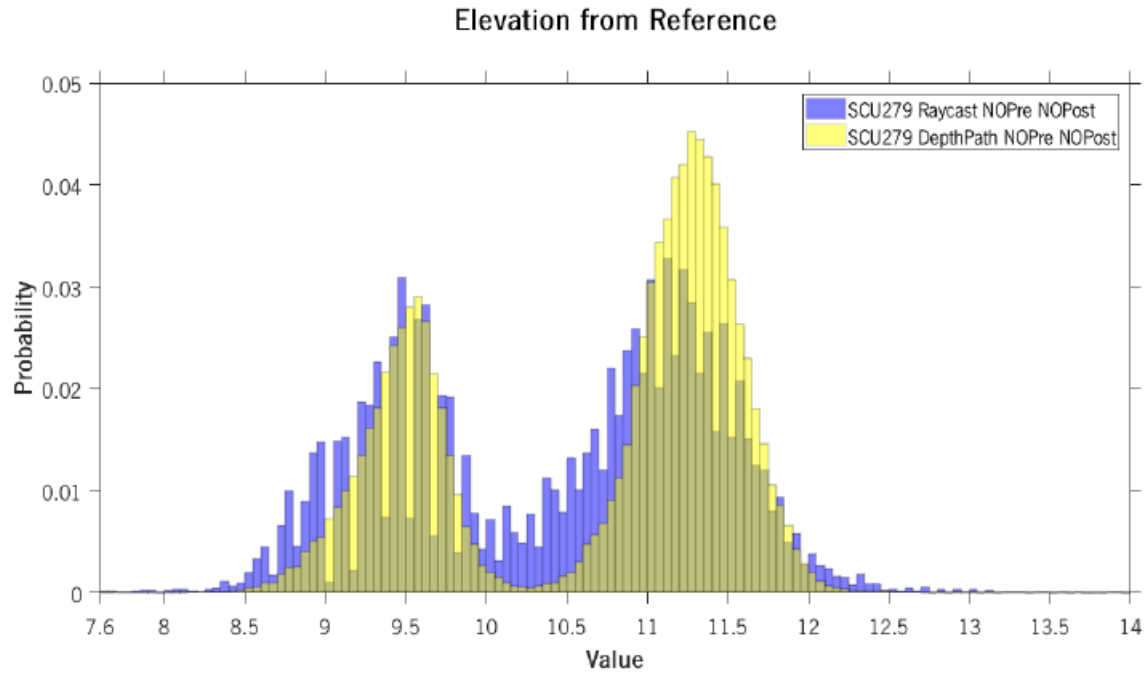

2. SC Pre and Post Processing comparison

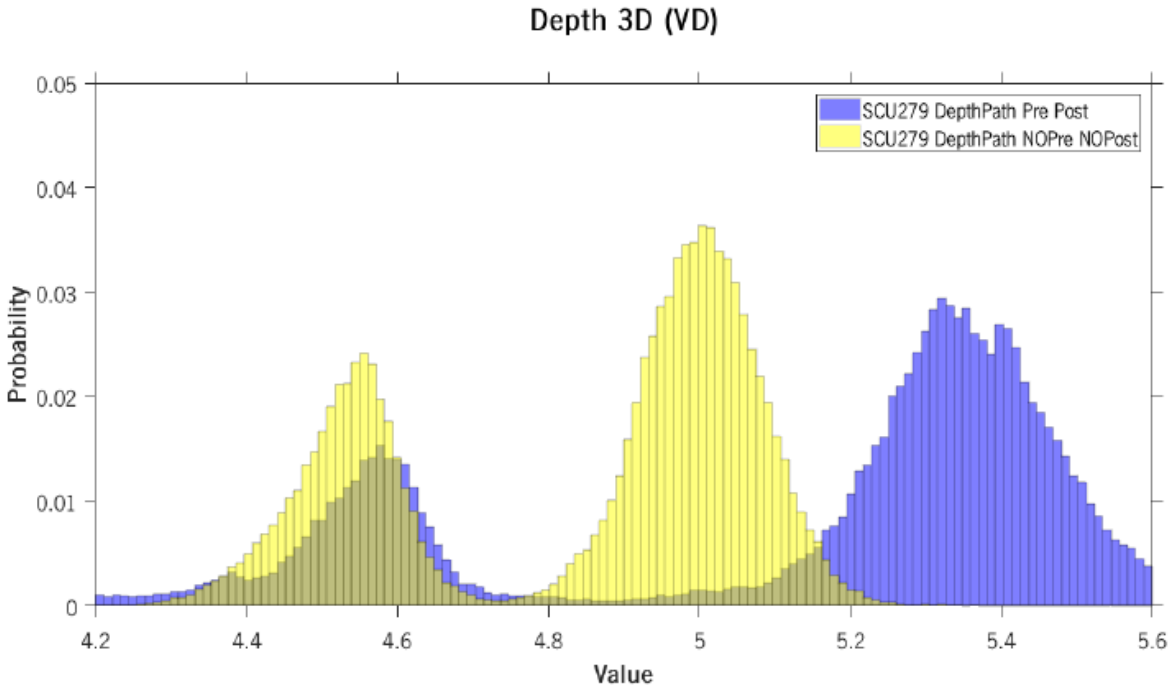

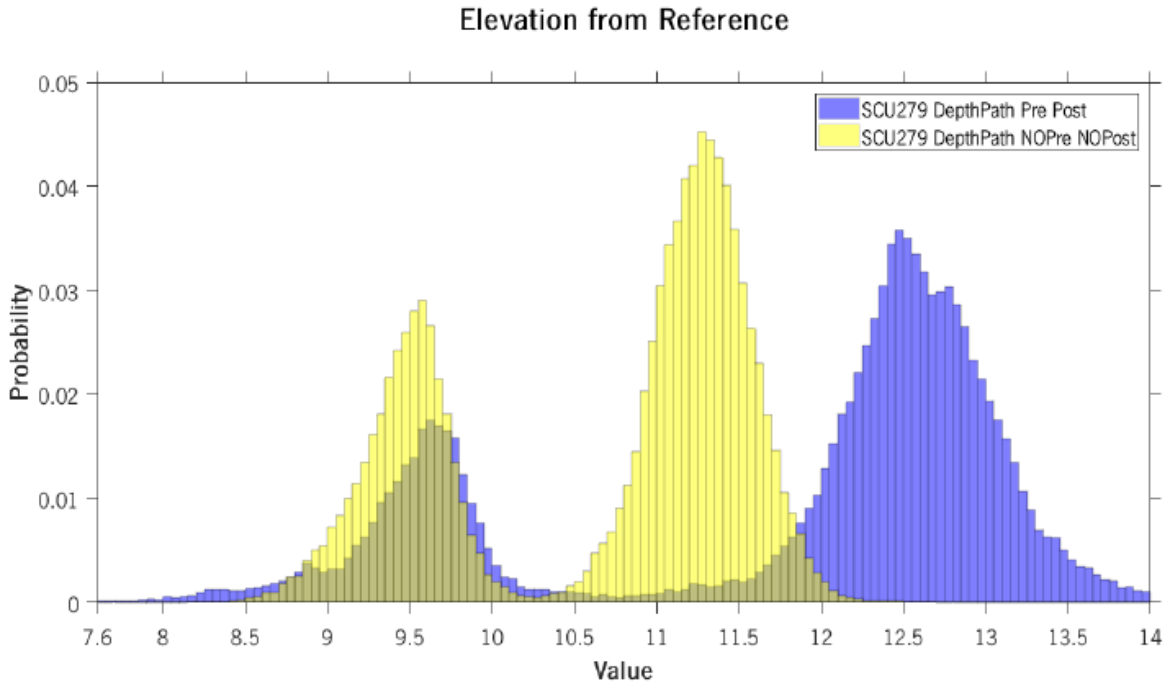

3. ECU algorithm comparison

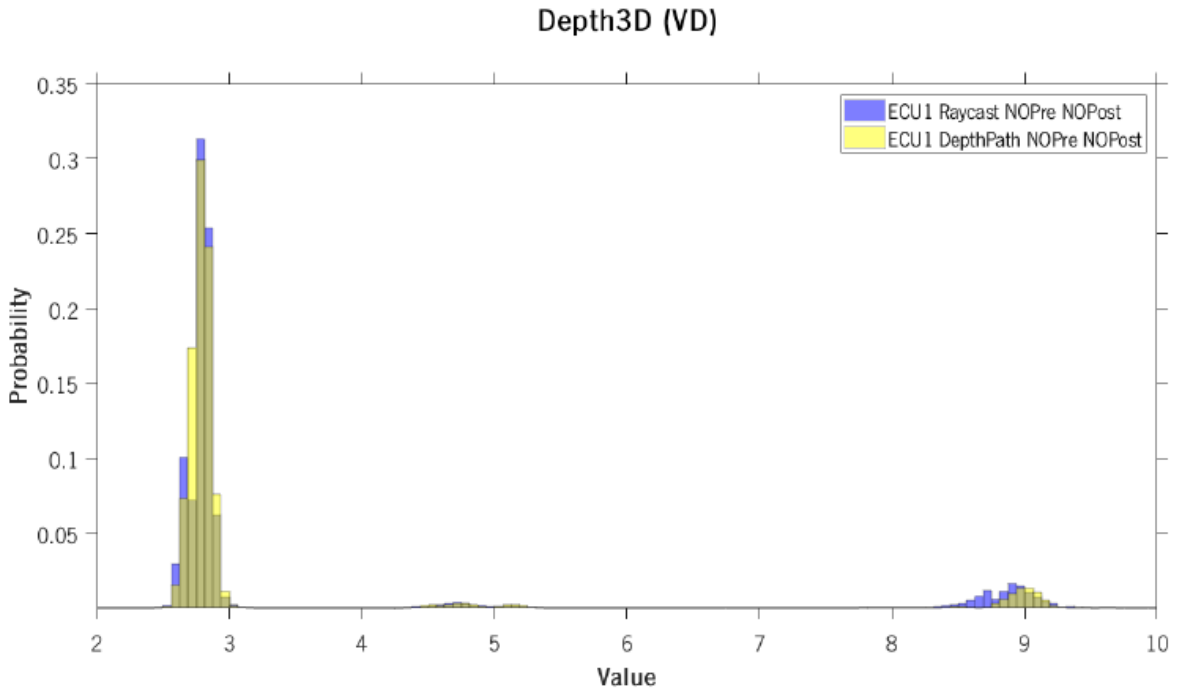

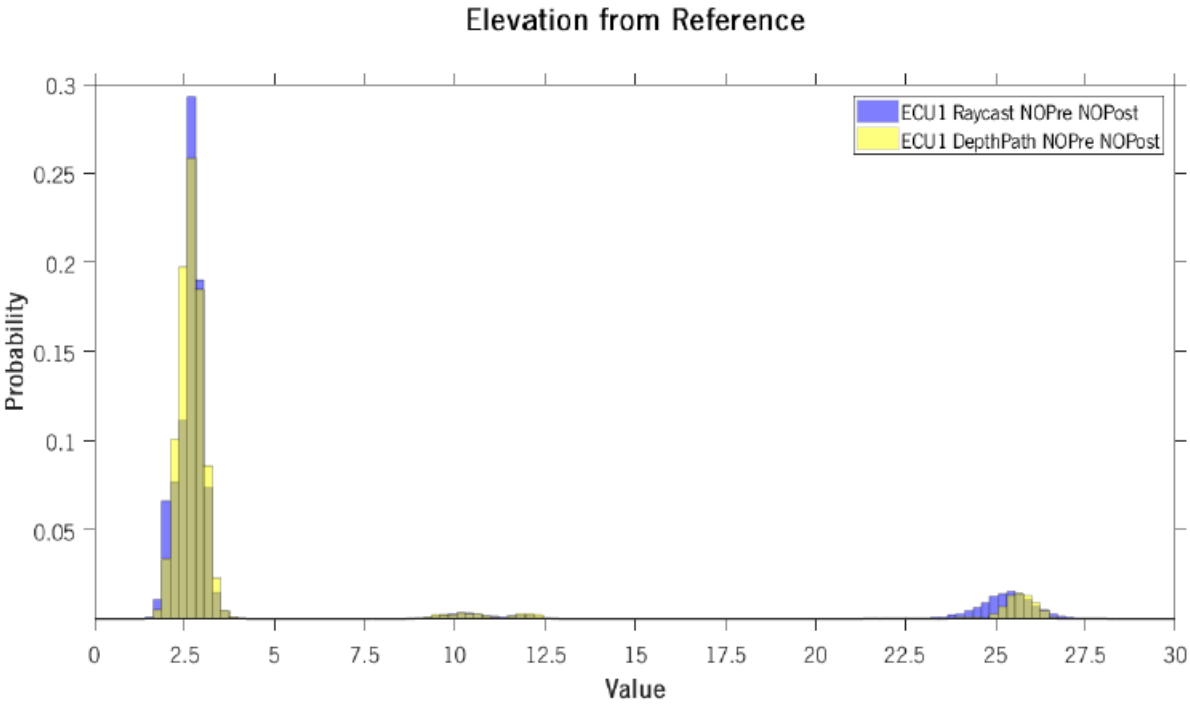

4. ECU Pre and Post Processing comparison

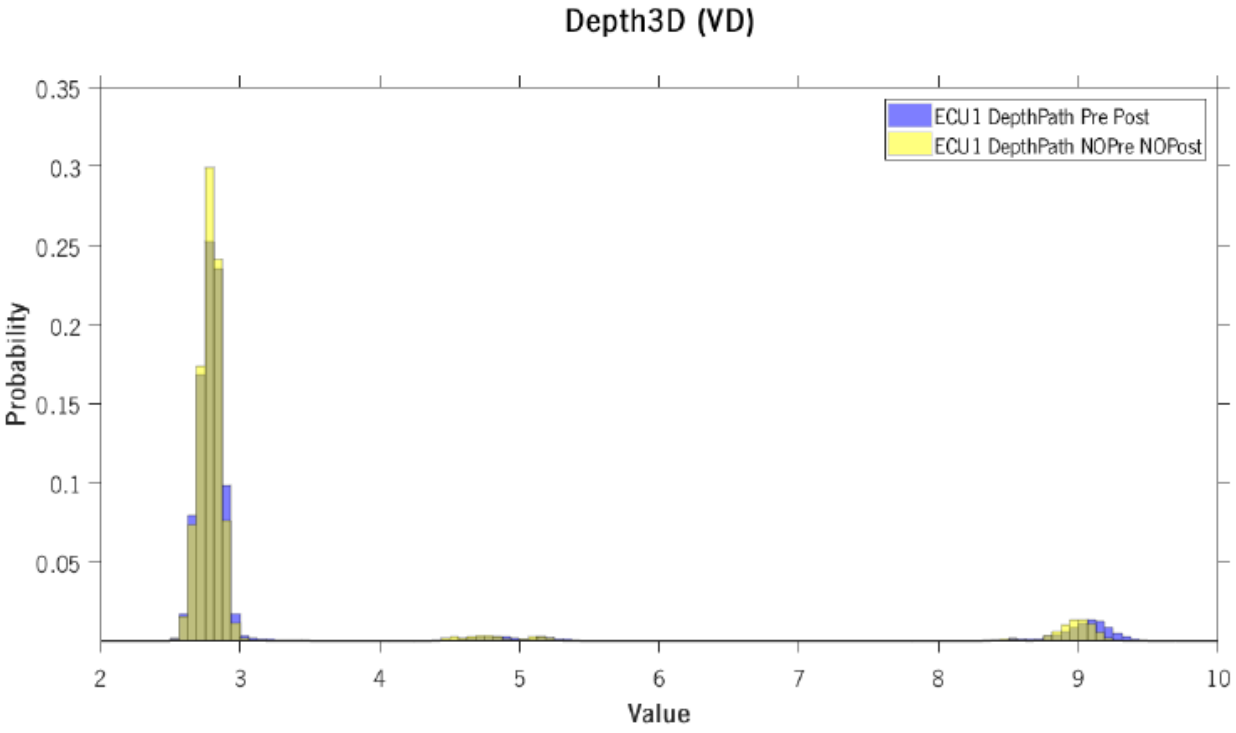

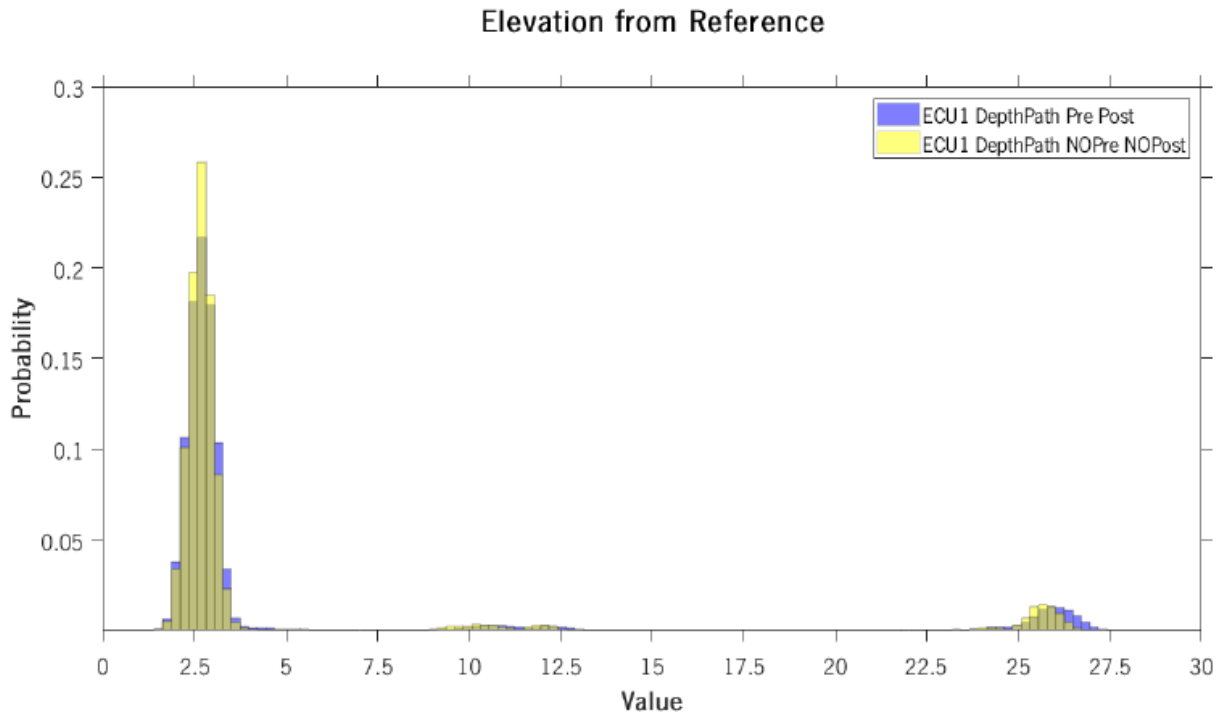

ANNEX B

1. Depth Path **with** BDE

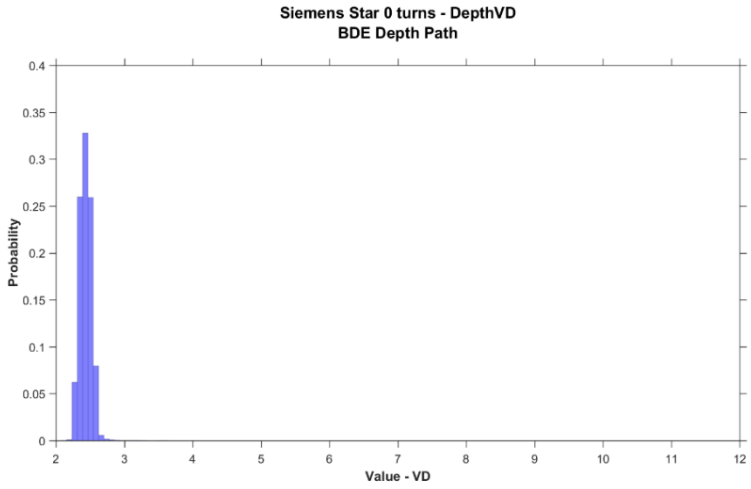

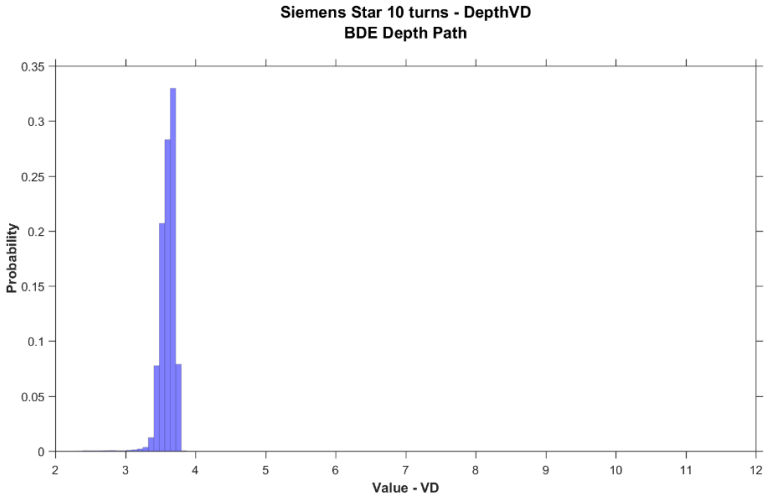

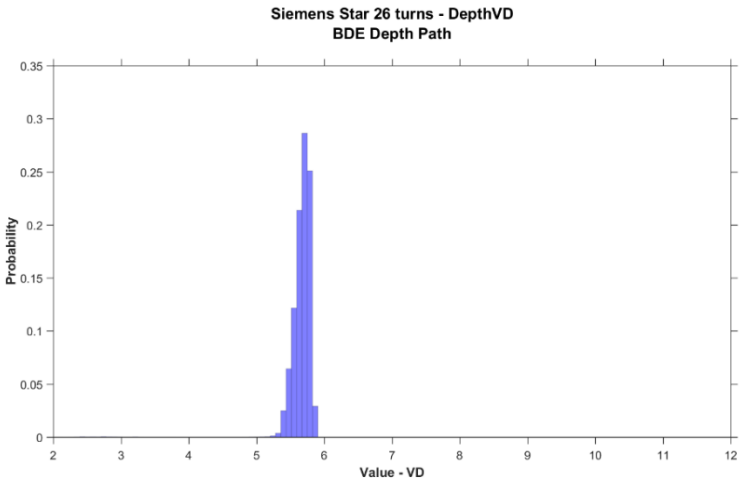

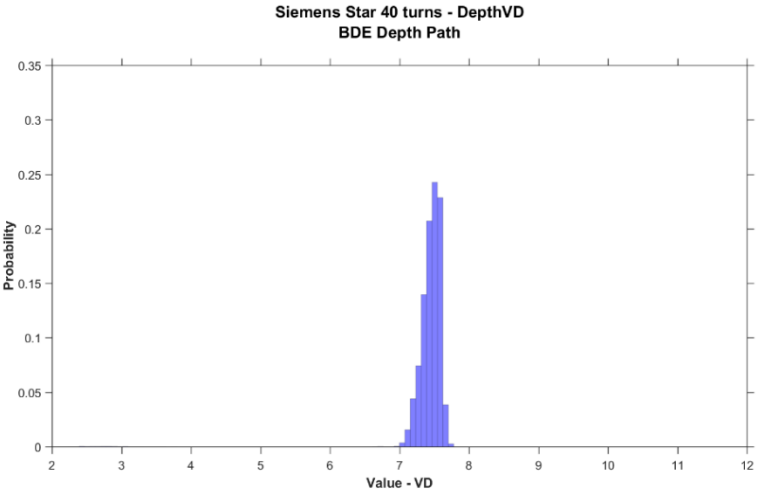

2. Raycast with BDE

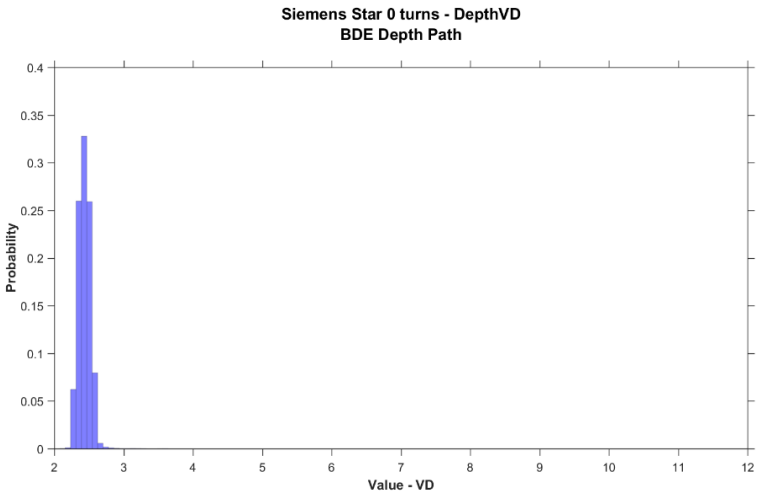

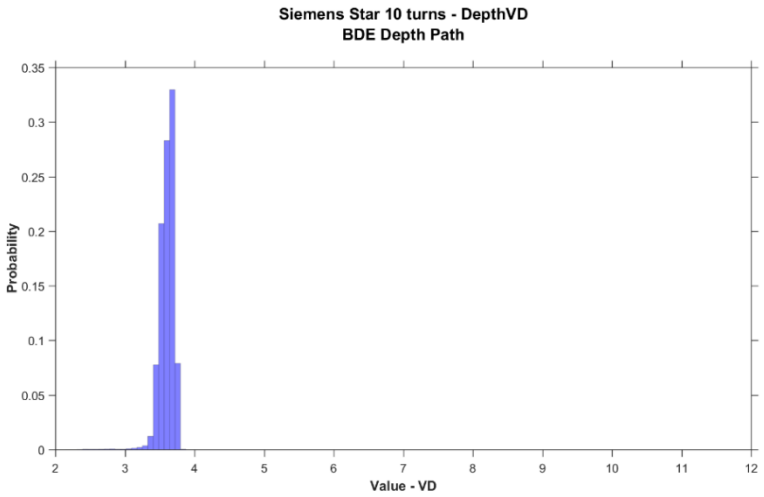

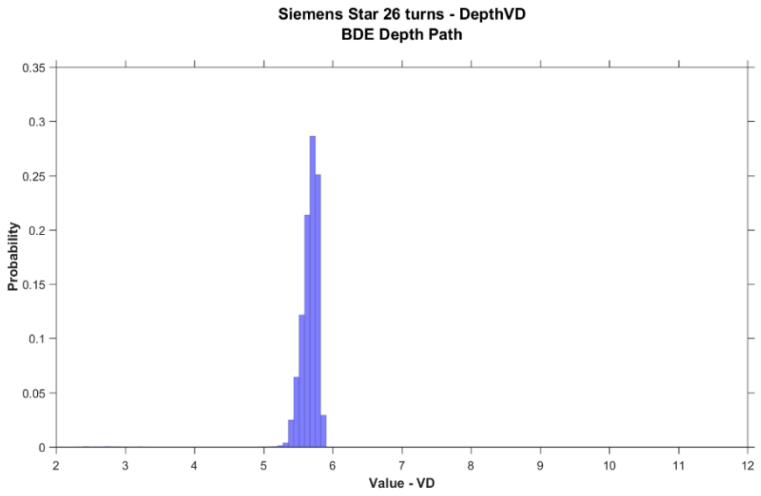

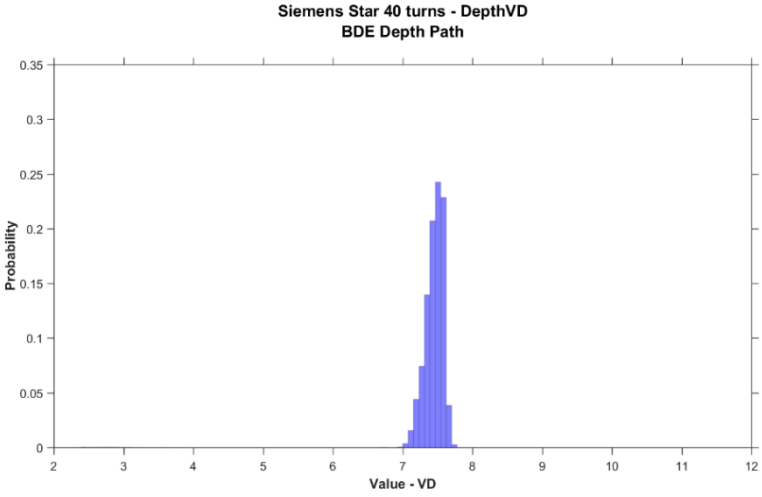

3. Depth Path without BDE

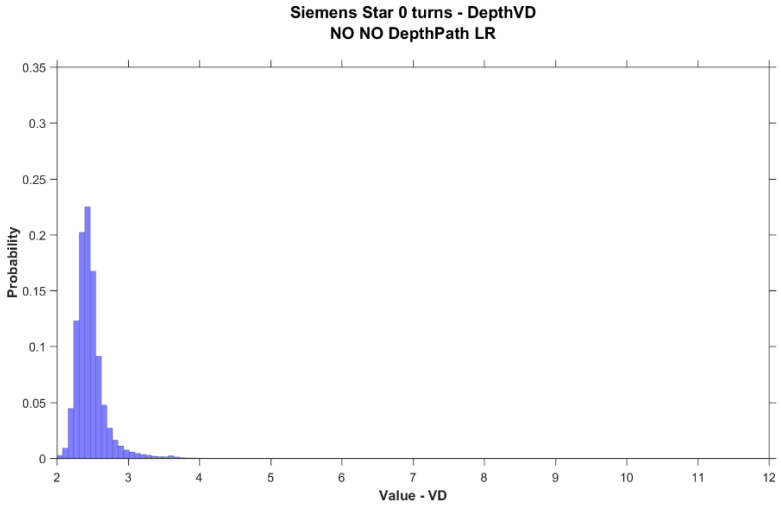

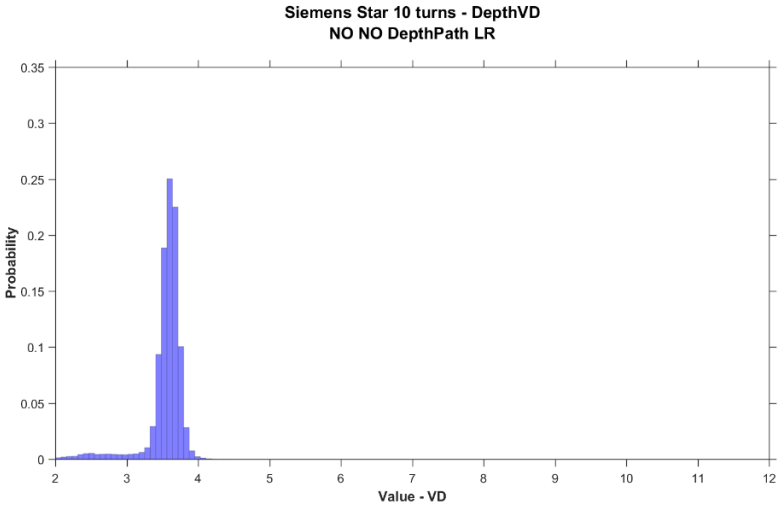

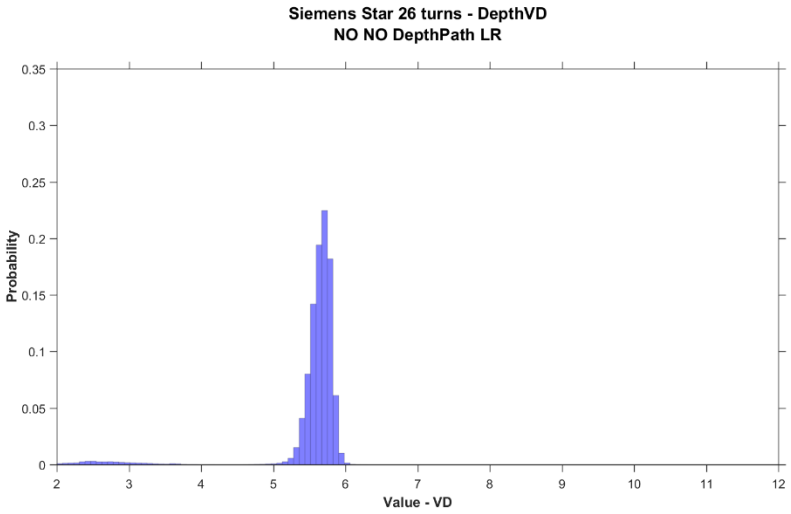

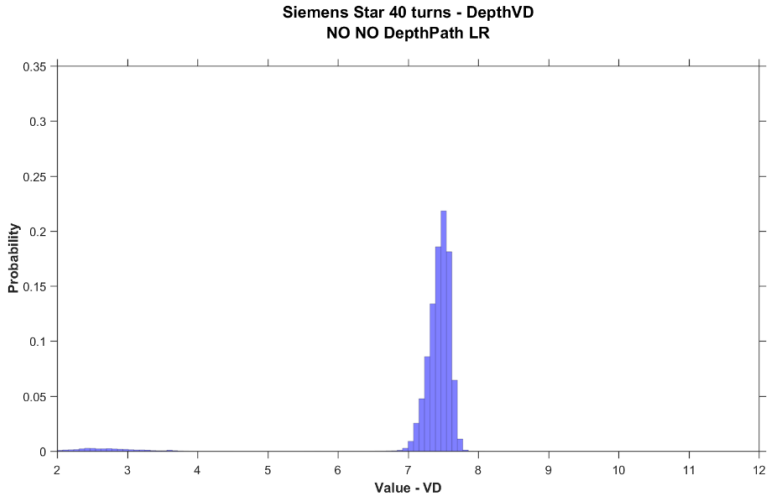

4. Raycast without BDE

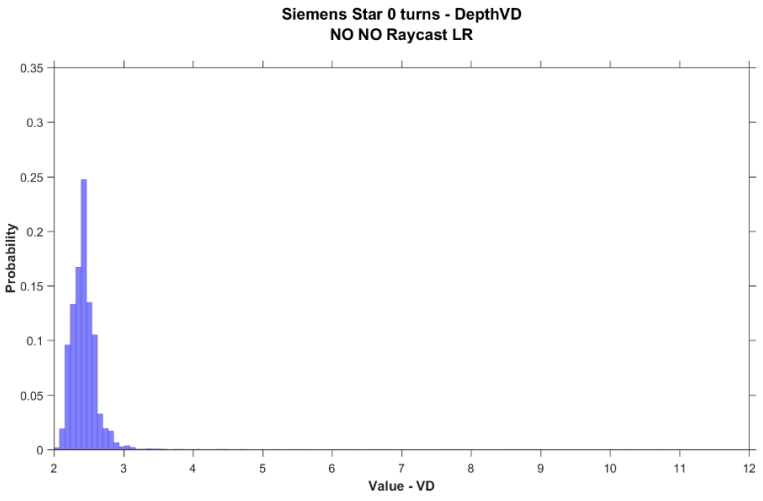

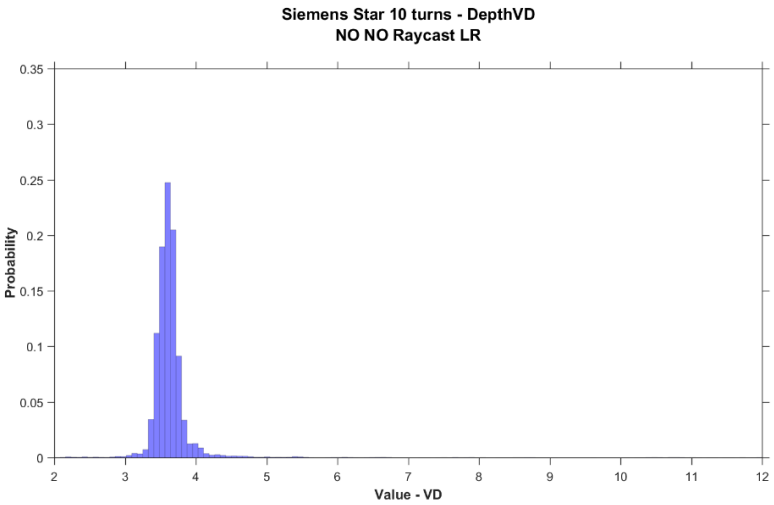

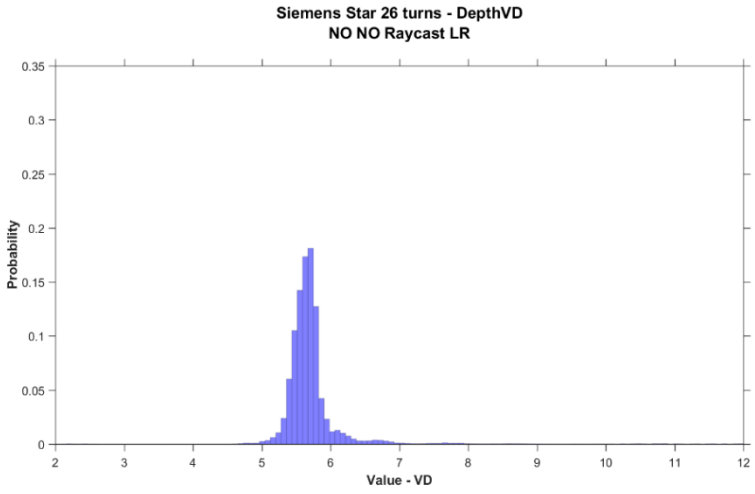

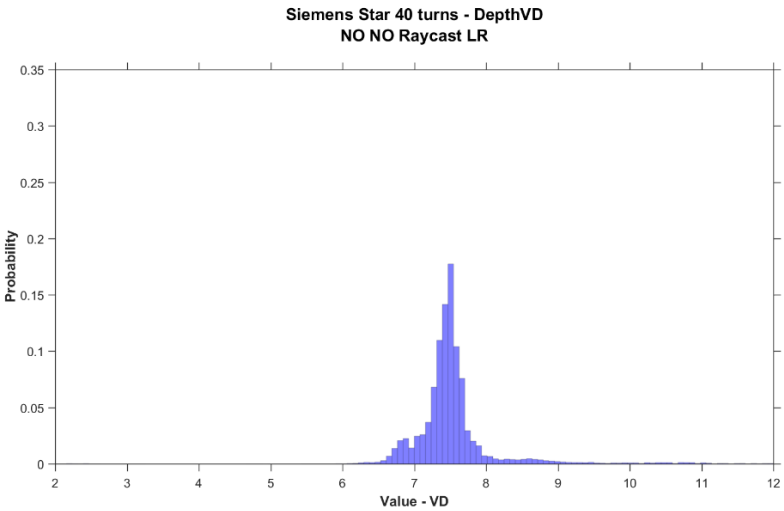

5. Graphics for Mean values and Standard Deviations

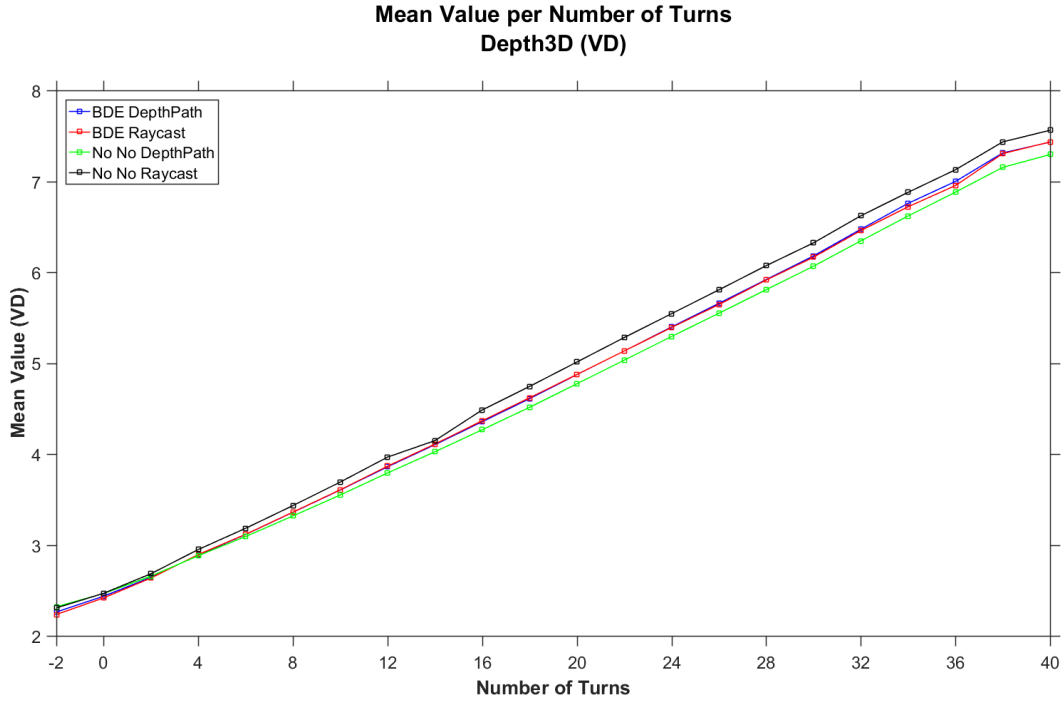

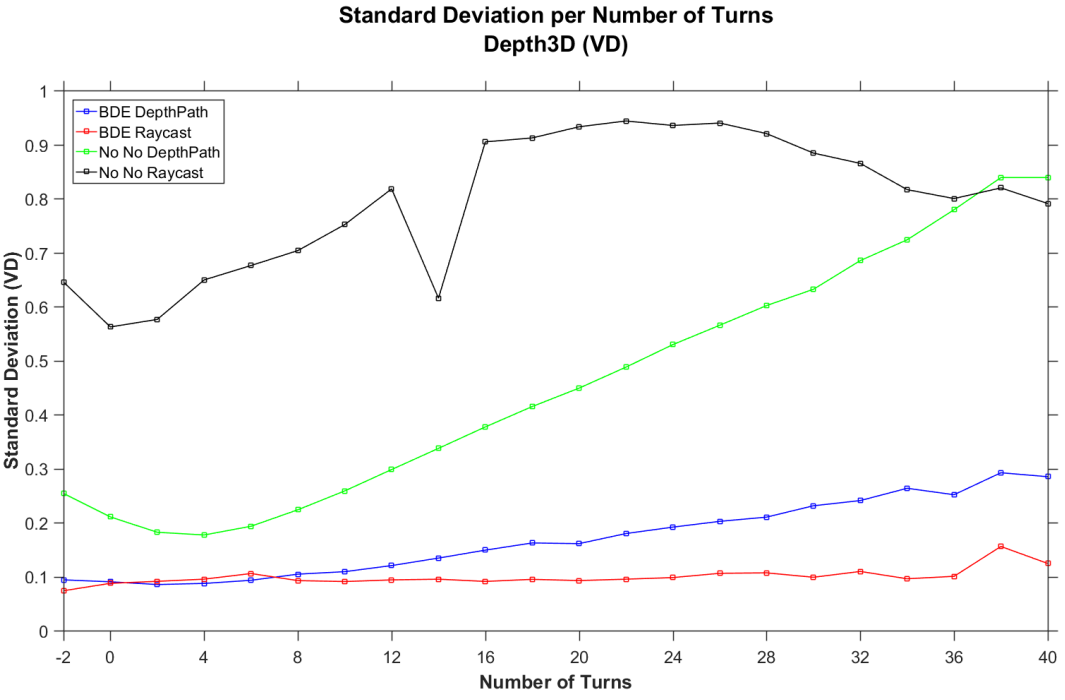

ANNEX D Calibration Plate Measurements

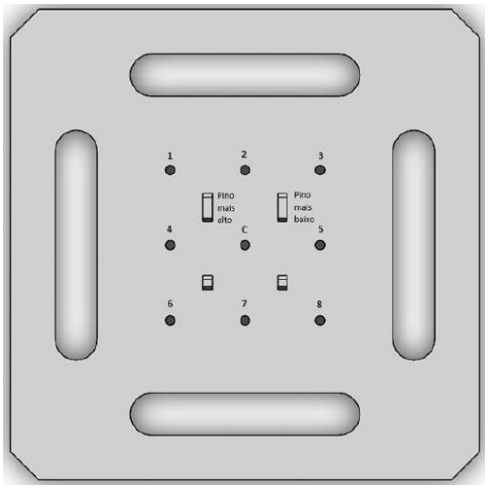

Distances from each hole to the central hole.

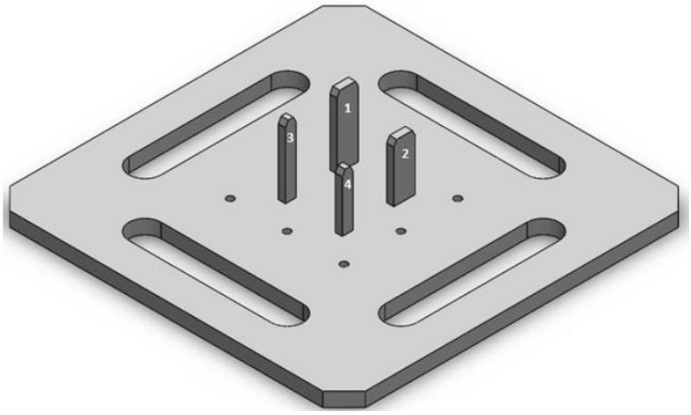

Heights of the pins

Nominal Values:

1C, 3C, 6C, 8C: 11.314 mm

2C, 4C, 5C, 7C: 8 mm

Values Measured by the Manufacturer:

1C: 11.229 mm

2C: 7.949 mm

3C: 11.308 mm

4C: 7.938 mm

5C: 8.051 mm

6C: 11.204 mm

7C: 8.027 mm

8C: 11.426 mm

Nominal Values:

1 and 3: 10 mm

2 and 4: 8 mm

Values Measured by the Manufacturer:

1: 10.100 mm

2: 8.054 mm

3: 10.098 mm

4: 8.047 mm

ANNEX E1 C_g and C_{gk} evaluations for the height of the Calibration Plate pins

Tolerance	300	micrometers		
StdDev	1.925590638	1.28543524	0.498260864	0.96802168
Cg	5.193211788	7.77946621	20.06980824	10.33034715
Min	8056	10096	8039	10074
Max	8063	10102	8041	10080
Average	8060.145833	10098.8125	8040.208333	10078.02083
Range	7	6	2	6
Cgk	4.129324651	7.47152901	15.52622665	3.450622902
Nominal	8054	10100	8047	10098

ANNEX E2 C_g evaluations for the XY position of the Calibration Plate holes

	Central Hole		Hole 1		Hole 2		Hole 3	
	XX	YY	XX	YY	XX	YY	XX	YY
StdDev	2.12264	4.538546	2.480645	3.046309	2.912044	3.989185	2.25424	4.870483
Average	-1523.12	4585.04	6993.08	12571.8	-1053.8	12599.92	-8918.28	12549.72
Min	-1527	4575	6987	12566	-1059	12592	-8922	12541
Max	-1518	4593	6997	12578	-1046	12606	-8915	12561
Range	9	18	10	12	13	14	7	20
Tolerance	300	micrometers						
Cg	4.711115	2.20334	4.03120	3.28266	3.43401	2.50677	4.43608	2.05318

	Hole 4		Hole 5		Hole 6		Hole 7	
	XX	YY	XX	YY	XX	YY	XX	YY
StdDev	2.17402	3.297029	1.203993	2.6533	1.273735	2.297825	4.088227	6.845027
Average	6896.56	4710.64	-9004.52	4744.6	6954.76	-3366.2	-1040.08	-3297.16
Min	6890	4701	-9007	4739	6953	-3370	-1046	-3308
Max	6900	4717	-9002	4749	6957	-3361	-1033	-3288
Range	10	16	5	10	4	9	13	20
Tolerance	300	micrometers						
Cg	4.59975	3.03303	8.30569	3.7688	7.85092	4.35194	2.44604	1.46091

ANNEX E3 C_g and C_{gk} evaluations for the distances from each hole to the central one

	Hole 1	Hole 2	Hole 3
StdDev	2.505083221	4.013310279	3.531556243
Average	11682.32101	8034.86678	10870.29961
Min	11676.74514	8026.655156	10863.76864
Max	11687.23415	8040.86519	10877.70307
Range	10.48900947	14.21003335	13.93442928
Nominal	11426	8027	11204
Tolerance	300	micrometers	
Cg	3.99188335	2.491708666	2.831612839
Cgk	-30.11490252	1.838317864	-28.66539712

	Hole 4	Hole 5	Hole 6	Hole 7
StdDev	2.180582559	1.235084526	1.805522446	6.619492942
Average	8424.589189	7479.353961	11621.80964	7891.198083
Min	8417.988477	7476.865252	11616.97035	7882.121098
Max	8428.097353	7481.908914	11625.31247	7901.714561
Range	10.10887643	5.043661945	8.342123773	19.593463
Nominal	8051	7938	11308	7949
Tolerance	300	micrometers		
Cg	4.585930469	8.096611845	5.538563101	1.510689729
Cgk	-52.52253771	-115.6860199	-52.39658723	-1.400002358